UNIVERSITÉ DE SHERBROOKE

Faculté de génie

Département de génie chimique et de génie biotechnologique

Vers le développement d'un pancréas bio-artificiel pour la transplantation

Towards the development of a bioartificial pancreas for transplantation

Thèse de doctorat

Spécialité: génie chimique

Rajesh GURUSWAMY DAMODARAN

Jury: Professeur Patrick VERMETTE (Directeur)

Professeur Denis GROLEAU (Rapporteur)

Professeur Tamas FÜLÖP

Professeur Stephen BADYLAK

Sherbrooke (Québec) Canada Décembre 2017

RÉSUMÉ

Le diabète sucré est déclenché par une perte de fonction et/ou du nombre total de cellules productrices d'insuline, les cellules β, que l'on trouve au sein des « Îlots de Langerhans » du pancréas. La greffe d'îlots est une des voies de traitement du diabète actuellement étudiée, et les avancées dans le domaine de l'ingénierie tissulaire pourraient améliorer la survie et la fonctionnalité des îlots transplantés. Lors de leur purification et de leur transplantation, les îlots subissent de nombreuses agressions : stress physiques et chimiques, la réponse immunitaire du patient greffé, infections post-opératoires, etc. Il est donc nécessaire de comprendre et d'améliorer les procédés de transplantation mais aussi de vérifier la fonctionnalité des îlots avant leur transplantation. Cette thèse a pour objectif de comprendre *in vitro* la fonctionnalité et la survie des îlots isolés en étudiant leur comportement dans un environnement 2D et dans un environnement 3D constitué de leur matrice extracellulaire native (MEC). Des pancréas de souris ont été décellularisés puis les îlots isolés ont été injectés dans le pancréas décellularisé. La viabilité et la fonctionnalité des îlots dans ce système ont été évaluées après 48h par coloration et par analyse de la sécrétion d'insuline par stimulation au glucose (GSIS). Ce manuscrit présente l'ensemble de la procédure de décellularisation du pancréas ainsi qu'une nouvelle technique d'injection d'îlots. La seconde partie de la thèse présente la solubilisation du pancréas décellularisé et l'immobilisation de ces extraits solubilisés sur des surfaces pour cultiver des îlots. Trois méthodes détaillées de solubilisation sont présentées (digestion à la pepsine, solubilisation par l'acide acétique et solubilisation par le NaOH). Des îlots isolés ont été cultivés sur ces surfaces biomimétiques et leur viabilité et fonctionnalité ont été évaluées. La dernière partie expérimentale de la thèse présente une comparaison du profil de sécrétion de l'insuline entre des îlots individuels et des populations d'îlots. Le profil cinétique a été modélisé à partir d'îlots cultivés seuls ou en groupe pendant 72h, et ce, *in vitro*. Trois profils cinétiques de sécrétion de l'insuline ont été observés (lent, rapide, et à taux constant), et nous avons analysé l'influence de la taille des îlots sur le profil cinétique de sécrétion. Les résultats observés lors des mesures traditionnelles de sécrétion d'insuline par stimulation au glucose (GSIS) sont discutés au regard des trois profils cinétiques de sécrétion.

Mots clés : Matrice extracellulaire, pancréas, îlots de Langerhans, cinétique de sécrétion d'insuline, transplantation d'îlots, pancréas décellularisé, extraction de protéines de la MEC.

ABSTRACT

Diabetes Mellitus involves the loss of function and/or absolute numbers of the insulin-producing β-cells normally located within the "Islets of Langerhans" of the pancreas. Islet transplantation is currently being investigated as a potential cure, and advances in tissue engineering is hypothesized to improve pancreatic islets survival and functionality. During isolation and transplantation, islets undergo physical damage, chemical damage, host-immune rejection, post-op infection, technical failures and graft failures. Therefore, it is essential to understand and improve the process of transplantation and, also, it is important to know the functionality of isolated islets before transplantation. This thesis aims to address these issues by understanding the functionality and survival of isolated pancreatic islets *in vitro*, by studying their behavior when cultured in 2D and 3D environments made of their native extracellular matrix (ECM). Also, insulin release kinetics of isolated single pancreatic islets was investigated and compared to those of pools of islets. The first experimental work includes the decellularization of mouse pancreata and infusing the freshly isolated islets into the decellularized pancreata. Glucose-stimulated insulin secretion (GSIS) and viability assays were performed on these islets to show the functionality and health of the islets after 48h of culture into the decelluarized pancreata. This section describes the full procedure of pancreas decellularization with a novel method to infuse islets into pancreata. The second experimental work describes the solubilisation of decellularized pancreata and the surface-immobilization of the extracts to culture islets. This study presents the detailed protocol of extraction of decellularized pancreata by three methods (pepsin digestion as well as acetic acid and NaOH solubilisation). The freshly isolated islets were cultured on these resulting biomimetic surfaces and the results of functionality and viability of these islets were discussed. The third experimental work focuses on the comparison of insulin kinetics between single islets and pools of islets. Freshly isolated individual islets and pools of islets were cultured *in vitro* for 72h and the kinetics of insulin release were modeled. Three modes of insulin secretion kinetics were revealed (slow-, fast- and constant-rate secretors), along with discussion on the effect of islet size on insulin release. In addition, the results of traditional GSIS on islets were compared with these secretion profiles.

Keywords: ECM, diabetes, pancreas, islets, insulin secretion kinetics, islet transplantation, decellularized pancreas, ECM protein extraction.

ACKNOWLEDGEMENTS

I would like to thank my research director Prof. Patrick Vermette for giving me this wonderful opportunity and space to work on this project and in his lab. I specially thank him for his valuable guidance and support throughout my studies.

I would like to thank the members of my jury (Prof. Stephen Badylak, Prof. Tamas Fülöp and Prof. Denis Groleau) for providing their valuable time to read and evaluate this thesis. Their feedback and inputs regarding this thesis are highly respected.

I very much appreciate the co-operations given by my colleagues Jamie sharp, Evan A. Dubiel, Parker Andersen, Carina Kuehn, Sylvain Vigier and Tim Spitters at Université de Sherbrooke, for their valuable feedbacks, inputs, suggestions and ideas during my studies.

A special thanks to Sylvain Vigier for the French translation of the thesis.

I would like to thank all my students Alexander, Anais, Sarah, Marc and Arnaud for helping in my experiments and data analysis.

The support provided by all the technicians Charles, Chantal, Isabelle, Valérie, Serge and Sonia are most valuable and very much appreciated.

I am most grateful to my friends Pavithran, Charith, Rajini, Giuliana, Barzin, Himmat, Djazia, David, Elaheh, Imad and Camila for sharing everything during the stay.

Finally, I am very much obliged to my wife Divya, my parents and my brother for their wonderful love and support during this journey.

TABLE OF CONTENTS

LIST OF FIGURES

LIST OF TABLES

LIST OF ABBREVIATIONS

2D	two dimensional
3D	three dimensional
ANOVA	analysis of variance
BSA	bovine serum albumin
$CaCl_2$	calcium chloride
CMD	carboxymethyl-dextran
CO_2	carbon dioxide
DAB	3,3'-diaminobenzidine
DAPI	4', 6-diamidino-2-phenylindole, dihydrochloride
DMEM	Dulbecco's modified Eagle medium
ECM	extracellular matrix
ELISA	enzyme-linked immunosorbent assay
FBS	fetal bovine serum
FDA	Food and Drug Administration
GAG	glycosaminoglycan
GSIS	glucose-stimulated insulin secretion
HBSS	Hank's balanced salt solution
IBMX	3-isobutyl-1-methylxanthine
IEQ	islet equivalent
INS-1	rat insulinoma cells
KRBH	Krebs-Ringer buffer with HEPES

MTT	3-(4,5-dimethylthiazol-2-yl)-2,5-diphenyltetrazolium bromide
P	probability
PBS	phosphate buffered saline
RPMI	Roswell Park Memorial Institute medium
RGD	Arg-Gly-Asp
RT	room temperature
T1DM	type 1 diabetes mellitus
T2DM	type 2 diabetes mellitus
TCPS	tissue culture polystyrene
τ_p	time constant
TUNEL	Terminal deoxynucleotidyl transferase dUTP nick end labeling

Chapter 1

INTRODUCTION

In 2015, the International Diabetes Federation estimated that 415 million people worldwide have been diagnosed with diabetes; with an estimated increase to 642 million by 2040. In 2017, the Canadian Diabetes Association reported that there are 11 million Canadians living with diabetes or prediabetes, the treatment of which still remains a huge physiological or medicinal, and socioeconomic problem.

In 1979, the terms type-I (T1DM) and type-II (T2DM) were assigned to classify the diabetic phenotypes; earlier it was called insulin dependent diabetes mellitus or juvenile diabetes, and non-insulin dependent diabetes mellitus or adult-onset diabetes, respectively [1].

T1DM is caused by the autoimmune destruction of insulin-producing β cells of the pancreas [2]. There are several factors including viral, bacterial, environmental, life style, and genetics which have all been associated with the pathophysiology of T1DM [3]. Due to the destruction of these cells, they can no longer produce insulin in response to glucose, thus, creating reliability on an exogenous supply of this hormone indispensable to normalize the blood glucose levels. This process is essential for long-term survival. A possible cure for T1DM came in 1966 when the first transplantation of a whole pancreas was successfully performed. Alike to other major organ transplantations, whole pancreas transplantation continues to have morbid risks including surgical complications, post-op infection, technical failures, donor obesity which all influence the success and long-term survival of such a graft [4]. Furthermore, the recipient also requires lifelong immunosuppressant drugs. Given this, transplanting islets of Langerhans may offer a less invasive, lower risk, alternative cure for T1DM. Recipients of islet transplantation attained insulin independence with normoglyceamia for a stipulated period of time, post-transplantation. This result combined with the less invasive nature of this transplantation reduced the overall post-surgical complications and improved the clinical outcome of the patient using less immunosuppressant drugs [5, 6].

The major limiting factors for islet transplantation include limitation of donors for the source of islets, immune rejection, damages of islets and of the extracellular matrix (ECM) during isolation as well as poor revascularization post transplantation [7].

Islets encapsulation could provide a possible solution to protect isolated islets. Three major advantages of islet encapsulation are: 1. to protect islets from host-immune rejection, 2. to re-establish the lost ECM to avoid anoikis and cell death and 3. to allow diffusion of molecules.

This thesis mainly focuses on the improvement of islet culture methods by providing information on islets behaviour *in vitro* on 2D and 3D ECM and the kinetics of insulin release revealing the full potential of isolated islets in terms of insulin secretion towards glucose stimulation.

Chapter 2 titled 'Tissue and Organ Decellularization in Regenerative Medicine' is a review of the scientific literature. Major tissues/organs used for decellularization including the recent techniques and chemicals involved in decellularization and their outcomes are discussed. This review also highlights the inevitability of ECM molecules and the possible immune reactions faced by these ECM scaffolds when transplanted. In addition, applications, status and perspective of decellularized tissues and organs are discussed in detail.

Chapter 3 consists of an experimental paper titled 'Decellularized Pancreas as a Native Extracellular Matrix Scaffold for Islets'. Mouse pancreata were decellularized and then isolated islets were perfused into the decellularized organ, thus, concluding that these islets were viable and functional after 48h *in vitro*.

Chapter 4 is an experimental paper titled 'Solubilisation of Decellularized Pancreata and Immobilization on Low-Fouling Surfaces for Islet Culture'. Briefly, the decellularized pancreata were solubilised using three different methods (pepsin, acetic acid and NaOH treatments). The extracted proteins were immobilized on low-fouling surfaces to culture freshly isolated pancreatic islets for 5 days. The results revealed that the islets were viable and functional after 5 days on the biomimetic surfaces.

Chapter 5 consists of an experimental paper titled 'Insulin Secretion Kinetics from Single Islets Reveals Distinct Sub-Populations'. 58 islets were freshly isolated from mouse pancreata and cultured on tissue culture polystyrene (TCPS) for 72h at four glucose concentrations. The results revealed that the islets responded to glucose by three different insulin secretion profiles (slow, fast and constant rate secretors), and most of the islets were characterized as slow secretors.

Chapter 6 presents a conclusion and future perspectives of the study.

Chapter 2

Tissue and Organ Decellularization in Regenerative Medicine

Foreword

Authors and Affiliations:

Rajesh Guruswamy Damodaran: Ph.D. Candidate, Université de Sherbrooke, Département de génie chimique et de génie biotechnologique.

Patrick Vermette: Professor, ingénieur, Université de Sherbrooke, Département de génie chimique et de génie biotechnologique.

Date of Submission: Januray 25th, 2017

State of Acceptance: Under review

Journal: Biotechnology Progress

Contribution:

This article constitutes the scientific literature review of this thesis. The contents of this work were submitted to *Biotechnology Progress*. The article was written by Rajesh Guruswamy Damodaran. All work was done under the direction and supervision of Patrick Vermette.

Résumé

L'augmentation de la demande en tissus et organes à transplanter a entrainé l'essor de la recherche sur la décellularisation tissulaire. La préparation d'organes et de tissus décellularisés implique l'élimination de leur contenu cellulaire et génomique tout en conservant la structure complexe de la matrice extracellulaire (MEC) pour jouer le rôle de support possédant une fonction physiologique. De nombreux tissus et organes ont été décellularisés avec succès et utilisés en recherche ou comme produits commerciaux. Différentes techniques sont utilisées : traitements mécaniques, chimiques ou biologiques, qui possèdent toutes leurs avantages et inconvénients. Cet article de revue présente les récents développements dans les méthodes de décellularisation, l'importance de la nature des détergents utilisés, ainsi que le rôle de la MEC soit comme support physique, soit comme support et source des signaux pour la survie cellulaire, la différenciation cellulaire et l'homéostasie. Nous présentons également les applications et les statuts actuels des bioproduits commercialisés à partir de tissus et d'organes décellularisés.

Mots clés : décellularisation; recellularisation; ensemencement cellulaire; organes artificiels; détergents; matrice extracellulaire (MEC); cellules souches; commercialisation

Abstract

The advancement and improvement in decellularization methods can be attributed to the increasing demand for tissues and organs for transplantation. Decellularized tissues and organs, which are free of cells and genetic materials while retaining the complex ultrastructure of the extracellular matrix (ECM), can serve as scaffolds to subsequently embed cells for transplantation. They have the potential to mimic the native physiology of the targeted anatomic site. ECM from different tissues and organs harvested from various sources have been applied. Many techniques are currently involved in the decellularization process, which come along with their own advantages and disadvantages. This review focuses on recent developments in decellularization methods, the importance and nature of detergents used for decellularization, as well as on the role of the ECM either as merely a physical support or as a scaffold in retaining and providing cues for cell survival, differentiation and homeostasis. In addition, application, status and perspectives on commercialization of bioproducts derived from decellularized tissues and organs are addressed.

Keywords: Decellularization; Recellularization; Cell seeding; Artificial organs; Detergents; Extracellular matrix (ECM); Stem cells; Commercialization

2.1 Introduction

Increased demand for tissues and organs for transplantation has expanded the fields of research on decellularization. Preparation of decellularized tissues and organs involves removal of cells and genetic materials from the tissue or organ and retention of the complex ultrastructure of the extracellular matrix (ECM) to serve as a natural scaffold. The ECM is produced by the native cells and serves as a mechanical support and cues for cell migration, attachment, differentiation and function [8, 9]. Many tissues and organs have been successfully decellularized and used for research and commercial purposes. Different techniques including physical, chemical and biological methods are currently applied in decellularization and these have their own pros and cons.

The two important criteria to be fulfilled during a decellularization procedure are: 1. retention of the native structures and 2. removal of a maximum of cell components. Several tissues and organs such as the small intestine, bladder, placenta and liver, only to name a few, have been decellularized and used as ECM scaffolds [10-13]. Recent advances in regenerative medicine and tissue engineering have paved the path for investigating the use of whole decellularized organs for transplantation. Many *in vitro* and *in vivo* studies support that ECM-based scaffolds made of decellularized tissues and organs have beneficial effects on cells, including stem cells, in terms of their attachment, proliferation, viability and functionality. In favor to that, these scaffolds have a low immunogenicity, which facilitates their *in vivo* applications [13, 14].

Over the past 20 years, decellularized tissues and organs have been commercially available for wound healing. Companies are working to commercialize ECM-based products for organ transplantation, which some are in clinical trials.

The objective of this review is to give an update on the most important tissues and organs that are used for decellularization, the importance of ECM as a complete set of biomolecules, the techniques and chemicals applied in decellularization operations, the rationale behind using ECM-based bioproducts, as well as applications, perspectives and path to commercialization.

2.2 Major tissues and organs used for decellularization

2.2.1 Liver

The liver is one of the important organs, which has been decellularized for regenerative medicine. The first successful liver decellularization was done by surface treatment with detergents and the resulting bioproduct was recellularized with rat hepatocytes to assess functionality [15]. Surface treatment refers to decellularizing a tissue or an organ by immersion in decellularizing solutions as opposed to perfusion decellularization, which involves perfusing solutions within the tissue or organ. Studies on liver decellularization report the perfusion of detergents through the network of veins and arteries, then its recellularization and *in vivo* transplantation [16-18]. For example, seeding rat hepatocytes into decellularized liver and subsequent transplantation in rats showed that less damages occurred to the cells following an 8h transplantation, as revealed by TUNEL staining [16]. In a separate study, when human liver stem cells were seeded in decellularized rat liver, differentiation into functional hepatocytes was observed as well as the presence of epithelial and endothelial-like cells [19]. Research on achieving human-sized whole liver has also been attempted with pigs by decellularizing the organ with SDS (sodium dodecyl sulfate) [20, 21].

2.2.2 Heart

Heart decellularization techniques started initially with heart valves by surface decellularization using detergents and subsequent recellularization with different cell types [22-24]. Introduced in 2008, decellularization of whole hearts from rats was done by perfusion methods and the resulting scaffolds were seeded with cardiac and endothelial cells; contraction in cell patches was observed after 4 days [25]. Recent advances in heart decellularization aim to improve perfusion processes during decellularization and cell seeding with progenitors as well as to achieve decellularization of organs from larger animals [26-30]. Allo-transplanted porcine heart seeded with mesenchymal stem cells (MSCs) showed thrombosis in arteries as well as the presence of inflammatory cells and the observation was similar to decellularized heart transplanted without mesenchymal stem cells [31]. In addition, a 14-day culture of human cardiomyocytes in human decellularized heart showed visible contraction when electrically stimulated [32].

2.2.3 Lungs

Decellularized lungs were considered as a source of bioartificial organs for transplantation in end-stage lung diseases. The first successful perfused decellularization was reported in 2010 following methods initially applied to heart and liver [33]. Recent works on decellularizing lung involve the improvement of decellularization process and cell seeding methods, as well as studies on the role of stem cells [33-35]. Attempts to decellularize human lungs are step closer to fill the gap in the demand for organ transplantation [36, 37]. Stabilization of endothelial cells by seeding adipose-derived stem cells into decellularized lungs could be a potential solution to regenerate the vasculature of decellularized lungs [38]. Seeding mesenchymal stromal cells in decellularized lung in suspension bioreactor resulted in differentiation of the cells into collagen-1 alpha-1 producing cells [39]. In another study, human-induced pluripotent stem cells (iPSC)-derived endothelium and ventralized iPSC were seeded in decellularized lungs resulting in retention of epithelial progenitors phenotype by expressing Nkx21 and endothelial phenotype by expressing CD31 [40]. Transplantation of decellularized rat lung seeded with epithelial and endothelial cells maintained the animals alive without ventilation for 6h [33].

2.2.4 Pancreas

The first perfused decellularization of pancreas was carried out in 2009 with a porcine organ [41] and then applied to mouse [42]. The decellularized tissues were used to seed cells and islets and their *in vitro* functions were studied as well as the biocompatibility of these bioartificial pancreata was investigated *in vivo* [41-44]. Later, rat pancreata were decellularized and a new method was introduced to infuse islets into the ducts, veins and arteries [45]. Decellularized pancreata were seeded with human stem cells, an AR427 acinal cell line, MIN-6 cells and islets, and cell attachment as well as basic cell functions were studied [42-45]. Recently published work from our group demonstrated that islets infused into the ductal system of decellularized pancreata were functional by releasing insulin in response to glucose stimulation after 48 days *in vitro [46]*.

2.2.5 Small intestinal submucosa (SIS)

One of the first usages of SIS was during 1989, as a vascular graft for dogs [47]. SIS biomaterials are widely used in regenerative medicine, for example to reconstruct urethra, cornea, oesophageal, and heart [48-51]. Recently, SIS seeded with urothelial cells showed formation of new vessels, proliferation of smooth muscle cells, epithelization and maintenance of the opening of urethra when compared to unseeded scaffold [52]. Reconstruction of cornea was accomplished successfully in 106 cases by preserving vision at third month of post-surgery using porcine SIS [53]. Seeding autologous oral mucosa epithelial cells along with SIS resulted in muscular regeneration and re-epithelization after 8 weeks of surgery and the results were superior to SIS with no cells [54]. Applying FDA-approved SIS ECM seeded with mesenchymal stem cells resulted in a lower response of the adaptive immune system in a porcine model, when compared to SIS-ECM with no cells [55].

2.2.6 Bladder

Urinary bladder has been one of the oldest organs selected for decellularization. Recent studies on ECM derived from decellularized bladder has indicated a beneficial effect on neuron survival, stem cells, spinal cord and open wounds [56-59]. Urinary bladder-derived ECM has shown greater advantage than cardiac-derived ECM in remodelling and for attracting site-specific cells (cardiomyocytes) after implantation [60]. The implantation of large segments (>24cm^2) of urinary bladder into porcine bladder showed infiltration of smooth muscle cells and promoted angiogenesis after 30 days [61]. Vesicles derived from urinary bladder ECM had a positive effect on neuron neurite growth and on spinal cord injury repair [57, 58]. Urinary bladder-derived ECM also had a better effect on the treatment of open wounds when compared to conventional therapies [56]. Bioproducts made from urinary bladder-derived ECM are available in different formulations such as sheets (Cytal® Burn Matrix, also marketed as MatriStem® Burn Matrix, ACELL (Columbia, USA); the product is applied directly on wounds), powder (MicroMatrix®, ACELL (Columbia, USA)) and hydrogels (not available commercially).

2.2.7 Kidneys

The initial method of decellularization of whole kidneys was achieved by perfusion techniques and the resulting products were used to seed and differentiate stem cells [41, 62]. Advances in kidney decellularization include *in vitro* and *in vivo* studies on rat and mouse kidneys to investigate the functionality of recellularized kidneys with endothelial, epithelial and renal progenitor cells [63, 64].

2.2.8 Bones and cartilage

The successful removal of cells from bones and cartilages was achieved in 2011[65]. Recent advancements in cartilage and bone repair include utilizing adipose-derived stem cells, multipotent stromal cells seeded on decelluarized cartilage ECM to study the mechanical properties and bone regenerative capacity [66, 67].

2.2.9 Plants

Recent advancements in tissue and organ decellularization have extended their boundaries to apply perfused decellularization protocols on plant leaves and eventually recellularize them with cardiomyocytes resulting in contractile function successfully for 21 days [68].

2.3 Recent decellularization methods

Over the years, several studies have been conducted to understand the utility of decellularized tissues and organs in regenerative medicine. Table 1 below provides a summary of recent studies highlighting the various techniques and their corresponding results on decellularized tissues and organs.

Table 1: Recent studies involving decellularization methods and their outcomes.

Organ or tissue	Species	Applications	Methods	Chemicals	Results	References
Liver	Mouse	Culture of mouse hepatocytes	Non-thermal irreversible electroporation	-	Cell integration into the host liver parenchyma	[69]
	Rat	Hepatocyte seeding and transplantation into rat	Perfusion through portal vein	SDS (0.01, 0.1 and 1%)	Preservation of functional and structural characteristics of microvascular network and display of liver-specific functions	[16]
		Decellularization using increasing detergent concentration	Perfusion through portal vein	1, 2 and 3% Triton X-100 + 0.1% SDS	Retention of laminin in the basement membrane and collagen IV	[70]
		Minimizing ECM damage	Arterial perfusion under oscillation	1% Triton X-100 + 1% SDS	Fast, homogenous, higher concentration of hepatocyte growth factor compared to the native	[71]

Organ or tissue	Species	Applications	Methods	Chemicals	Results	References
			pressure conditions		tissue, high GAG concentration and gentle method of decellularization	
	Pig	Comparison of three detergent mixtures for decellularization and recellularization with rat hepatocytes	Perfusion de-cellularization and freeze-thaw	1% SDS; 1% Triton X-100 + 1% sodium deoxycholate; 1% sodium deoxycholate + 1% SDS	Cell removal, preservation of ECM structure and biocompatibility, achieved by 1% Triton X-100 + 1% sodium deoxycholate	[18]
Kidneys	Pig	Study on decellularization methods	Perfusion using a high-throughput de-cellularization apparatus	water and 0.5% SDS	Preservation of important ECM components, intact vasculature tree, *in vitro* biocompatibility for cells and preservation of gross anatomy after 2 weeks of implantation	[72]
Heart	Rat	Recellularization with aortic endothelial cells and	Coronary perfusion	1% SDS	Performance of basic functions	[73]

Organ or tissue	Species	Applications	Methods	Chemicals	Results	References
		rat neonatal cardiomyocytes				
	Zebra fish + Mouse	*In vitro* proliferation and migration of human cardiac precursor cells	Freeze-thaw cycles		Exhibition of pro-proliferative and chemotactic effect with human cardiac precursor cells by Zebra fish ECM including structural preservation and cardiac contractile function	[74]
	Pig	Comparison of two detergents	Surface treatment	1% Triton X-100 + nucleases + trypsin and sodium deoxycholate with and without nucleases	Complete cell removal and preservation of ECM structures by Triton X-100 + nucleases + trypsin	[75]
Myocard -ium	Pig	Comparison of decellularizing agents and recellularization with	Surface treatment	1% SDS; 1% Triton X-100; 0.5% trypsin	Effective decellularization by SDS and retention of ECM microstructures.	[76]

Organ or tissue	Species	Applications	Methods	Chemicals	Results	References
		rat myocardial fibroblasts			Display of different beating magnitudes of seeded cells: largest beating magnitude in trypsin, moderate in SDS and none in Triton X-100-treated scaffolds	
Teeth	Human	Comparison of decellularization methods	Surface treatment	10% formaldehyde, PBS + EDTA + 2.5% sodium hypochlorite; PBS + EDTA + 40v (40 volume or 12%) hydrogen peroxide; PBS + 2.5% sodium hypochlorite + Ryozime®; PBS + EDTA + 40 v hydrogen peroxide + Ryozime®	Maximal removal of biological particles and less damage to the structures obtained with PBS + EDTA + 40 v hydrogen peroxide + Ryozime®	[77]

Organ or tissue	Species	Applications	Methods	Chemicals	Results	References
Bones and cartilages	Rat	Calvaria regeneration *in vivo* and recellularization with mesenchymal stem cells	Surface treatment	0.5% SDS + 0.1% ammonium hydroxide	Formation of new bone and merging with the host bone after 3 months. Proliferation and osteogenic differentiation of mesenchymal stem cells	[78]
	Pig	Tissue characterization and recellularization with murine fibroblasts and porcine chondrocytes	Surface treatment	1% SDS	Retention of compatible tension properties of intact tissue but reduction in compression. No cytotoxicity on recellularized cells	[79]
	Bovine	Tissue characterization and recellularization with human adipose mesenchymal stem cells	Surface treatment	10 mM Ethylenediaminetetra-acetic acid disodium salt dihydrate (Na_2EDTA, pH 7.2–7.4)	Chondrogenic differentiation of human adipose mesenchymal stem cells	[80]
Skeletal Muscle	Pig	Comparison of decellularization	Surface treatment	1% SDS; 1% SDS	Formation of jelly-like hydrogel by using	[81]

Organ or tissue	Species	Applications	Methods	Chemicals	Results	References
		methods and formulation of hydrogel scaffolds		+ 0.2% sodium deoxycholate; 1% SDS + 1% Triton X-100; 1. 0.2% Trypsin/0.1% EDTA, 2. 0.5% Triton X-100, 3. 1% Triton X-100/0.2% sodium deoxycholate	0.2% trypsin/0.1% EDTA, 0.5% Triton X-100, and 1% Triton X-100/0.2% sodium deoxycholate treatment	
Nerve	Rat	Reconstruction of long gap nerve injury	Surface treatment	(Dulbecco's modified Eagle medium + 10% fetal bovine serum and 4% penicillin/streptomycin/amphotericin B) + (DMEM with 10% fetal bovine serum and 2% penicillin/streptomycin/ amphotericin) + PBS	Exhibition of functional nerve regeneration *in vivo*	[82]
Skin	Mouse	Comparison of detergent-free decellularization	Surface treatment	(50nM latrunculin B + Dulbecco's modified Eagle medium) + 0.6	Retention of matrix composition and biomechanical property	[83]

Organ or tissue	Species	Applications	Methods	Chemicals	Results	References
		with ionic and anionic detergents for decellularization		mol/L potassium chloride + 1.0 M potassium iodide	with detergent-free decellularization method, but, bio-functionally all methods responded equally	
Trachea	Rabbit	*In vivo* transplantation	Freeze-drying, detergent and sonication	1% SDS	Exhibition of necrosis and animal death in 7-24 days and integration of decellularized scaffold into the host structure was observed	[84]
Spleen	Rat	Recellularization of bone marrow mesenchymal stem cells (BMSCs)	Freeze-thaw cycles and perfusion decellularizatio n	0.1% trypsin, 0.05% EDTA, 3% Triton X-100	Differentiation of BMSCs into functional hepatocyte-like cells	[85]
		Culture of rat hepatocytes	Perfusion decellularizat-ion	0.1% SDS	Survival and secretion of urea and albumin for 10 days in culture	[86]

Organ or tissue	Species	Applications	Methods	Chemicals	Results	References
Pancreas	Mouse	Recellularization of MIN-6 cells and AR42J	Perfusion decellularizat-ion	0.5% SDS	Upregulation of insulin gene *in vitro*, less immune reaction and angiogenesis after 14 days *in vivo*	[42]
		Recellularization of MIN-6 cells and *in vivo* implantation	Freeze-thaw at -80^{0}C for one day followed by perfusion decellularizat-ion	1% Triton X-100 + 0.1% ammonium hydroxide	Biocompatibility and angiogenesis induction	[44]
	Rat	Comparison of three perfusion routes for decellularization and recellularization of islets	Perfusion decellularizat-ion	1% Triton X-100 + 0.5% SDS	Reach of islets into parenchymal space of the pancreas after infusion through ductal system	[45]

BMSCs: bone marrow mesenchymal stem cells; ECM: extracellular matrix; GAG: glycosaminoglycans;

PBS: phosphate-buffered saline; SDS: sodium dodecyl sulfate

2.4 Chemicals used for decellularization

Any decellularizing procedure involves disruption of the ECM. The selection of decellularizing agents causing the least possible damage to the ECM is vital. The choice of decellularizing agents depends on the nature of the tissue or organ. A decellularization operation involves notable changes in the tissue and organ color, starting from its original color to become translucent. The process consists in removing cellular components and nuclear materials. Destruction of the cell membrane, dissolution of cellular components and removal of nucleic acid materials are the key steps.

Alkalis and acids dissolve cellular components and wash nucleic acids [87]. Detergents solubilize cell membranes and remove cellular components and nucleic acids [88].

Detergents are soluble amphiphiles, which can solubilize biological membranes. They have both hydrophilic and hydrophobic groups with a more hydrophilic nature than biological membranes. They can be classified according to their charges: non-ionic, anionic, cationic and zwitterionic detergents [89, 90]. Triton X-100, a non-ionic detergent, is commonly used for cell lysis and permeabilization [91, 92]. The hydrogen bonds in lipid bilayers are disrupted by the polar head group of Triton X-100, breaking the cell plasma membrane [89]. In some studies, Triton X-100 has been reported to be the best decellularizing agent compared to other detergents and that for many tissues and organs including ligaments, small intestine, annulus fibrosus, liver and aortic valves [49, 93-96]. On the other hand, some studies demonstrated that Triton X-100 had poor cell removal capacity for many tissues and organs such as veins, cornea, urethra, heart and kidneys [25, 97-100].

Another detergent commonly used in decellularization protocols is sodium dodecyl sulfate (SDS). SDS is an anionic detergent, used mainly in commercial applications such as in cleaning and in the making of cosmetics. SDS is also well known in biochemistry for its use in the SDS-PAGE technique. Its application in decellularization can be counterintuitive when aiming to preserve the tissue or organ ECM structure intact, as SDS is known to denature proteins [101]. SDS solubilizes membrane proteins and thus helps effectively in the decellularization process. SDS incorporates into the outer membrane layer by increasing its curvature, creating a stress which results in membrane disruption [102]. SDS proved to be superior when compared to other

detergents in removing cells and genetic materials in many tissues and organs including aorta, veins, heart, kidneys and urethra [25, 97, 99, 100, 103]. Triton X-100 and SDS have also shown negative influence on tissues and organs used for decellularization but, on the other hand, when these two detergents were used in combination, the mixture allowed efficient decellularization and preservation of ECM structures and this has been tested on tendons, kidneys, small intestinal submucosa and liver [18, 50, 104, 105].

Another ionic detergent/bile salt frequently used in decellularization is sodium deoxycholate (SDC). After adhering to the membrane, SDC incorporates its cholate moiety into the lipid membrane, resulting in pore formation and membrane disruption [106]. SDC, alone or in combination with other detergents, has shown to be effective in removing cells while retaining ECM structures in decellularized tissues [23, 107].

CHAPS, 3-[(3-cholamidopropyl)dimethylammonio]-1-propanesulfonate hydrate, is another detergent used in decellularization. CHAPS is a zwitterionic detergent with a hydrophilic side and a hydrophobic back. CHAPS does not result in pore formation; instead, the molecules seem to directly break the lipid membrane [108]. CHAPS has proven to be milder and to have greater ability to retain mechanical strength in lungs [34, 37, 109].

Other chemicals applied in decellularization protocols are acids and bases. Both acids and bases had a negative impact on the ECM mechanical strength [110]. Acetic acid-treated bovine pericardia had reduced tensile strength but, on the other hand, it supported the growth of human mesenchymal stem cells and, hence, proved to be biocompatible [111]. Peracetic acid along with ethanol was used to sterilize decellularized scaffold materials, a well-known and FDA-approved method for medical devices [13]. However, the use of peracetic acid for decellularization resulted in incomplete cell removal from tumor ECM, porcine liver and kidneys [112, 113]. Decellularization of skin using NaOH had a cytotoxic effect on fibroblasts, however, prolonged washing of the scaffold helped in decreasing this cytotoxic effect [114]. Alcohols or acetone solutions can be used in the pre-treatment of tissues for lipid removal. It is easier to lyse and remove cells after eliminating lipid contents [115]. Acetone/alcohol combinations had a negative effect on tissue dehydration and greater influence on modifying mechanical properties and morphology of temporomandibular joint from pig jaws, as compared to SDS-treated tissues [116].

Along with chemicals, the use of enzymes in decellularizing techniques can be advantageous. It is not possible to decellularize tissues or organs only with enzymes. However, enzymes are involved in the removal of cell debris. The most commonly used enzymes are trypsin, nucleases, collagenase, thermolysin, α-galactosidase and dispase [110, 117].

2.5 Rationale for using extracellular matrix (ECM)-based products

ECM proteins have shown positive influence on cell growth, function and differentiation and examples of biomimetic surfaces have been reviewed by us [118].

An important class of ECM-derived proteins is that of collagens, as reviewed elsewhere [119]. Collagen is in fact an abundant source of ECM proteins. For example, collagen microspheres can differentiate oligodendrocyte progenitors into oligodendrocytes and collagen-immobilized nanowires had a positive influence on human microvascular endothelial cells [120, 121]. Fibronectin and laminin showed numerous positive effects on cell survival and functions both *in vitro* and *in vivo* [122, 123]. In the past years, our group has verified the positive effects of various ECM peptides and proteins. For example, immobilization of fibronectin, fibrinogen and fibrin on polymer surfaces enhanced the proliferation of smooth muscle cells [124]. Also, embedding pancreatic islets and endothelial cells in fibrin showed increased insulin secretion and preservation of islet integrity [125]. Culturing young porcine islets in fibrin exhibited the protective nature of fibrin towards hydrogen peroxide [126].

In addition to whole ECM proteins, functional peptides derived from the ECM can influence cell behaviour [127-130]. Peptide motifs from collagen I (GTPGPQGIAGQRGVV), collagen IV (MNYYSNS), fibronectin (PHSRN) and laminin (YIGSR) can enhance cell attachment [131, 132]. Arginine-glycine-aspartic acid (RGD), a peptide sequence found in fibronectin, vitronectin, laminin, collagen types I and IV, has a high affinity for integrin-mediated cell attachment and spreading, functionality and tissue development [133-137]. The RGD sequence co-immobilized with the SVVYGLR sequence was used to enhance the adhesion of endothelial cells[130]. Three ECM-derived peptides, laminin (IKLLI and PDSGR) and cadherin (HAVDI) supported the adhesion and survival of insulin-containing cultures for 5 days [129]. Rat insulinoma INS-1 cells cultured on immobilized ECM proteins and peptides (RGD &

CDPGYIGSR) showed higher glucose-stimulated insulin secretion compared to surfaces bearing no peptides [127].

Hyaluronic acid, a polysaccharide, helped in neuron survival and controlled self-renewal and differentiation of human embryonic stem cells [138, 139]. Many studies demonstrated that proteoglycans from the ECM are involved in molecular events of cell adhesion, proliferation and migration [140].

These are just examples of the effects ECM components can have on cells allowing for appreciating the potential impact of bioproducts made from decellularized tissues and organs. As reviewed by us and others, [118], [141] [142], other ECM proteins have been applied to produce biomimetic materials and surfaces and these include: collagen types I, III and IV, gelatin, fibronectin, vitronectin, polysaccharide nanofibers, proteoglycans, nidogen and laminins, as well as ECM-mimicking peptides including YIGSR,RGD, DGEA, KRSR, IKVAV, P15, and GFOGER, to list a few.

Furthermore, following their implantation, decellularized scaffolds are repopulated by host cells and are even degraded, resulting in a functional tissue containing site-specific cells [143]. Decellularized tissues or organs, with or with no cells, can chemo-attract progenitor cells towards the implantation site [144, 145]. The degrading ECM molecules are also involved in various biological activities and growth factor signaling [146, 147]. Therefore, these matrices made from decellularized tissues and organs act as bioactive scaffolds by modifying the host environment to create a more suitable solution for healing, repair and even regeneration.

ECM scaffolds made from decellularized tissues and organs also provide mechanical support in many conditions. They possess different physical characteristics, which are often difficult to reproduce with synthetic materials [148]. The ECM provides a mechanical support for the recellularizing cells to attach to the matrix. It is very important for scaffolds made from decellularized tissues and organs to have certain mechanical properties matching the site of implantation of the tissue or organ to be substituted. Creating less damage to the tissue during decellularization could yield better mechanical properties and more intact vasculature structure, facilitating the induction of angiogenesis post-implantation [44]. Also, the presence of ECM proteins and functional peptides in 3D scaffolds allows for recreating environments more physiological for cell culture, as opposed to traditional 2D cultures on flat surfaces.

2.6 Immunogenicity of ECM-based scaffolds

Most decellularization protocols involve removing cell materials, which could cause major immunogenic reactions: hyperacute rejection, acute immune rejection, chronic immune rejection, and inflammatory reactions. Hyperacute rejection is a severe reaction of vascularized xenografts, triggered a few minutes to a few hours after implantation [149, 150]. This hyperacute rejection is mainly caused by the α-Gal epitope (galactose-α(1,3)-galactose) expressed on many cell surfaces and is less common in human and old-world monkeys. Pigs have been modified genetically to remove the Gal epitope to avoid xenograft rejections, but the application of this method is resulting into an acute immune rejection by non-Gal antibodies circulating at low levels, a few days to a few weeks after implantation [151]. Chronic immune rejection is associated with allograft transplantation by introducing donor-specific antibodies [152]. Also, the presence of DNA in decellularized tissues and organs can potentially cause inflammatory reactions [153].

Collagens with lower immunogenicity is achieved by removing N-and C- terminal telopeptides by pepsin type-I treatment, which are referred to as atelocollagen [154]. Atelocollagens have been clinically applied in wound healing and as bone substitutes [154].

Host response towards bioproducts made from ECM materials are different and are based on the product's properties, species and methods of preparation; five different commercially available products were tested on rats and resulted in distinct morphological appearance of the implantation site[155]. Similarly, the immune reaction from the decellularized heart tissue (SynerGraft®) had a mixed reaction after implantation. In one study [156], SynerGraft® exhibited much less HLA (human leukocyte antigen) class I and II antibodies, as claimed by the company; however, in another study [117], macrophage infiltration after implantation was observed into the tissue decellularized using the SynerGraft® process [149]. In addition to that, porcine small intestinal submucosa had both positive and negative inflammatory responses when implanted into rodents [157-159].

Another important factor to be studied in detail is the response of host innate and adaptive immune response towards implanted xenograft materials. The polarization of T helper cells 1 (Th1) and macrophages (M1) results in a pro-inflammatory response and T helper cells 2 (Th2)

and macrophages (M2) are involved in the anti-inflammatory response, which leads to constructive tissue remodelling[160].

Many studies have different conclusions on host-decellularized tissues/organs interactions and responses. Therefore, a detailed scientific understanding of the outcomes following decellularized product implantation including the responses of host tissues towards the implanted decellularized materials is vital [161].

2.7 Applications, status and perspective of decellularized tissues and organs

Engineered substitutes could be a possible cure for patients in the last stage of tissue or organ failure. The increase demand for tissues and organs for transplantation and the encountered immune rejection of xenograft transplantations have pushed researchers to find alternative tissue and organ sources.

Decellularized tissues and organs have a great potential to serve as carriers for transplanting autologous tissue made from the host cells or site-specific functional cells. Regardless of the availability of genetically engineered animals to harvest tissues or organs for transplantation, the rejection of the transplanted graft by the host appears inevitable [162]. This situation can potentially be solved with scaffolds and other bioproducts made from decellularized tissues and organs since antigenic elements of cell components are supposed to be completely removed. Recent advances involving recellularization of human-induced pluripotent stem cells in decellularized scaffolds could be a way to avoid the intake of immunosuppressive drugs required after organ transplantation [40, 163].

Achieving a functional tissue or organ is the goal of any decellularized scaffolds carrying either functional cells or stem cells. Failure of re-endothelialization of the organ with functional endothelium is one of the main reasons for organ loss in transplantation and a major hindrance in developing functional decellularized scaffolds. However, many studies have shown promising results on re-endothelialization and these could be considered as a potential solution to solve re-endothelialization problems [164, 165].

Materials and scaffolds made from decellularized tissues and organs have been commercially available for many applications. ECM-derived products from animal sources have been commercially available for more than 20 years and are applied in the treatment of many tissue regeneration processes and statistically, many years ago, over 200,000 patients have been implanted with xenogeneic decellularized scaffolds [166]. Many animal and human tissue-derived decellularized commercial products like Oasis® (porcine small submucosa, Cook Biotech, Inc., Indiana, USA), GraftJacket® (human dermis, Acelity L.P. Inc., Texas, USA), DermACELL® (human dermis, Novadaq Technologies Inc., Mississauga, Canada), Alloderm® (human dermis, Allergan plc (NYSE: AGN, Dublin, Ireland)), NeoForm™ (human dermis, California, USA), Strattice™ (porcine dermis, Allergan plc (NYSE: AGN, Dublin, Ireland)), Restore™ (porcine small intestine (DePuy Orthopedics, Inc., Indiana, USA), Prima™ Plus (porcine heart valve, Edwards Life Sciences LLC, California,USA), AlloSkin™ AC (human dermis, AlloSource, Centennial, CO, USA), MatriStem® (mucosa of urinary bladder, ACell, Columbia, USA), Biodesign® (small intestine, COOK MEDICAL INC., Bloomington, IN, USA), Lyoplant® (pericardium, Aesculap, Inc., Center Valley, PA, USA)[167, 168].

Most of the biological scaffolds are marketed as surgical mesh devices [168]. Scaffolds made from decellularized tissues or organs have the potential to be marketed under the category of 510(K) of the FDA (Food and Drug Administration) [169]. Under 510(K) clearance, a company must register to notify (PreMarket Notification or PMN) the FDA 90 days in advance of marketing a medical device. The FDA would assess the notified device to make sure it falls under the already existing three classifications of devices in the market, for which a premarketing approval (PMA) is not required. The claim must be made by the company to support its device is substantially equivalent to the ones already available in the market. 510(K) devices can fall under 3 classes: class I, class II and class III, depending on the assurance of safety and effectiveness.

Table 2: Regulatory requirements for 510(k) devices [170].

Regulatory requirements	**Class I**	**Class II**	**Class III**
General controls	All general controls are complied with and provide reasonable assurance	General controls are insufficient to provide reasonable assurance	General controls are insufficient to provide reasonable assurance
Secondary controls	No further secondary controls are required	Information required to perform secondary controls are sufficient and hence secondary controls are performed for gaining reliable assurance of the device	Information required to perform secondary controls are insufficient and hence secondary controls cannot be performed for gaining reliable assurance of the device
Premarket notification/approval	Eligible directly for premarket notification	Eligible directly for premarket notification	Requires premarket approval prior to notification
Device/product risk	Low	Medium	High

Note: General controls refer to a comprehensive set of regulatory authorities to be complied for by any medical device to be marketed. Special controls are controls to be complied where general controls are insufficient.

Oasis®, MiroMesh® and PhotoFix® are a few examples of 510(K)-cleared commercially available bioproducts derived from decellularized tissues and organs [167, 171].

Decellularized tissues which are intended to be implanted or transplanted have the potential to be marketed under the category *Human Cells, Tissues, and Cellular and Tissue-Based Products*

(HCT/Ps) of the FDA. HCT/Ps are products regulated by two different divisions, namely, the *Center for Devices and Radiological Health (CDRH)* & the *Center for Biologics Evaluation and Research (CBER)*, or sometimes as a combination of both [172]. DermACELL® (a decellularized human dermis) and Allopatch HD® (an acellular human dermis) are examples of HCT/Ps products [167, 173]. Miromatrix Medical Inc. (Eden Prairie, Minneapolis), a USA-based biotechnology company founded in 2009, is involved in developing fully functional human organs by perfusion technology, primarily applied to the liver and, upon completion, extended to the kidneys. Miromesh™ and Miroderm™ (derived from porcine liver) are products launched by the company. AxoGen Inc. (Alachua, Florida) from the USA develops a technology to regenerate peripheral nerve injuries. AxoGuard® is derived from pigs and is used as a nerve connector. Another USA-based company, Humacyte, Inc. (Morrisville, North Carolina), develops acellular grafts to repair vascular damages; some of their products are under Phase III clinical trials.

2.8 Conclusions

The selection of a technique or chemicals to decellularize a specific tissue or organ is an important decision to achieve complete decellularization and to retain intact the ECM. Perfusion decellularization has allowed fast and complete decellularization of many whole tissues and organs using either SDS or Triton X-100. Many whole organs have been successfully decellularized and subsequently seeded with different cell types. Recent advances in recellularizing decellularized tissues and organs involve the use of induced pluripotent stem cells to attain the native function of the tissue. Decellularized tissues or organs offer both mechanical support and cues from the ECM for cell growth and function *in vivo.* Many bioproducts derived from decellularized tissues and organs are commercially available, along with that, regenerative medicine companies are working to market functional whole organs to meet the demand. Extracting purified proteins from ECM or synthesizing new motifs are costly affairs compared to decellularizing a tissue, therefore, decellularized tissues and organs could be a potential source of substitutes for transplantation, provided they are devoid of cellular components, maintain the necessary functionality and are less immunogenic.

2.9 Acknowledgements

This research project was supported by the Université de Sherbrooke and NSERC through a Discovery Grant awarded to Patrick Vermette (Grant # 250296-2012).

Chapter 3

Decellularized pancreas as a native extracellular matrix scaffold for pancreatic islet seeding and culture

Foreword

Authors and Affiliations:

Rajesh Guruswamy Damodaran: Ph.D. Candidate, Université de Sherbrooke, Département de génie chimique et de génie biotechnologique.

Patrick Vermette: Professor, ingénieur, Université de Sherbrooke, Département de génie chimique et de génie biotechnologique.

Date of Submission: July 1st, 2017

State of Acceptance: Published

Journal: Journal of Tissue Engineering and Regenerative Medicine

Contribution:

This article constitutes an experimental study of this thesis. The content of this work is published in *Journal of Tissue Engineering and Regenerative Medicine*. All experimental work was performed by Rajesh Guruswamy Damodaran. All data were analysed by Rajesh Guruswamy Damodaran and Patrick Vermette. The article was written by Rajesh Guruswamy Damodaran. All work was performed under the direction and supervision of Patrick Vermette.

Titre en français :

Pancréas décellularisé comme support naturel pour les îlots

Résumé

Le diabète se caractérise par une perte de fonction ou du nombre de cellules productrices d'insuline, les cellules-β, dans les îlots pancréatiques. La transplantation d'îlots est une des thérapies étudiées comme traitement du diabète, et des développements dans les méthodes d'ingénierie tissulaire peuvent améliorer la survie et la fonctionnalité des îlots transplantés. La transplantation des îlots les soumet à l'anoïkis, à l'hypoxie et aux attaques du système immunitaire, ce qui les fragilise et peut conduire à la destruction du greffon. Les avancées récentes en ingénierie tissulaire permettent d'utiliser des organes décellularisés comme supports aux cellules greffées. Le pancréas décellularisé pourrait être un bon support pour la transplantation d'îlots dans la mesure où l'on peut conserver correctement sa matrice extracellulaire (MEC) et son système vasculaire. Pour cette étude, le pancréas de souris a été décellularisé par perfusion d'une solution de 0,5% de dodecyl sulfate de sodium (SDS). Avec différentes techniques de caractérisation, nous montrons que le pancréas perd l'intégralité de ses cellules mais conserve une part importante de sa MEC. Des îlots isolés sont injectés dans le pancréas décellularisé via le canal collecteur et la fonctionnalité des îlots est confirmée par réponse à la stimulation au glucose (GSIS) après 48h. La re-cellularisation du pancréas par des cellules INS-1 exprimant la GFP montre que ce support est biocompatible et non-toxique après 120 jours. Ces données suggèrent que le pancréas décellularisé ensemencé par des cellules endocrines pourrait devenir un organe bioartificiel potentiellement utilizable dans le traitement du diabète.

Mots clés : matrice extracellulaire; biomatériaux; pancréas décellularisé; fonction des îlots pancréatiques; pancréas bio-artificiel; cellules INS-1 marquées au GFP

Abstract

Diabetes Mellitus involves the loss of function and/or absolute numbers of insulin-producing β-cells in pancreatic islets. Islet transplantation is currently being investigated as a potential cure, and advances in tissue engineering methods can be used to improve pancreatic islets survival and functionality. Transplanted islets experience anoikis, hypoxia and inflammation-mediated immune response, leading to early damage and subsequent failure of the graft. Recent development in tissue engineering enables the use of decellularized organs as scaffolds for cell therapies. Decellularized pancreas could be a suitable scaffold as it can retain the native extracellular matrix (ECM) and vasculature. In this study, mouse pancreata were decellularized by perfusion using 0.5% sodium dodecyl sulphate (SDS). Different characterizations revealed that the resulting matrix was free of cells and retained part of the pancreas ECM including the vasculature and its internal elastic basal lamina, the ducts with their basal membrane as well as the glycosaminoglycan and collagen structures. Islets were infused into the ductal system of decellularized pancreata and glucose-stimulated insulin secretion (GSIS) results confirmed their functionality after 48h. Also, re-cellularizing the decellularized pancreas with GFP-tagged INS-1 cells and culturing the system over 120 days confirmed the biocompatibility and non-toxic nature of the scaffold. GFP-tagged INS-1 cells formed pseudo-islets which were, over time, budding out of the decellularized pancreata. Decellularized pancreatic scaffolds seeded with endocrine pancreatic tissue could be a potential bioengineered organ for transplantation.

Keywords: extracellular matrix (ECM) scaffolds; pancreas decellularization; pancreatic islets functionality; bioartificial pancreas; GFP-tagged INS-1 cells; cell and islet seeding

3.1 Introduction

Type-1 diabetes is caused by the autoimmune destruction of insulin-producing β cells of the pancreas [2]. These cells then can no longer produce insulin in response to glucose. Hence the patient depends completely on an exogenous supply of insulin to normalize the circulating blood glucose levels for long-term survival. A possible cure for type-1 diabetes came in 1966, when the first transplantation of a whole pancreas was successfully performed [174]. Akin to other major organ transplantation, whole pancreas transplantation continues to have morbid risks including surgical complications, post-op infection, technical failures, donor obesity which all influence the success and long-term graft survival [4]. The recipient also requires lifelong immunosuppressant drug administration. Given this, transplanting islets of Langerhans offers a less invasive, lower risk, alternative cure for type-1 diabetes. It reduces the overall post-surgical complications and improves the clinical outcome of the patient using immunosuppressant drugs [5, 6].

Over 1500 islet transplantation procedures have been carried out worldwide since 2000, but only approximately 7.5% of the transplanted patients remain insulin independent 5 years following transplantation [175, 176]. Current transplantation procedures involve the infusion of islets into the liver portal vein [177]. The major disadvantages of intraportal islet infusion are bleeding and thrombosis, while other factors like anoikis, hypoxia and inflammation-mediated immune response also result in impairment of islet function and graft loss [178-184].

Encapsulating islets could be a possible solution to protect the transplanted islets. The two main aims of encapsulating islets are to protect islets from the host immune response and to allow diffusion of molecules such as oxygen, nutrients, glucose, insulin and waste metabolites. Current research focuses majorly on two materials for encapsulation, namely, alginate and fibrin [185-187]. The requirement to use poly-lysine to stabilise alginate gels results in decreased graft function *in vivo* [188]. Also, the use of high fibrinogen and thrombin concentrations to prepare fibrin gels has a negative impact on pancreatic islets [189]. Therefore, there is still a need to find suitable materials for encapsulation, which would more closely mimic the native environment of the pancreas and trigger acceptable and desirable host immune response.

The pancreas extracellular matrix (ECM) has a big impact on islet biology apart from its physical structural support. The ECM mediates signalling for islets and β-cells survival, function, differentiation, proliferation and migration [190-194]. Scaffolds can be successfully obtained

following decellularization of organs and tissues [39, 63, 195-197]. A previous study on pancreatic scaffolds shows promising results in production and recellularization of a decellularized pancreatic tissue [42]. Encapsulating islets with ECM proteins has shown enhanced function of islets [198]. Implantation of cell-free decellularized pancreas proved to be a biocompatible scaffold by triggering angiogenesis *in vivo* after 14 days [44]. Therefore, we hypothesized that a decellularized pancreas, as scaffold to culture pancreatic islets, would create a favourable microenvironment for islet viability and functionality by preserving at least, part of the native pancreatic ECM.

In this study, mouse pancreata were decellularized using 0.5% sodium dodecyl sulfate (SDS) infused through the ductal system. Separately, green fluorescent protein (GFP)-tagged INS-1 cells and pancreatic islets were perfused into the decellularized pancreas. Histological and immunohistochemical characterization, glucose-stimulated insulin secretion (GSIS) as well as scanning electron microscopy (SEM) and microscopic observations were performed to study *in vitro* the nature of the decellularized tissue and its influence on GFP-transfected cells and islets.

3.2 Materials and methods

3.2.1 Pancreas decellularization

Mice (CD-1® IGS, Charles River, Boston, MA, USA) were sacrificed under a CO_2 atmosphere, as approved by the Université de Sherbrooke's ethical committee (protocol no. 367-14). A total of 28 pancreata were used in this study. The full experimental procedure of the pancreas decellularization is presented in Figure 1 and as a supplemental video (Supplemental Video 1). The pancreas was injected with phosphate buffer saline (PBS) (BP6651, Fisher Scientific) through the pancreatic duct at the duodenal end using a 26-gauge needle. Reaching all sections of the pancreas using the needle during perfusion helps in obtaining a complete decellularization. Once the buffer reaches the entire pancreas, the needle was clamped along with the pancreas using a hemostat. The entire pancreas was mounted on a circulation system and the decellularization was achieved with a modified protocol which is described elsewhere [42]. Briefly, the pancreas was continuously perfused with 0.5% sterile SDS (616-0302, Biorad) using a Masterflex® L/S Easy-Load II peristaltic pump at the flowrate of 8 mL min^{-1} for 12 h, then washed with sterile Milli-Q water for 15 minutes, followed by perfusing Milli-Q water containing benzonase (90 U mL^{-1})

(E1014, Sigma-Aldrich) for 15 minutes. The final wash was performed again with Milli-Q water for 15 minutes. Then, perfusion continued with PBS containing 10% FBS and a penicillin/streptomycin mix (10 000 U mL^{-1}) (15140-122, Life Technologies) for 24 h followed by a final perfusion of Dulbecco Modified Eagle Medium (DMEM, D5523, low-glucose, Sigma-Aldrich) containing 10% FBS and the penicillin/streptomycin mix for 36 h.

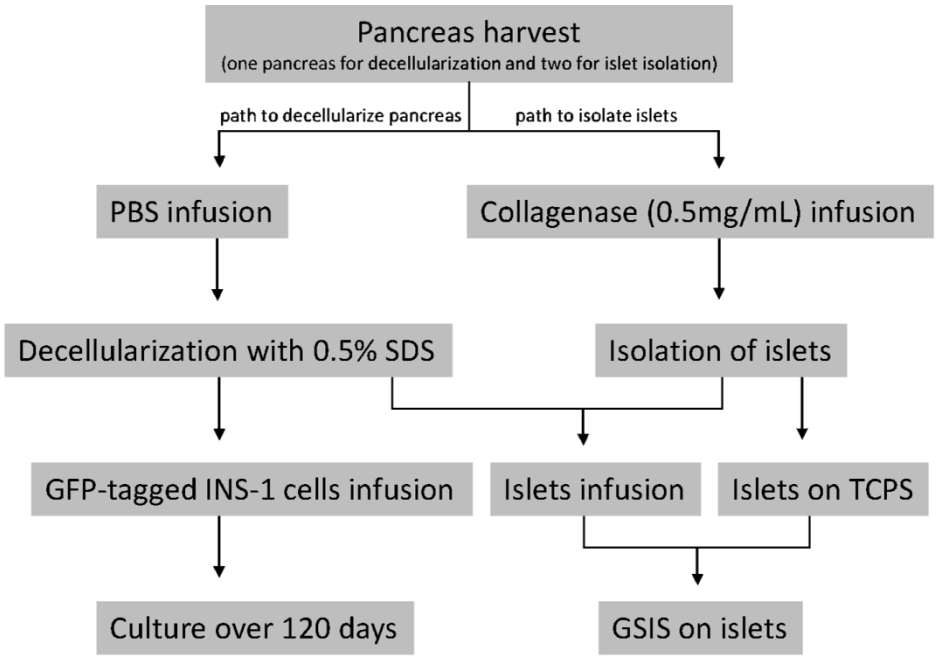

Figure 1 Experimental procedures for pancreas harvesting and decellularization including cells and islets infusion as well as scaffold and cells/islets characterization. One full pancreas is used for decellularization and two for islet isolation

3.2.2 Histological and immunohistochemical analyses

The decellularized pancreata, with and without pancreatic islets, were fixed with 4% paraformaldehyde (PFA) (P6148, Sigma-Aldrich) overnight and processed in a tissue processor (Thermo Fisher Scientific, Shandon Citadel 1000). A standard procedure was followed for paraffin embedding and tissue sectioning [194]. The paraffin-embedded tissues were sliced to a 4-µm thickness and sections were stained with hematoxylin and eosin (H&E), alcian blue and nuclear

fast red. For immunohistochemistry, sections were deparaffinized and hydrated. Blocking was done using a blocking buffer (X0909, Dako) for 30 minutes at 37^0C and then incubated with monoclonal antibody (ab9569, Abcam) for overnight at 4^0C. Then, the sections were incubated with a secondary antibody (A11001, Abcam) for 1 h at room temperature and counterstained with 4,6-diamidino-2-phenylindole, dihydrochloride (DAPI, D1306, Invitrogen). Sections were viewed and imaged under an epifluorescence microscope (Nikon Eclipse TE2000).

3.2.3 Decellularized pancreas microstructure analysis by scanning electron microscopy (SEM)

Samples were freeze-fractured and fixed with 2.5% glutaraldehyde in PBS (pH 7). After two washes with PBS (pH 7), the samples were fixed with 1% osmium tetroxide, then rinsed twice with distilled water. Dehydration was done with successive ethanol treatments prior to critical-point drying with liquid carbon dioxide. The samples were mounted on stub and metal coated with gold/palladium and viewed via a Hitachi S-3000N scanning electron microscopy (SEM).

3.2.4 Decellularized pancreas permeability by dye infusion

Undiluted food colorant (propylene glycol & propylparaben) was added to the pre-clamped needle on a completely decellularized pancreas. The dye-containing solution was infused into the pancreatic duct by gravity. The entire process of dye infusion was video-recorded.

3.2.5 Mouse islet isolation and islets infusion into decellularized pancreata

Mice were sacrificed as mentioned earlier. The pancreas was infused through the duct with dissociation medium reconstituted with 2.5 mg mL^{-1} of collagenase (C9263, Sigma-Aldrich). The dissociation medium comprises L15 medium (L-4386, Sigma-Aldrich), 15mM HEPES, 10mM nicotinamide, 1 mg mL^{-1} glucose, 2% FBS, 0.35 mg mL^{-1} $NaHCO_3$ and a penicillin/streptomycin mix. Then, the pancreas was removed and transferred into 15mL centrifuge tubes containing the same ice-cold mixture and incubated at 37ºC in a water bath for 18±2 min with regular interval shaking. Ice-cold HBSS (H1387, Sigma-Aldrich) supplemented with 5% FBS, 10mM

nicotinamide, and 0.35 mg mL^{-1} $NaHCO_3$ was added to stop the collagenase action. To avoid crowding of tissues while handpicking islets, a portion of digested tissues was transferred to bacteriological Petri dishes and diluted with HBSS. Islets were then picked using a 10µL micropipette under an optical microscope (Carl Zeiss, SteREO Lumar, between 6.5x to 80x) and stored temporarily in dissociation medium without collagenase. The isolated islets were re-suspended in 250µL of islet medium, constituted with DMEM (D5523, low-glucose, Sigma-Aldrich):RPMI (1:1), 5% FBS, 10mM nicotinamide, 15mM HEPES, and the same penicillin/streptomycin mix. Islets were injected very slowly into the decellularized pancreas using a 3mL syringe, which was connected with the 26g needle pre-clamped on the pancreas. Decellularized pancreata infused with islets were cultured in 12-well plates with islet medium for 48 h. The percentage of islet retention inside the decellularized pancreas was calculated by subtracting the escaped islets from the initial number of islets infused.

3.2.6 Glucose-stimulated insulin secretion (GSIS)

GSIS assays were performed on decellularized pancreata containing islets and on islets in traditional tissue culture polystyrene (TCPS) plates. Samples were pre-incubated in 2.8mM glucose for 1h and then sequentially in: 1) 2.8mM, 2) 20mM, 3) 20mM + 50µM 3-isobutyl-1-methylxanthine (IBMX, I5879, Sigma-Aldrich) and 4) 2.8mM, at 37°C and 5% CO_2, in Krebs buffer made with 25mM HEPES, 115mM NaCl, 24mM $NaHCO_3$, 5mM KCl, 1mM $MgCl_2$ and 0.1 % (w/v) bovine serum albumin. Insulin was measured after each incubation using a Mouse High Range Insulin ELISA (80-INSMSH-E01, Alpco). Since each decellularized pancreas contained a different number of islets, insulin concentrations were normalized to one islet. Performing GSIS on GFP-INS-1 cells-infused decellularized pancreata was not possible because of continuous formation and release of pseudo-islets from the matrix.

3.2.7 Seeding GFP-transfected INS-1 cells to assess cytocompatibility and cell distribution

Lentiviral transfected GFP-INS-1 cells were cultured with DMEM [199]. Cells were trypsinized and re-suspended in 250μL of medium and injected into the decellularized pancreas using a 3mL syringe connected to the 26g needle pre-clamped on the pancreas. This experiment was done mainly to investigate cytocompatibility and to determine how long the matrix can support cell growth, as well as to evaluate cell distribution within the matrix.

3.3 Results

3.3.1 Pancreas decellularization

The mouse pancreata were infused with 0.5% of SDS through the duodenal end of the ductal system. The complete process of decellularization takes ca. 12 h of perfusion. However, visible changes in color and size of the tissue can be observed from 2 h (Fig. 2). The infused solutions travel through the main duct and reach all parts of the pancreas. The total time taken for a dye to diffuse through the decellularized pancreas is approximately 7 min.

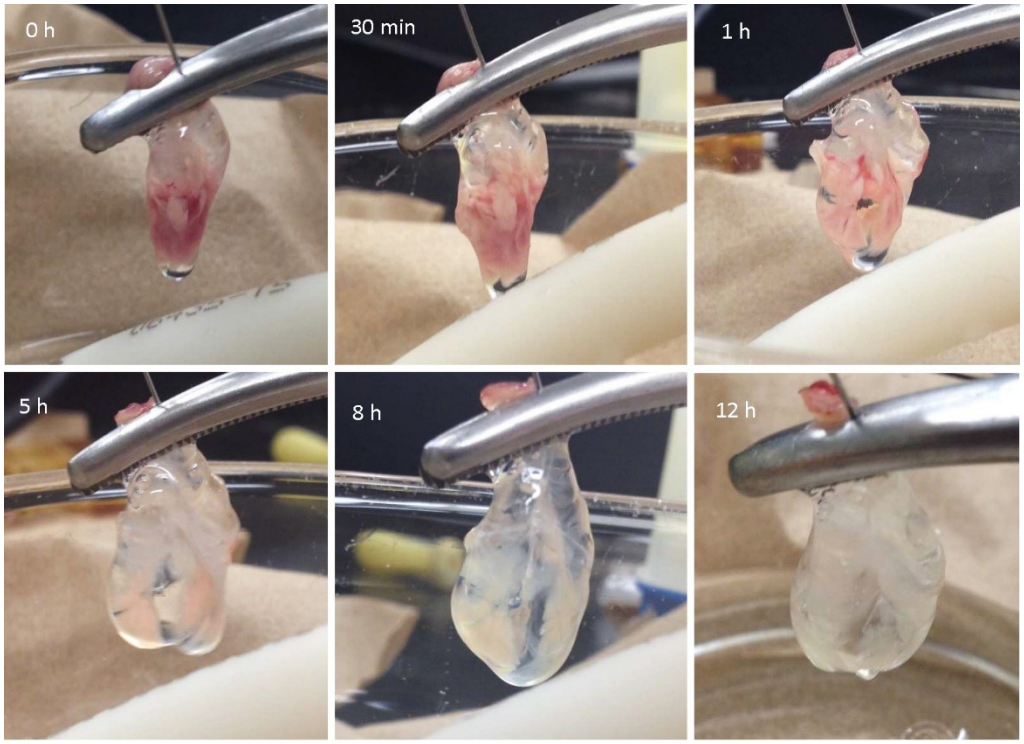

Figure 2 Pictures of the pancreas during decellularization over 12 hours.

The different existing techniques of decellularization includes physical methods such as agitation in suspension, freeze-thaw cycles, vascular perfusion, as well as ultrasonic and manual disruption [200]. Chemical methods involve the use of detergents, solvents as well as acid, alkali, and ionic solutions while biological treatments use enzymes [110, 200, 201]. The greatest challenges among the previously mentioned techniques are to achieve maximal removal of cell debris and to retain the ECM components with minimal damage. The use of perfusion techniques has an edge over other techniques by minimizing the diffusion distance to achieve maximal decellularization in the shortest possible time period [42, 201]. SDS, an anionic detergent, effectively solubilizes both nuclear and cytoplasmic cellular membranes and several studies confirmed SDS to be effective in achieving maximal cell extraction with limited damage to the extracellular matrix [42, 72, 100, 116, 202]. The use of SDS (0.5%) for the purpose of decellularization has been reported in commercially available allogenic dermal graft [203]. The use of benzonase (endonuclease) helps removing nucleic acids by cleaving the mid nucleotide sequences [204]. Many studies reveal that benzonase is very effective in removing more than 99% of the DNA content from scaffolds [42, 110, 205].

3.3.2 Characterization of decellularized pancreata

Hematoxylin/eosin (H&E) and alcian blue/nuclear fast red staining revealed that the decellularized pancreas was completely free of cells and of nuclear materials. Eosin-stained collagen and alcian blue-stained glycosaminoglycans (GAGs) can be depicted in Figures 3B and 3D. A previous study that uses a similar technique of decellularization on mouse pancreas had similar H&E staining of the resulting scaffolds [42]. The metrics to define decellularization is the lack of visible nuclear material in tissue sections stained with H&E [110].

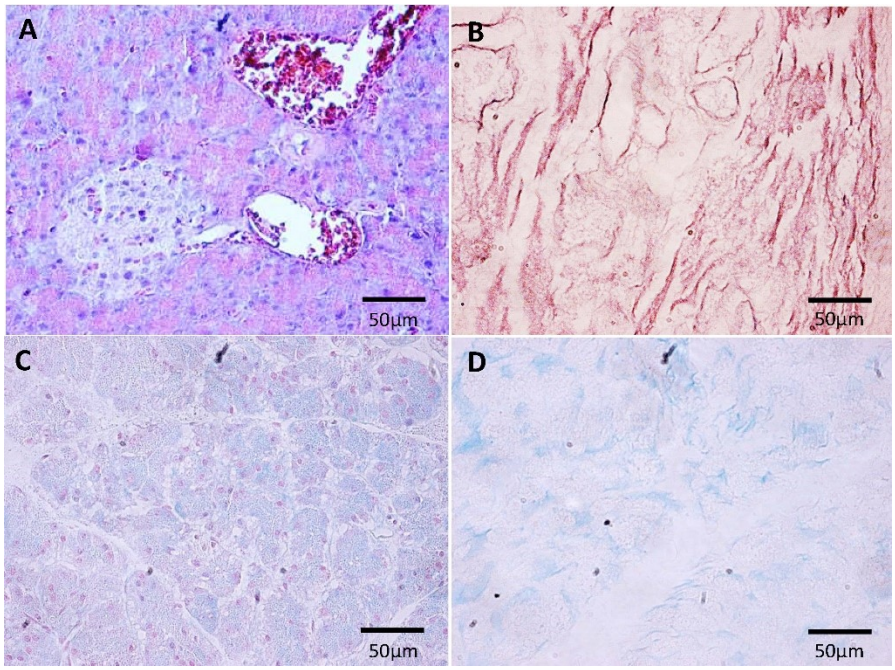

Figure 3 Hematoxylin/eosin (H&E) histological staining of (A) native pancreas and (B) decellularized pancreas. Alcian blue/nuclear fast red histological staining of (C) native pancreas and (D) decellularized pancreas.

SEM analysis of the scaffold revealed that the decellularized pancreata were free of cells leaving only spaces left empty by the solubilized cells (Fig. 4C). Since our technique involves injecting the solution through the ductal system for decellularization, the vasculature system was not disturbed and appeared to be intact. The vasculature retained the internal elastic basal lamina as substantiated by its scalloped appearance, which confirms that the process of decellularization

was not too harsh and allowed for maintaining some microstructural aspects of the pancreas ECM (Fig. 4D) [42]. Laminin-rich basal lamina of the vasculature is involved in Rac activity and is known to promote the sprouting of endothelial cells [44, 206]. It can then be hypothesised that the formation of new blood vessels after implantation can be enhanced by preserving the vasculature ECM intact. In our study, the decellularization process removed the layer of ductal cells from the ducts, as seen in intact ductal system (Fig. 4B), leaving ducts with a layer of basal membrane (Fig. 4E). SEM revealed that the 3D network of collagen fibers was retained from the decellularization, collagen being the most abundant protein of the pancreatic ECM (Fig. 4F) [207].

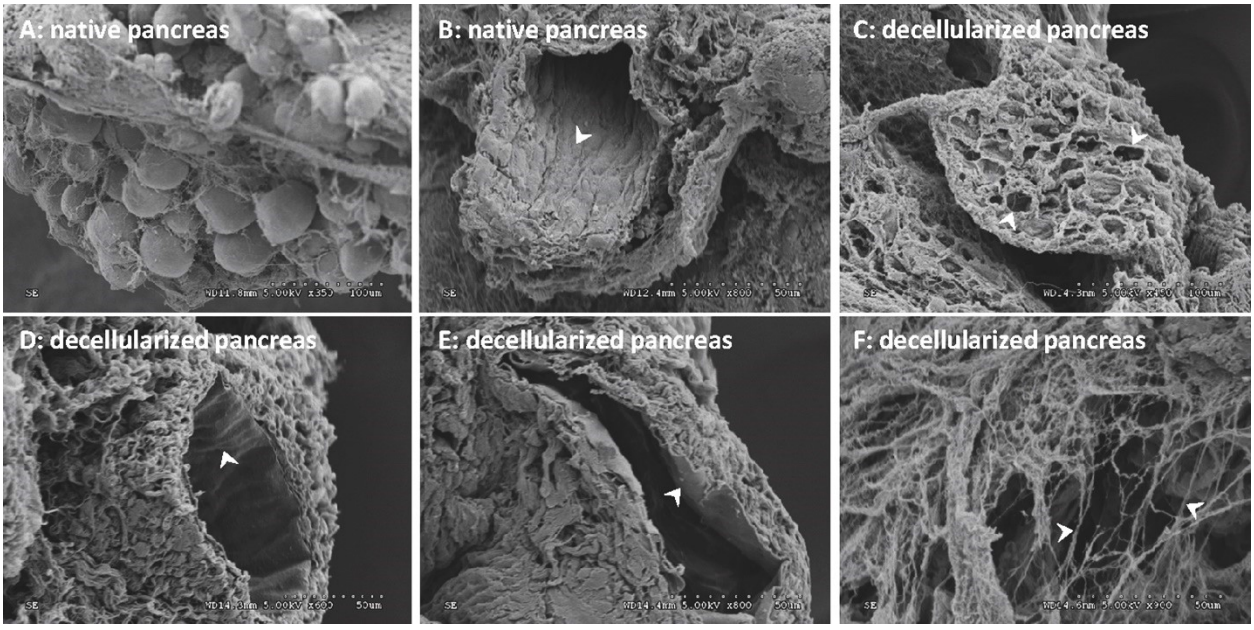

Figure 4 Comparison of native and decellularized pancreata by scanning electron microscopy (SEM). A) Clusters of pancreatic cells along with an ECM network. B) Intact duct with ductal cells (white arrow). C) Decellularized pancreas showing empty cellular spaces. D) Scalloped structure of inner wall of blood vessel. E) Basal lamina of decellularized ductal port. F) Structures showing collagen fibrils.

3.3.3 Localization of infused pancreatic islets within decellularized pancreata

The isolated islets were injected slowly into the main duct of the pancreas yielding a retention percentage of islets within the decellularized pancreas of approximately 70%. Immunohistochemistry analysis (Fig. 5B) revealed that the infused islets were not clumped together in the duct. Figure 5B also reveals that β-cells within the islets remain positive for insulin.

We believe that islets within the decellularized pancreas (Supplemental Fig. 1; Appendix A) were mainly located and attached to the ductal system. It has been reported in a previous study that some islets also move to the decellularized parenchymal matrix when they are infused through the ductal system [45]. Studies on pancreatic duct revealed the following information: i. the duct has close association with islets in adult rats, as most islets are connected to the ducts; ii. islet morphogenesis is influenced by ducts by budding out epithelial cells; and iii. ductal ECM contains laminin-1, fibronectin and collagen IV, which could improve β-cells survival [190, 208-210].

3.3.4 Functionality of pancreatic islets seeded within decellularized pancreata

GSIS results confirmed that the islets were functional after 48 h of culture in decellularized pancreata. When compared to islets maintained in tissue culture polystyrene (TCPS) plates, islets in decellularized pancreata responded to glucose and secreted more insulin (Fig. 5A). However, comparing islets cultured in TCPS plates to those in 3D scaffolds, such as in decellularized pancreata, is difficult since the diffusional barrier is potentially affecting the GSIS response in 3D matrices [211]. Islets or β-cells cultured with ECM molecules showed improved survival and GSIS, by activating NF-κB signaling and integrin matrix interactions [187, 212-215]. Previously, decellularized pancreata were re-cellularized with human amniotic fluid-derived stem cells and porcine islets [43], AR42J acinar cell line [42], MIN-6 β-like cells [42, 44], and rat islets [45]. In the particular study using porcine islets, the islets were seeded on decellularized pancreata and not within the organ. Also, islets functionality was not investigated [43]. An important finding from [45] is that the ductal system was the most efficient route for pancreas decellularization and subsequent islets infusion. But as the GSIS was carried out only immediately after infusing the islets into the decellularized matrix, the effect of the matrix on islets was not reported [45]. Although findings from those studies are of great importance, the use of decellularized pancreata to maintain islet functionality could not be confirmed.

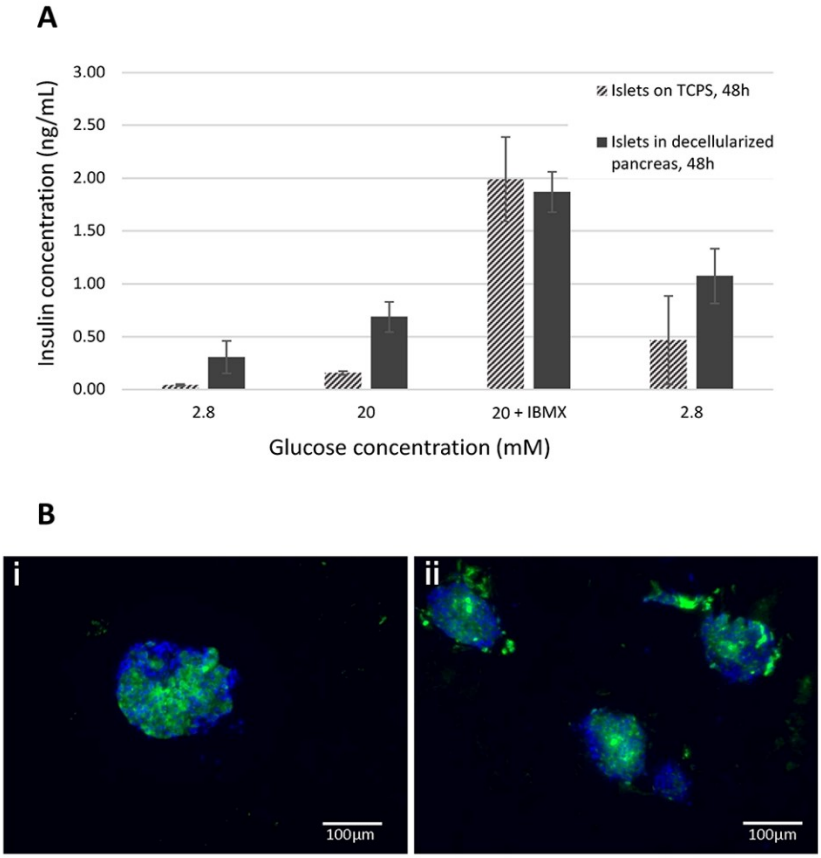

Figure 5 (5A) Glucose-stimulated insulin secretion (GSIS) assay on islets maintained in tissue culture polystyrene (TCPS) plates and cultured in decellularized pancreata for 48 h. Insulin concentration given per islet. (5B) Immunohistochemistry staining positive for insulin and DAPI, Green - Insulin and Blue - DAPI.

3.3.5 GFP-transfected INS-1 cells infused in decellularized pancreata

GFP-INS-1 cells infused in the decellularized pancreas were maintained in culture for up to 120 days, demonstrating that decellularized pancreata provide a cyto-compatible environment (Fig. 6). The metabolic activity of INS-1 cells and pancreatic islets were also determined (Supplemental Fig. 2; Appendix A). An observation was made during culture: individual cells formed pseudo-islets (see Fig. 6F). The pseudo-islets were budding out from the matrix during the culture. Such behaviour with beta-like cells has never been reported. Although INS-1 cells proliferation was not quantified, as it is not possible to reliably estimate cell numbers because of constant release of cells from the decellularized pancreas, microscopic observations revealed that cells were

proliferating and forming pseudo-islets. A similar observation was made with pancreatic acini cells; when cultured on basal lamina, the cells rearranged into 3D acini-like structures and retained their differentiated morphology [216].

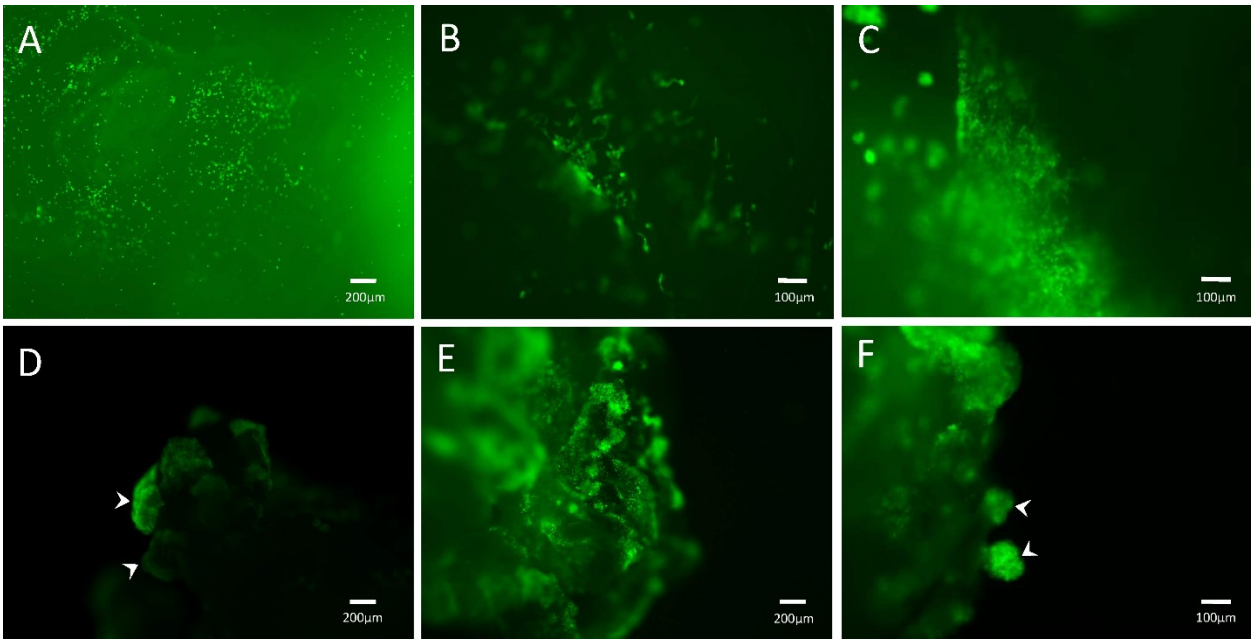

Figure 6 Green fluorescent protein (GFP)-transfected INS-1 cells (A) on a decellularized pancreas at Day 0. Cells were visible in the duct at (B) Day 3 and (C) Day 10. D) Cells at Day 60 forming pseudo-islets (indicated by white arrows). E) Cells at Day 120. F) Decellularized pancreas releasing pseudo-islets from the matrix (indicated by white arrows).

3.4 Conclusion

Decellularized pancreata can serve as a biocompatible scaffold to subsequently infuse pancreatic islets and are non-toxic and free of cellular components. They retain ECM and preserve inner vasculature structures. This study provided new insights on pancreas decellularization and its applications: 1. A new technique has been adapted to perform perfusion decellularization of whole pancreata and subsequent seeding of pancreatic cells and islets without the need to dismantle the organ from the perfusion system; 2. A GSIS analysis on infused islets after 48h of *in vitro* culture demonstrated for the first time that infused islets remain functional into decellularized pancreata; 3. Cytocompatibility has been shown with beta-like cells for 120 days *in vitro*, opening new windows of opportunity for stem cell culture and differentiation for longer period; 4. Beta-like

cells cultured in decellularized pancreata formed pseudo-islets and were budding out of the matrix; and 5. Decellularized pancreata could serve as an ECM scaffold "bag" to carry islets for transplantation. This study goes one step closer to *in vivo* testing, as this method could be an innovative approach in developing a bioartificial pancreas for transplantation.

3.5 Acknowledgements

We thank Jamie Sharp and Evan Dubiel for their technical support. We thank Parker Andersen for providing GFP-transfected INS-1 cells. We thank Charles Bertrand for his technical support on SEM. We thank Tim Spitters for his advice on MTT staining and technical support. This research project was supported by NSERC through a Discovery Grant awarded to Patrick Vermette (Grant # 250296-2012).

Chapter 4

Solubilisation of decellularized pancreata and immobilization on low-fouling surfaces for islet culture

Foreword

Authors and Affiliations:

Rajesh Guruswamy Damodaran: Ph.D. Candidate, Université de Sherbrooke, Département de génie chimique et de génie biotechnologique.

Evan A Dubiel, Ph.D. Université de Sherbrooke, Département de génie chimique et de génie biotechnologique.

Patrick Vermette: Professor, ingénieur, Université de Sherbrooke, Département de génie chimique et de génie biotechnologique.

Date of Submission: Dec 3rd, 2017

State of Acceptance: Under review

Journal: ACS Biomaterials Science & Engineering

Contribution:

This article is the second experimental work of this thesis. The content of this work was submitted to *ACS Biomaterials Science & Engineering*. All experimental work was performed by Rajesh Guruswamy Damodaran. Technical advice was given by Evan A Dubiel. All data analysis was performed by Rajesh Guruswamy Damodaran and Patrick Vermette. The article was written by Rajesh Guruswamy Damodaran. All work was performed under the direction and supervision of Patrick Vermette.

Titre en français :

Solubilisation de pancréas décellularisés et immobilisation sur des surfaces à faible encrassement pour la culture d'îlots pancréatiques

Résumé

La matrice extracellulaire (MEC) joue un rôle important dans la physiologie des îlots de Langerhans. Ainsi, l'étude d'îlots sans leur MEC native peut conduire à des erreurs d'interprétation de leur fonctionnement. Des surfaces biomimétiques ont été préparées à partir de molécules de la MEC de pancréas de souris décellularisés et de MEC solubilisée suivant trois méthodes distinctes (pepsine, acide acétique et NaOH). Ces trois méthodes ont permis une solubilisation allant de partielle à totale. Les extraits de pancréas décellularisés ont été greffés sur des surfaces à faible adhérence et mis en culture avec des îlots. Des cellules ont migré à l'extérieur des îlots sur toutes les surfaces sauf sur celles anti-adhérentes. Différentes morphologies de cellules ont été observées. Les îlots cultivés sur ces surfaces étaient viables et fonctionnels après 5 jours de culture, sauf pour les surfaces greffées avec les extraits solubilisés avec le NaOH qui montrèrent une certaine toxicité.

Abstract

Investigating islets without their native extracellular matrix (ECM) may lead to aberrant responses. Biomimetic surfaces were prepared from ECM of decellularized mouse pancreata solubilized using pepsin, acetic acid or NaOH. All three methods resulted in solubilisation. Decellularized pancreata were grafted on low-fouling surfaces to support mouse islets. Cell outgrowth from islets was observed on all surfaces except for low-fouling surfaces. Differences in cell morphology on biomimetics were noted. Islets were functional and viable after 5 days, except on NaOH-solubilized extracts, which exhibited some cytotoxicity. This study reports for the first time the solubilisation of a decellularized pancreas and its immobilization on low-fouling surfaces.

The extracellular matrix (ECM) plays an important role in islet biology. Losing the ECM during isolation of islets aimed for clinical transplantation results in rapid anoikis of islets (within 48h) [183]. The ECM is synthesised by the native cells, is mainly involved in mechanical support and provides cues for cell migration, attachment, differentiation and function [8, 9]. It is necessary to appreciate the importance of the ECM in islet behaviour to maintain these islets healthy. Considering the importance of the ECM and its role in islets viability and functionality, culturing islets on tissue culture polystyrene (TCPS) can result in false interpretations masking the islets responses towards the targeted treatment. Comparisons of results obtained with TCPS and surface-immobilized ECM proteins/peptides highlight the influence of the ECM on islets insulin secretion and viability [127, 129].

ECM proteins as well as ECM-derived peptides can have various positive effects on islets and beta cells. Culturing rat islets on fibronectin improved proliferation and prevented apoptosis [217, 218]. Laminin-derived (IKLLI and PDSGR) and cadherin-derived (HAVDI) peptides supported the adhesion and survival of dissociated pancreatic islets for 5 days [129]. The integrin-binding tripeptide RGD sequence found in type I collagen, laminin, fibronectin, vitronectin and fibrinogen improved the survival and function of rat insulinoma beta cells (INS-1 cells) *in vitro* [127]. Culturing human islets on ECM proteins like collagen (types I and IV), fibronectin, and laminin had a positive influence on cell attachment, insulin secretion and cell survival [219]. In addition, islets cultured in 3D fibrin gels are more functional *in vitro* and *in vivo* than in 2D [220].

The re-establishment of the lost pancreatic ECM environment can contribute to islets function and survival *in vitro*, a step closer to producing an *in vivo*-mimicking environment. A decellularized pancreas incorporates ALL of the individual proteins/peptides that make up the islet ECM. Decellularized pancreas immobilized on a surface thus more closely represents a true biomimetic interface in comparison to previous studies that analyze individual proteins/peptides. Also, studies on individual proteins/peptides have shown positive results, however, studies on combination of these proteins/peptides can be costly. Extracting the ECM from the pancreatic tissue would be of great interest to design biomimetic materials. Various studies involving solubilization of pancreatic ECM were performed, highlighting the importance of ECM in regenerative medicine [42, 221, 222].

In the present study, biomimetic surfaces were prepared from decellularized mouse pancreata solubilized by three methods: pepsin digestion, acetic acid and NaOH. Decellularized pancreatic extracts were grafted on low-fouling carboxymethyl-dextran (CMD) surfaces to limit non-specific interactions between the islets and the underlying TCPS surface. Pancreatic mouse islets were isolated and cultured on these biomimetic surfaces for 5 days. Cell attachment and morphology, cell viability and glucose-stimulated insulin secretion (GSIS) were investigated to screen the effects of the biomimetic surfaces on islets.

Complete pancreas decellularization was achieved, as described in the section 3.2.4, by perfusing 0.5% sodium dodecyl sulfate (SDS) through the duodenal end of the ductal system [223]. Perfusion decellularization with SDS through ductal system of the pancreas eliminates almost all cellular components [223]. Decellularized pancreata were frozen overnight at -80°C and freeze-dried for 48h. The freeze-dried samples were finely chopped into tiny pieces, before solubilisation. The samples (1 mg mL^{-1}) were solubilized using three methods: 1. pepsin digestion (1 mg mL^{-1} in 0.01M HCl at 37^0C for 48h), 2. 0.01M acetic acid for 48h at 37^0C under agitation at 60 rpm, and 3. 1M NaOH for 15 min at 60°C in a water bath. NaOH and acetic acid resulted in complete solubilisation of pancreata, while pepsin digestion resulted in partial solubilisation (Supplemental Fig. 3; Appendix A). Once solubilisation/digestion was completed, the sample pH was adjusted at around 5.5 and then immobilized on CMD surface to culture islets since the isoelectric point of unpurified collagen is approximately pH 5.8 [224]. The islet culture was performed at pH 7.

The protein content of the solubilised decellularized pancreata was estimated using a Bradford protein assay kit (protein assay kit, 500-0006, Bio-Rad), using the microassay procedure for microtiter plates and the absorbance was measured at 595nm [225]. Different methods of solubilization could yield different compositions of proteins [226, 227].

Protein content of the three extracts was estimated (Fig. 7). NaOH solubilisation yielded the highest protein/peptide content (ca. 1.2 mg mL^{-1} from a 10 mg mL^{-1} solution of decellularized pancreas), as compared to the acetic acid treatment and pepsin digestion.

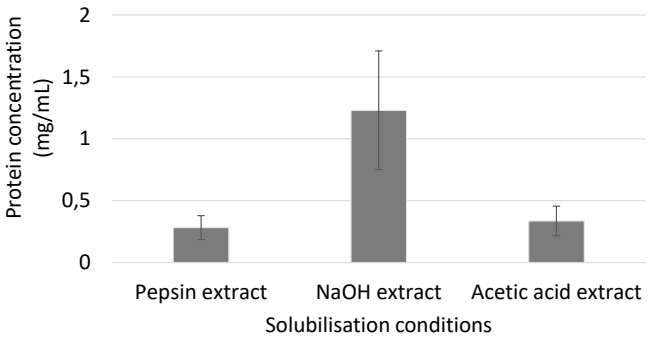

Figure 7. Protein content estimated by a Bradford protein assay of decellularized pancreata solubilised by pepsin, NaOH and acetic acid.

Synthesis of carboxylmethyl-dextran (CMD) has been described elsewhere [128]. 96-well tissue culture polystyrene (TCPS) plates were first modified by plasma polymerization of n-heptylamine to introduce functional amine groups [228]. CMD was grafted on the n-heptylamine-functionalized surfaces, as described elsewhere [130]. The CMD-grafted surfaces were rinsed with 1M NaCl twice at an interval of 12h and then followed by rinsing with Milli-Q water twice at an interval of 12h. After rinsing, the surfaces were sterilized under UV for 20 min and stored in Milli-Q water at 4°C until use. CMD surfaces have excellent low-fouling properties towards many cell types and proteins, allowing for better discrimination of the effects of the molecules of interest [127].

Surface-immobilization of solubilised pancreata was carried out by activating for 10 min the CMD surfaces with 200mM of 1-ethyl-3-(3-dimethylaminopropyl)carbodiimide (EDC)/N-hydroxysuccinimide (NHS) in sterile solutions and under agitation at room temperature. Activated CMD surfaces were then rinsed twice with sterile Milli-Q water [127, 229]. Solutions from decellularized pancreata (100 µL/well) containing 30µM of $CaCl_2$ [229] were added and plates were incubated for 3h at 37°C under agitation (70 rpm). After incubation, the surfaces were rinsed with sterile PBS and utilized immediately. All procedures for surface-immobilization were done under aseptic conditions.

Small pieces (ca. 1cm in radius) of tissue culture polystyrene (TCPS) from 6-well plates bearing the different layers were sent for X-ray photoelectron spectroscopy (XPS) analysis, as described elsewhere [128]. Three different spots on each surface were analysed.

All the surfaces were analysed by XPS (Table 3). Atomic ratios of the elements are determined from survey spectral analysis. There was an increase in nitrogen content of all biomimetic surfaces compared to CMD surfaces, the latter incubated in Milli-Q water at 4^0C for 2 weeks. Similarly, an increase in N/C ratios was seen for the biomimetic surfaces. It is difficult to confirm grafting of decellularized pancreatic extracts using XPS high-resolution spectra [128] (presented in Supplemental Fig. 4; Appendix A). There was no augmentation in the binding energy at 288-289 eV (peptide bonds) on all surfaces bearing ECM extracts when compared to CMD surfaces. The breakdown of proteins into small peptide fragments during solubilisation could be a possible reason for the unreliable XPS high resolution spectra detection, as previously reported [3,[128]]. Confirmation of surface-grafted peptides, given their small size, needs to be complemented by a cell test.

Table 3. X-ray photoelectron spectroscopy (XPS) atomic concentration (%) and atomic ratios of the different surfaces obtained from XPS survey spectra.

	Atomic concentration (%)			**Atomic ratio**		
	O 1s	**C 1s**	**N 1s**	**O/C**	**N/C**	**N/O**
n-heptylamine plasma polymer surfaces	1.37 (± 0.09)	90.52 (± 0.19)	8.06 (± 0.19)	0.01	0.08	5.85
CMD surfaces in Milli-Q water at 4°C for 2 weeks	16.88 (± 0.16)	79.57 (± 0.40)	3.11 (± 0.39)	0.21	0.03	0.18
Biomimetics bearing pepsin extracts	18.97 (± 0.70)	75.77 (± 0.82)	4.58 (± 0.04)	0.25	0.06	0.24
Biomimetics bearing NaOH extracts	18.76 (± 0.45)	75.81 (± 0.80)	4.42 (± 0.40)	0.24	0.05	0.23
Biomimetics bearing acetic acid extracts	18.85 (± 0.61)	75.58 (± 1.02)	4.73 (± 0.40)	0.24	0.06	0.25
Pepsin control surfaces	14.71 (± 0.04)	80.59 (± 0.15)	4.48 (± 0.11)	0.18	0.05	0.30

Islets were isolated as described in section 3.2.5. Each condition comprised 20 islets with 200µL of medium/well in a 96-well plate.

As described in the section 5.2.6, viability was assessed at the end of the GSIS assay. A GSIS assay was performed on islets after 5 days in culture on the different biomimetic and control surfaces. As described elsewhere, samples were pre-incubated with 2.8mM glucose for 1h and then sequentially with: 2.8mM, 28mM, 28mM + 50µM 3-isobutyl-1-methylxanthine (IBMX, I5879, Sigma-Aldrich) and 2.8mM at 37°C and 5% CO_2 [127]. Solutions were collected after each incubation and stored at -20°C. Insulin in the solutions was measured using a Mouse High Range Insulin ELISA assay (80-INSMSH-E01, Alpco).

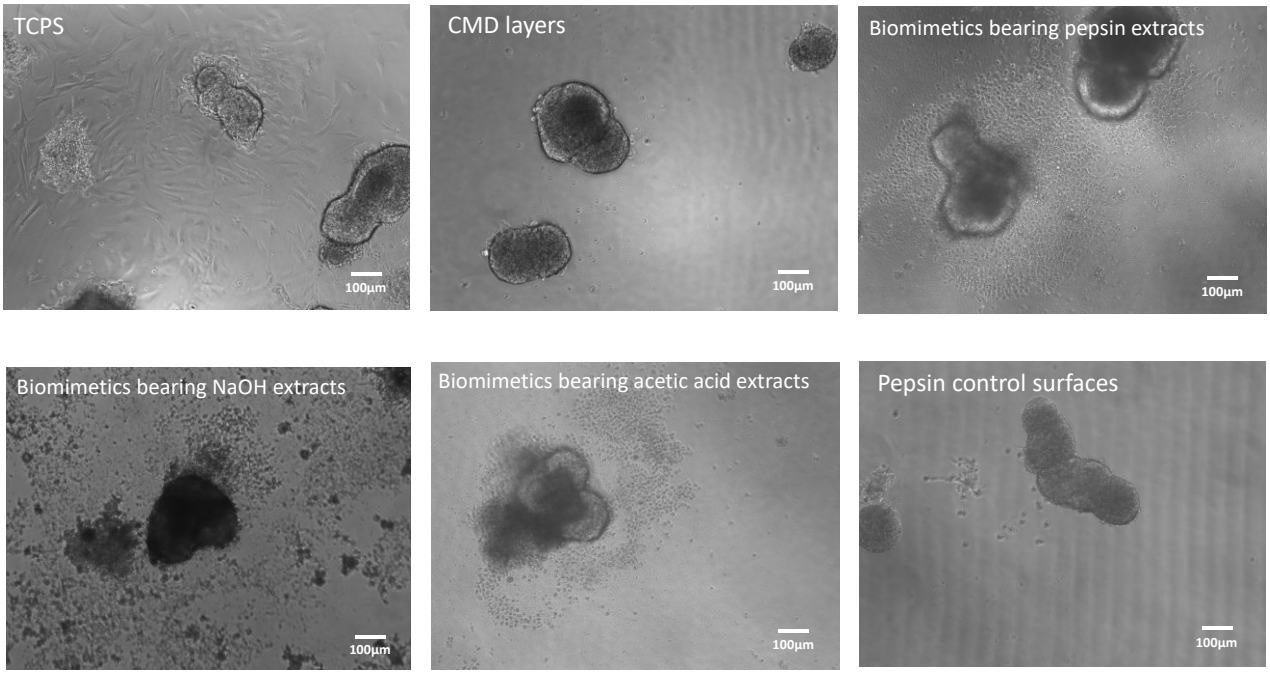

Figure 8. Microscopic images of islets after 5 days of culture on a CMD low-fouling layer, TCPS and a pepsin control surface (i.e., "pepsin control surfaces" refer to activated CMD surfaces incubated in a solution with only pepsin without decellularized pancreata, to check the effect of immobilized pepsin on cells) and on the biomimetic surfaces bearing decellularized pancreatic extracts obtained from acetic acid, NaOH and pepsin treatments.

Islets morphology in all conditions at Day 5 is shown in Figure 2. CMD surfaces retained their low-fouling properties, as illustrated by the absence of islets attachment to the surface. However, over time, islets tended to aggregate (Fig. 8). Islets on TCPS started attaching to the surface from Day 3 and cell outgrowth was subsequently observed; cells seen on the surface appear fibroblastic at Day 5 (Fig. 2). Islet attachment and cell outgrowth were observed sooner, from Day 1, on surfaces bearing acetic acid- and pepsin-solubilised pancreata. However, the cell morphology was very different than that observed on TCPS at Day 5 (Fig. 8). On surfaces bearing NaOH-solubilised pancreata, cell attachment was observed, but to a lesser extent, compared to surfaces made with acetic acid- and pepsin-treated pancreata. Also, dissociation of islets was observed with NaOH-solubilisation (Fig. 2). Little cell attachment was seen on pepsin control surfaces (Fig. 2). Not all islets are spheroidal and islet shape alone cannot be considered as a sign of distress of islets; difference in the isolation process and animals could explain variation in insulin release [230-232]. Islet morphology at Day 0, 1 and 3 on all surfaces are shown in Supplemental Figures 5-7; Appendix A.

In all conditions, islets secreted insulin in response to glucose after 5 days of culture (Supplemental Figs. 8-9; Appendix A). Overall, insulin secretion in response to glucose was higher on islets cultured on the biomimetic surfaces when compared to those on CMD and TCPS (Supplemental Figs. 8-9; Appendix A). The stimulation indices calculated from the ratio of the insulin concentration at high-glucose + IBMX concentration to that at high-glucose concentration confirm islets are responding to IBMX (Fig. 9). With the stimulation indices calculated from ratios of insulin concentration at high glucose to that at low glucose, it is difficult to conclude on islet functionality (Supplemental Figs. 10; Appendix A). Ratios of insulin concentration at last low-glucose concentration to that at first low-glucose from glucose-stimulated insulin secretion (GSIS) assays revealed that islets responded to glucose gradients and returned to basal secretion levels (Supplemental Figs. 11; Appendix A).

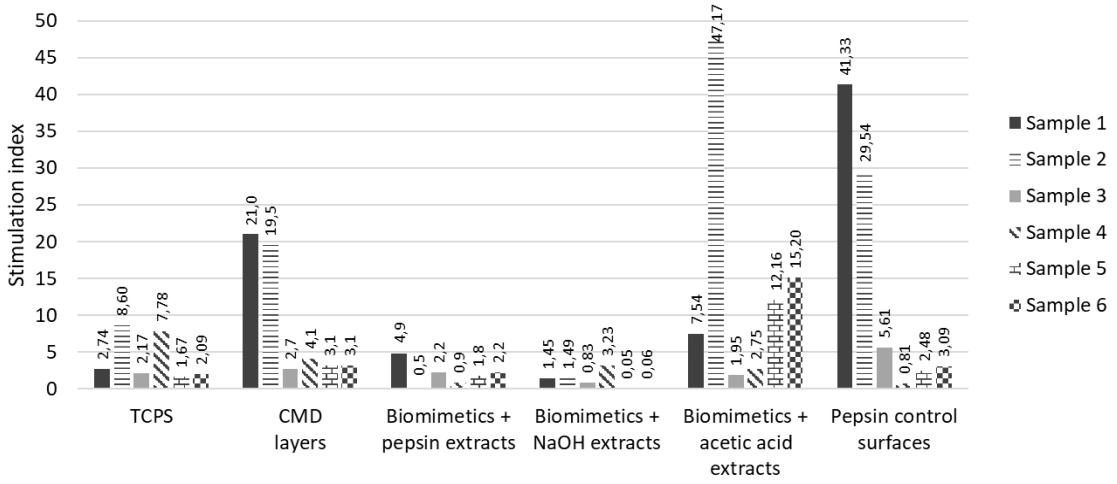

Figure 9. Stimulation indices (ratio of insulin concentration at high glucose-IBMX concentration to that at the high-glucose) from glucose-stimulated insulin secretion (GSIS) assays on murine islets cultured on the different surfaces

Live/dead staining revealed that islets cultured on all surfaces, except those produced from NaOH-solubilised pancreata, were viable after the GSIS assay at Day 5 (Fig. 4). In addition to the observed low level of insulin secreted from islets cultured on biomimetic surfaces made with NaOH soluble extracts, islets viability was lower for that condition (Fig. 4). This observed cytotoxicity was reported earlier, when skin was decellularized by NaOH [114]. We hypothesize that NaOH toxicity could have resulted from an insufficient washing of the surfaces.

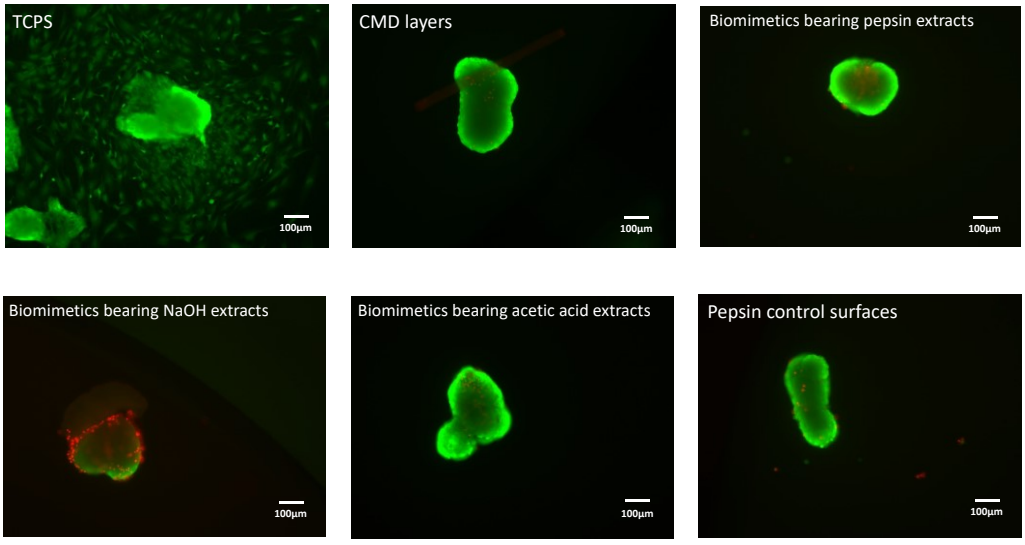

Figure 10. Viability of islets cultured on the different surfaces after a GSIS assay, by staining with fluorescein diacetate (live - green) and propidium iodide (dead - red).

To conclude, decellularization of mouse pancreata followed by ECM solubilization was achieved using three solubilization protocols. These solubilized ECM contents were immobilized on CMD surfaces. Isolated mouse islets were cultured successfully for five days on biomimetic surfaces and remained viable for the culture period. Their functionality was retained partially. NaOH solubilization yielded the highest protein content but the resulting surfaces were cytotoxic as compared to the other surfaces made of pepsin and acetic acid extracts. Surfaces bearing ECM contents resulted in higher insulin secretion compared to the control surfaces (TCPS and CMD). Characterization of the solubilized proteins from the ECM and the different cell types from the islets found on surfaces will be performed in future studies. This work reports, for the first time, the solubilisation of a decellularized pancreas and its successful immobilization on low-fouling surfaces.

Acknowledgements

This research project was supported by NSERC through a Discovery Grant awarded to Patrick Vermette (Grant # 250296-2012). The authors declare no competing financial interest.

Chapter 5

Insulin secretion kinetics from single islets reveals distinct sub-populations

Foreword

Authors and Affiliations:

Rajesh Guruswamy Damodaran: Ph.D. Candidate, Université de Sherbrooke, Département de génie chimique et de génie biotechnologique.

Alexandre Poussard: Université de Sherbrooke, Département de génie chimique et de génie biotechnologique.

Benoît Côté: Université de Sherbrooke, Département de génie chimique et de génie biotechnologique.

Parker L. Andersen, Ph D.: Université de Sherbrooke, Département de génie chimique et de génie biotechnologique.

Patrick Vermette: Professor, ingénieur, Université de Sherbrooke, Département de génie chimique et de génie biotechnologique.

Date of Submission: Dec 6th, 2017

State of Acceptance: Published

Journal: Biotechnology Progress

Contribution:

This article is the last experimental work of this thesis. The content of this work has been accepted in *Biotechnology Progress*. All experimental work was performed by Rajesh Guruswamy Damodaran and Alexandre Poussard. Technical advice was given by Parker L. Andersen. All data analysis was performed by Rajesh Guruswamy Damodaran, Alexandre Poussard and Patrick Vermette. Mathematical models were derived by Benoît Côté. The article was written by Rajesh Guruswamy Damodaran. All work was performed under the direction and supervision of Patrick Vermette.

Titre en français : L'analyse du profil cinétique de sécrétion d'insuline par des îlots uniques montre l'existence de populations distinctes d'îlots.

Résumé

Le diabète de type II évolue avec une sécrétion d'insuline inadéquate et une augmentation de l'exposition à un taux élevé de glucose dans le sang. *In vitro*, la sécrétion d'insuline par les îlots en réponse à la stimulation par le glucose suggère que tous les îlots ne répondent pas de façon équivalente. Nous faisons donc l'hypothèse que tous les îlots isolés du pancréas ne sécrètent pas l'insuline de manière unique. Pour vérifier cette hypothèse, nous avons mesuré et modélisé la cinétique de sécrétion d'insuline sur des îlots individuels, isolés de pancréas de souris, et soumis à une stimulation chronique au glucose (2.8-20 mM). L'analyse cinétique sur 58 îlots distincts exposés 72h à une concentration élevée en glucose montre l'existence de différents profils de sécrétion : lent, rapide, et sécrétion à taux constant ; le profil de sécrétion lent étant le plus observé (50%). Il existe donc une variation temporelle dans la réponse au glucose. Lors de courtes expositions (<4h) à un taux élevé de glucose, très peu d'îlots réagissent pas une sécrétion d'insuline maintenue dans le temps. Ce modèle permet également d'analyser l'influence de la taille des îlots sur la sécrétion d'insuline, sans montrer d'effet clair de ce paramètre. Pour une forte concentration en glucose, la quantité d'insuline sécrétée normalisée par rapport au volume de l'îlot montre une tendance de sécrétion plus grande par les îlots de petite taille. De plus, pour des concentrations élevées en glucose, la sécrétion d'insuline mesurée sur des îlots individuels est similaire à celle mesurée pour des populations d'îlots, tandis que pour des concentrations faibles en glucose, nous n'observons pas les mêmes profils de sécrétion pour les îlots individuels et les groupes d'îlots.

Mots clés : modélisation de la sécrétion; concentration de glucose; îlots individuels; taille d'îlots; sécrétion rapide; sécrétion lente; sécrétion à taux constant

Abstract

Type II diabetes progresses with inadequate insulin secretion and prolonged elevated circulating glucose levels. Also, pancreatic islets isolated for transplantation or tissue engineering can be exposed to glucose over extended timeframe. We hypothesized that isolated pancreatic islets can secrete insulin over a prolonged period of time when incubated in glucose solution and that not all islets release insulin in unison. Insulin secretion kinetics was examined and modeled from single mouse islets in response to chronic glucose exposure (2.8-20mM). Results with single islets were compared to those from pools of islets. Kinetic analysis of 58 single islets over 72h in response to elevated glucose revealed distinct insulin secretion profiles: slow-, fast- and constant-rate secretors, with slow-secretors being most prominent (ca. 50%). Variations in the temporal response to glucose therefore exist. During short-term (<4h) exposure to elevated glucose, few islets are responding with sustained insulin release. The model allowed studying the influence of islet size, revealing no clear effect. At high-glucose concentrations, when secretion is normalized to islet volume, the tendency is that smaller islets secrete more insulin. At high-glucose concentrations, insulin secretion from single islets is representative of islet populations, while under low-glucose conditions pooled islets did not behave as single ones. The characterization of insulin secretion over prolonged periods complements studies on insulin secretion performed over short timeframe. Further investigation of these differences in secretion profiles may resolve open-ended questions on pre-diabetic conditions and transplanted islets performance. This study underlines the importance of size of islets in insulin secretion.

Key words: insulin secretion modeling; glucose concentration; single islets; islet size; fast secretors; slow secretors; constant-rate secretors.

5.1 Introduction

Isolated pancreatic islets are used to perform studies on islet biology, tissue engineering methods and transplantation as well as on diabetes. Islets exist in different sizes throughout the pancreas. *In vitro*, it is believed that the rate of insulin secretion is proportional to the size of the islets but some studies revealed that smaller islets secrete more insulin than larger ones. Smaller islets are believed to have a larger number of β-cells relative to the other cell types and higher oxygen diffusion [233-237]. Those studies often involve the stimulation of islets with a single glucose concentration and only for a few hours (up to 2h).

Many studies involving glucose-stimulated insulin secretion (GSIS) show that the exocytosis of cytoplasmic insulin granules occurs in a biphasic manner both *in vitro* and *in vivo*. This was first reported in 1968.[238-241] The first phase of insulin release occurs within 1 to 10 minutes by the pre-docked insulin granules at the plasma membrane from a readily releasable pool (RRP). The granules from the reserve pool, which lies further from the plasma membrane, are used to refill the RRP [239, 242] and this constitutes the second phase. This secondary release is slow and sustained as long as glucose concentration remains high.[239, 243, 244]

A slowdown in both first and second phases of glucose-stimulated insulin secretion is considered to be an early indication of β-cells dysfunction in type-2 diabetes [240]. Investigating insulin and glucose relationship is important but this is hard to perform *in vivo* since direct detection of insulin is difficult and insulin degradation is fast (4-6 min) [245]. When investigated *in vivo*, kinetics of insulin secretion in response to glucose has been carried out often for short periods of time (0 to 2h) [246, 247] and has demonstrated that not all islets secrete in unison [248].

During and after isolation, islets undergo physical, enzymatic and chemical damages leading to functional loss [249]. The most common practice to evaluate islet function is the GSIS assay that investigates insulin secretion in a static manner. A GSIS assay takes a “snapshot” of the insulin released following a short period of time following islet incubation in glucose solutions. Typically, insulin is measured from the same population of islets after a series of one-hour incubations in different glucose conditions. Glucose concentrations used in GSIS assays can vary between studies. GSIS assays currently applied represent modified versions of the erstwhile functionality experiment reported in 1967 on isolated rat islets, wherein functionality was determined by incubating the islets with 1.6mM and 16.6mM glucose in Krebs bicarbonate solution and the insulin release was measured over 90 minutes *in vitro* [250]. Pancreatic islets

isolated for transplantation or tissue engineering can be exposed to high glucose concentrations over extended periods of time, both *in vitro* and *in vivo*.

Practically, batch-to-batch variability of tissues and enzyme cocktails used in isolation, low isolation yields, large number of required animals as well as animal variation, when non-human tissues are utilized [251, 252], are all imposing a financial burden on the usage of islets. Considering that few islets can be obtained from each isolation from mice (typically, 200 to 250 islets per mouse; in our laboratory around 150),[253] there is a need to develop models that would use fewer islets per condition.

The objective of this work was to model the insulin secretion profile to categorize islet sub-populations by developing and using an assay investigating insulin secretion kinetics from isolated single islets. The responses of single islets were also compared to those of pooled islets. Single islets refer here to one islet per culture well as opposed to pooled islets (10 islets) which correspond to 10 islet equivalents per culture well. In addition, the effect of islet size and glucose concentration on the kinetics of insulin secretion was studied. To reach these goals, the kinetics of insulin secretion from isolated single islets exposed to four glucose concentrations were investigated for a period of 72h and compared to those of populations of 10 islets.

5.2 Materials and methods

5.2.1 Mouse islet isolation

Female mice between 19g and 33g (CD-1® IGS, Charles River, Boston, MA, USA) were sacrificed under a CO_2 atmosphere, as approved by the Université de Sherbrooke's ethical committee (protocol no. 367-14). The pancreata were injected with a dissociation solution containing 0.5 mg mL^{-1} of collagenase (C9263, Sigma-Aldrich, Oakville, ON, Canada). Dissociation solution was composed of L15 medium (L-4386, Sigma-Aldrich), 15mM HEPES, 10mM nicotinamide, 1 mg mL^{-1} glucose, 2% (v/v) FBS, 0.35 mg mL^{-1} $NaHCO_3$ and a penicillin (100 U mL^{-1})/streptomycin (100 µg mL^{-1}) mix. Then, the pancreata were excised and transferred to 15 mL centrifuge tubes containing the same ice-cold mixture (for transportation) and incubated for 18±2 min in a 37°C water bath with regular interval shaking. Digestion was stopped by adding ice-cold HBSS (H1387, Sigma-Aldrich) supplemented with 5% (v/v) FBS, 10mM nicotinamide,

and 0.35 mg mL^{-1} $NaHCO_3$. Digested tissues were split in bacteriological Petri dishes and diluted with HBSS solution. Islets were then recovered by handpicking under an optical microscope (Carl Zeiss, SteREO Lumar. V12, between 6.5X to 80X) and placed in dissociation medium without collagenase.

5.2.2 Islet culture

Isolated islets were pre-incubated in RPMI 1640 (R1383, Sigma Aldrich) without glucose, supplemented with 10mM nicotinamide, 15mM HEPES and the penicillin/streptomycin mix, for 30 min at 37°C and 5% CO_2. For each experiment, islets were cultured in 1 mL of growth medium in 24-well plates containing either 2.8mM, 5.6mM, 11.2mM, or 20mM glucose. Growth medium was DMEM (D5523, low-glucose, Sigma-Aldrich):RPMI (1:1), with 5% (v/v) FBS, 10mM nicotinamide, 15mM HEPES, and the penicillin/streptomycin solution. Islets were counted, before and after sampling, to ensure islets were not accidentally removed during pipetting. Pictures were taken at 4X and 10X (Nikon Eclipse TE2000) to measure islet sizes using the ruler tool in Adobe Photoshop®. For spherical islets, the diameter was calculated by taking the mean of the biggest and smallest diameter of each islet. For those which were oval or cylindrical, mean diameters were estimated from the volume of a sphere equal to that of an ovoid or a cylinder determined from the respective formula for calculating volume and representing the corresponding islet.[128] Conversion between pixels and micrometer was performed using a scale previously established using pictures of a ruler at each magnification of the microscope. Islet equivalent was obtained by dividing the mean diameter by 150µm.[254] For ten islets (picked randomly), the total mean diameter was divided by 150µm.

5.2.3 Measurements of insulin secretion

Medium samples were collected at different time points for ELISA to test the insulin secretion. As described in the manuscript, one islet or ten islets were both incubated in 1 mL medium, resulting in the big difference in cumulative insulin concentration in the medium (Fig. 1A). Cultures were incubated for 72h and media (25 µL each) were collected over 8 time points (0.5, 1, 2, 4, 18, 24, 48 and 72 hours) under the microscope (SteREO Lumar. V12) to avoid picking

islets during collection. Insulin concentrations were corrected for volume sampling. Triplicates for each culture condition were performed. Insulin in the media was measured using an ELISA kit (80-INSMSH-E01, Mouse High Range Insulin ELISA, Alpco, Salem, NH, USA).

5.2.4 Modeling of insulin secretion

Insulin secretion was modeled from 58 single islets isolated from five mice and from 36 10-islet pools obtained from 9 mice (Fig. 11A). Considering the shape of the insulin secretion curves over time (Fig. 11 for typical examples), islets were categorized as Fast Secretors (Equation 1, first-order function), Slow Secretors (Equation 2, second-order function), or Constant-rate Secretors (Equation 3, linear regression (zero-order function)). Equations 1-3 were therefore used to fit the data. Full development of Equations 1 and 2 is presented in Supplemental Materials.

$$y = K_P A\left(1 - e^{-t/\tau_p}\right) \qquad \text{Equation 1 (Fast secretors)}$$

$$y = K'_p A\left[1 - \frac{1}{(\tau_2 - \tau_1)}\left(\tau_1\, e^{-t/\tau_1} - \tau_2\, e^{-t/\tau_2}\right)\right] \qquad \text{Equation 2 (Slow Secretors)}$$

y is the insulin concentration in function of time in ng mL^{-1}, t the time in hours, K_p and K'_p are the steady-state process gains in (ng of insulin/mL) (mM glucose)$^{-1}$, A the step input (i.e., the glucose concentration in which islets are incubated) in mM of glucose, τ_p is the time constant in hours for first-order systems, and τ_1 and τ_2, the two time constants for second-order systems in hours. The K_pA or K'_pA product represents the asymptotic (at plateau) value of cumulative insulin concentration in ng mL^{-1}. K_p and K'_p can be interpreted as the ratios of the predicted (modeled) cumulative insulin concentration at plateau to the glucose concentration used to incubate the islets.

$$y = mt \qquad \text{Equation 3 (Constant-rate Secretors)}$$

m is the rate of insulin secretion in ng mL^{-1} h^{-1} and t the time in hours.

τ_p and K_p as well as τ_1, τ_2, and K'_p were obtained after minimizing the sum of the squared errors with the Excel 2013 solver. For most curves, the function selected to fit the experimental points was that giving the best mathematical fit (i.e., the smallest error), but for some systems a visual inspection was also done to complement the mathematical fitting strategy to make sure that the trend of the experimental points was respected.

With a fast secretor (Fig. 11B), the insulin released increases rapidly at first (represented by τ_p in Eq. 1) and then gradually approached a steady state (plateau) concentration (K_pA in Eq. 1). In particular, the initial rate of release was characterized by an exponential function. Whereas with a slow secretor (Fig. 11C), the behaviour can be described by two (first-order) processes in series. Firstly, the concentration increases at a rate that can be represented by a first-order dynamic (τ_1 in Eq. 2). Then, it goes through another secretion phase that can be described by a second first-order function (τ_2 in Eq. 2). Finally, it levels off to a steady state (at plateau) value (K'_pA in Eq. 2). With a constant-rate secretor (Fig. 11D), the rate of insulin release is constant at any given time.

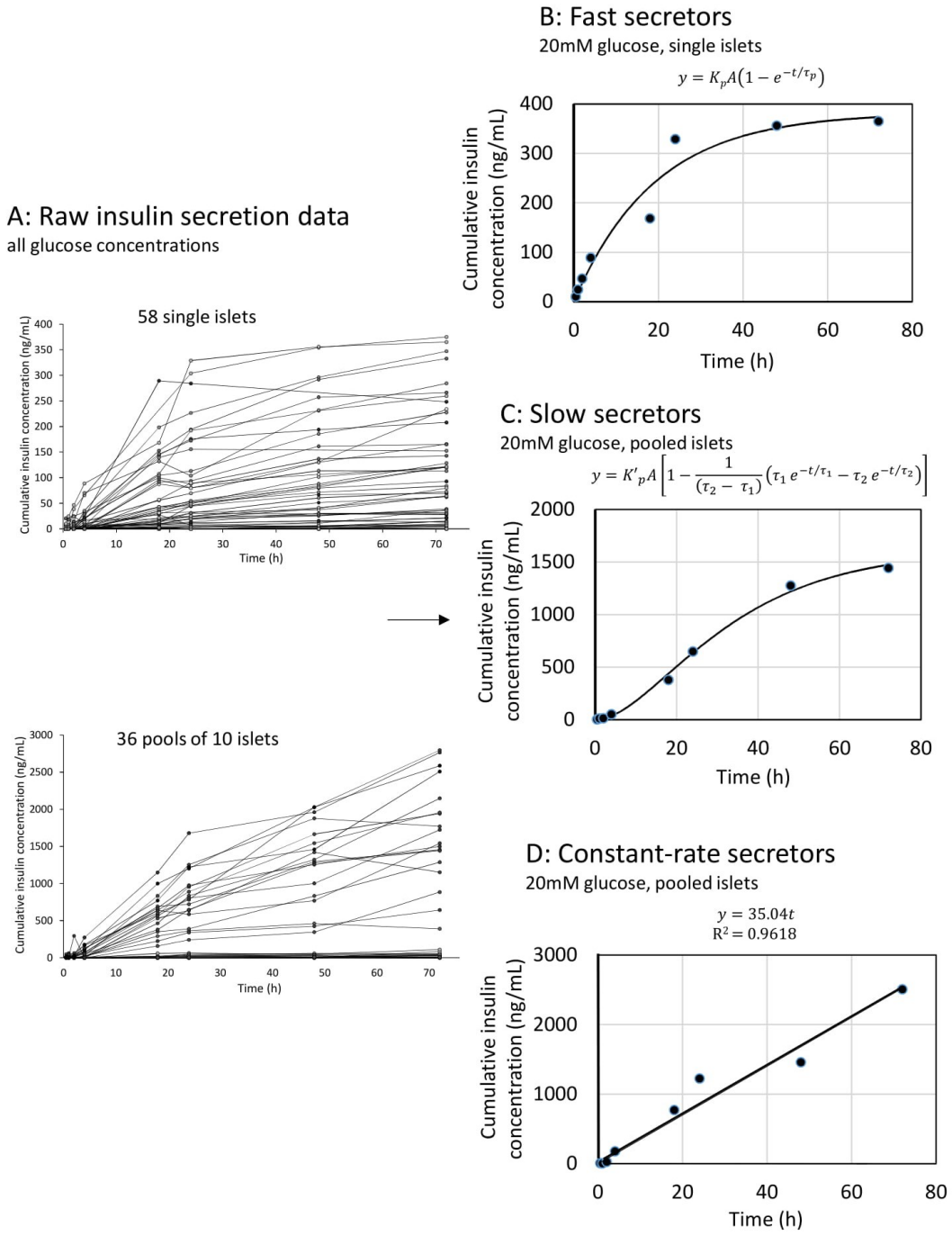

Figure 11. (A) Raw insulin secretion data from 58 single islets and 36 pools of 10 islets. Each set of data points from (A) was used to model the measured cumulative insulin concentration vs time allowing to identify (B) fast, (C) slow, and (D) constant-rate secretors. Each exemplified set of data points and curve is obtained from one glucose concentration. From those curves, time constants as well as as K_p and K'_p (fast and slow secretors) and rates of insulin secretion (constant-rate secretors) were derived.

5.2.5 Glucose-stimulated insulin secretion (GSIS)

A GSIS assay was performed from populations of 10 islets with an aim to verify the functionality of the islets and to compare GSIS with an insulin secretion profile over a 72h period. GSIS measurements were done with 10±2 islet equivalents (IEQ) in duplicate and three different experiments were performed separately. The assay solution was a Krebs buffer composed of 25mM HEPES, 115mM NaCl, 24mM $NaHCO_3$, 5mM KCl, 1mM $MgCl_2$ and 0.1 % (w/v) bovine serum albumin. Islets were first pre-incubated 1h, at 37°C and 5% CO_2, in Krebs buffer supplemented with 2.8mM glucose. Then, islets were sequentially incubated for 1h at 37°C and 5% CO_2 in 1) 2.8mM glucose, 2) 20mM glucose, 3) 20mM glucose + 50µM 3-isobutyl-1-methylxanthine (IBMX, I5879, Sigma-Aldrich) and 4) 2.8mM glucose, all made in Krebs buffer. Media were collected after every incubation and insulin was measured with the Mouse High Range Insulin ELISA mentioned above.

5.2.6 Islets purity and viability assessment

Purity and viability of the handpicked islets were performed separately on different sets of islets and verified for each culture for both kinetics and GSIS experiments. Purity was investigated by incubating handpicked islets in 200µL PBS in which 1mL of 0.01% dithizone (43820, Sigma-Aldrich) was added to stain the islets. After 5min, samples were observed under the stereo microscope (Leica stereomicroscope MZFLIII at 8x). Viability was verified at the beginning and at the end of each culture. Staining was done using fluorescein diacetate (FDA) (F7378, Sigma-Aldrich) and propidium iodide (PI) (P4170, Sigma-Aldrich) to visualize live (green) and dead (red) cells, respectively. Staining was performed by adding 20µL of a 1:10 diluted PI stock solution (0.5 mg mL^{-1}) and 20µL of a 1:100 diluted FDA stock solution (5 mg mL^{-1}) to 200µL of RPMI medium containing the islets. After 30s, 2mL of PBS were added and the whole suspension was observed under a fluorescence microscope (10X) and images were taken for analysis (Nikon Eclipse TE2000). The percentages of cell viability within the islets were obtained by counting the number of pixels in an image of particular intensity and color with a Python program developed in house, which uses functions from the Python Image Library (PIL). The Python program is available as Supplemental Materials.

5.3 Results

5.3.1 Islet characterization

The *in vitro* release of insulin from single endocrine mouse islets and populations of 10 islets was monitored over 72h following stimulation using four glucose concentrations i.e., 2.8mM, 5.6mM, 11.2mM and 20mM.

The mouse islets isolated by handpicking showed more than 95% viability, both post-isolation at Day 0 and at 72h (Fig. 12A). After isolation, the handpicked islets were almost exempt of exocrine tissues (Fig. 12B). In addition to the viability and purity, the GSIS results confirmed the functionality of the islets (Fig. 12C).

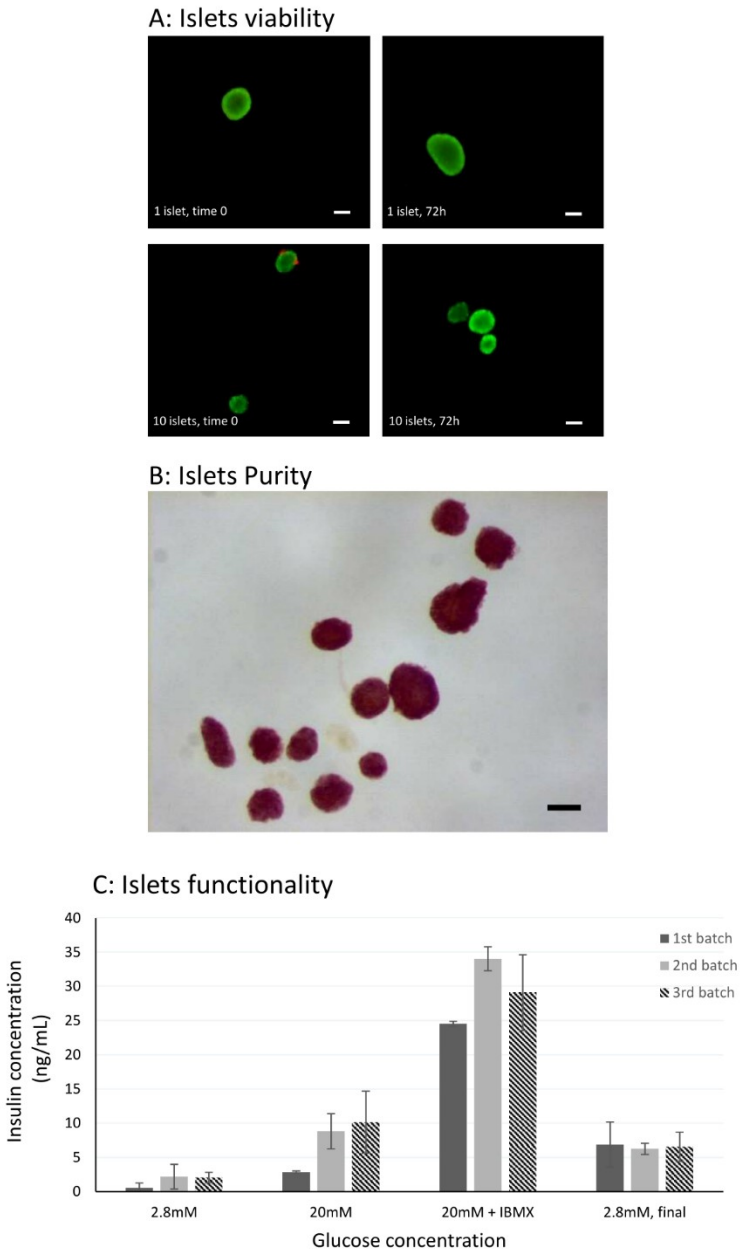

Figure 12. (A) Viability of islets measured by staining with fluorescein diacetate (FDA - green) and propidium iodide (PI - red). Islets viability at time zero: 97.9 % ± 4.3% and at 72 hours: 95.8 % ± 7.8%. Scale bars =100 µm. (B) Pool of ten islets stained with dithizone illustrating the presence of insulin-positive cells. Scale bars =100 µm. (C) Glucose-Stimulated Insulin Secretion (GSIS) from pools of 10 islets.

5.3.2 Kinetic analysis revealed distinct insulin secretion profiles: fast, slow and constant-rate secretors

Examples of typical insulin secretion profiles over time are illustrated in Figure 11. The three profiles are encountered in both single islets and pooled islets. At 2.8mM glucose, few single islets secreted insulin in the detectable range making the fitting of insulin secretion over time not possible for a majority (Figs. 13A and 14A).

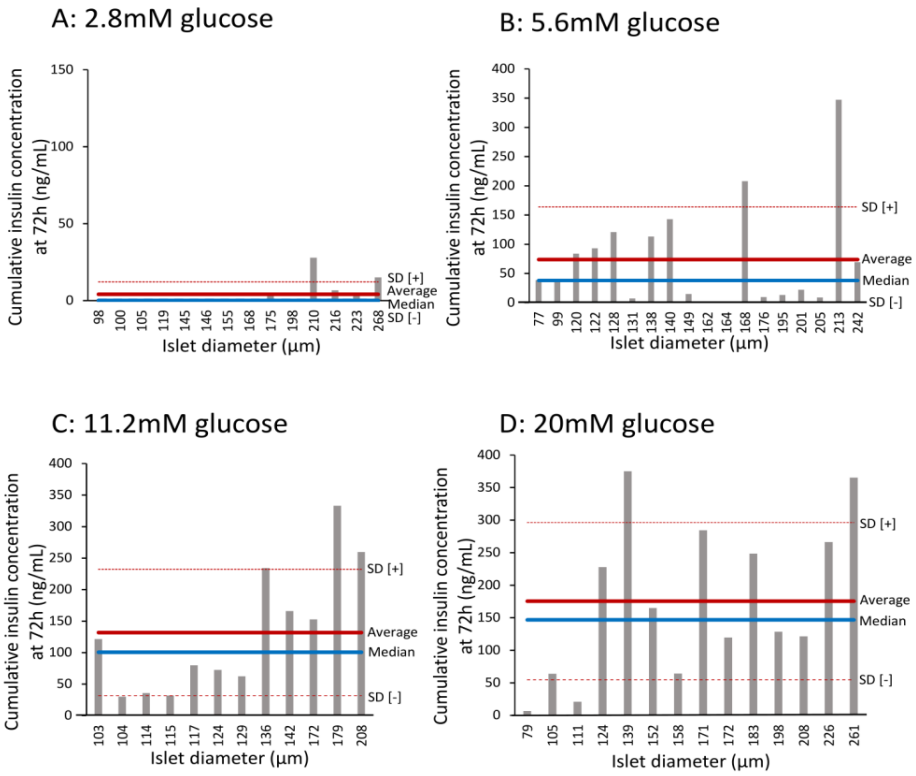

Figure 13. Measured cumulative insulin concentration over 72h from single islets maintained in (A) 2.8mM glucose, (B) 5.6mM glucose, (C) 11.2mM glucose, and (D) 20mM glucose.

For single islets, at 5.6mM, 11.2mM, and 20mM glucose, a majority of islets were slow secretors (Fig. 14). This is also valid for pools of 10 islets, but only for 11.2 and 20mM glucose (Fig. 14). When comparing the overall percentage distribution independently of the glucose concentration, a majority of islets were also slow secretors (Figs. 14C and 14D).

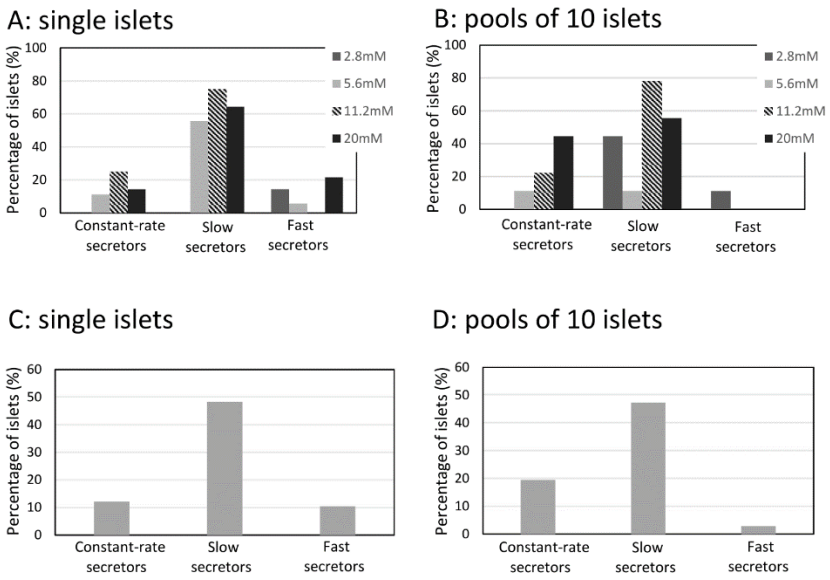

Figure 14. Percentage of islets fitted for insulin secretion kinetics for the four tested glucose concentrations: A) single islets and B) pools of 10 islets. Overall percentage of islets fitted for insulin secretion kinetics: C) single islets and D) pools of 10 islets. For A and B, 100 percent corresponds to the total number of islets for a given glucose concentration. For C and D, 100 percent corresponds to the total number of islets for either single islets or pools of 10-islet experiments. 58 single islets and 36 pools of 10 islets were used in total.

5.3.3 Effect of islet size on insulin secretion

No correlation between insulin secretion and islet size could be established, but few observations can be made. When comparing the medians and averages in Figure 13, it can be depicted that means and medians are close enough to each other for single islets at all glucose concentrations, illustrating that the data points are evenly distributed. Statistically this can be explained as there is less variation in insulin release among a majority of islets for the same concentration of glucose.

At 2.8mM glucose, some insulin secretion was observed with bigger islets (Fig. 13A), although insulin secretion from those single islets resulted in very low level of cumulative insulin concentration. The trend of insulin secretion from single islets remains the same when the

cumulative insulin concentrations secreted from single islets were normalized by Islet equivalent (IEQ) as well as by surface area and volume of islets (Supplemental Fig. 12; Appendix A).

At 5.6mM glucose, islets of smaller sizes secreted lower level of insulin compared to larger ones, but when insulin secretion was normalized per islet volume and per islet area, this trend was reversed or masked (Supplemental Figs. 13C and 13D; Appendix A).

At 11.2mM glucose, more insulin is secreted from larger islets (Fig. 15A). When cumulative insulin concentration was normalized by islet volume, this trend was masked (Fig 15B and Supplemental Fig. 14; Appendix A). At 20mM glucose, when insulin secretion was normalized per islet volume and per islet area, smaller islets secreted more insulin (Supplemental Fig. 15; Appendix A). No effect of islet size could be revealed on time constants and rates of insulin secretion (Supplemental Figs. 16-17; Appendix A).

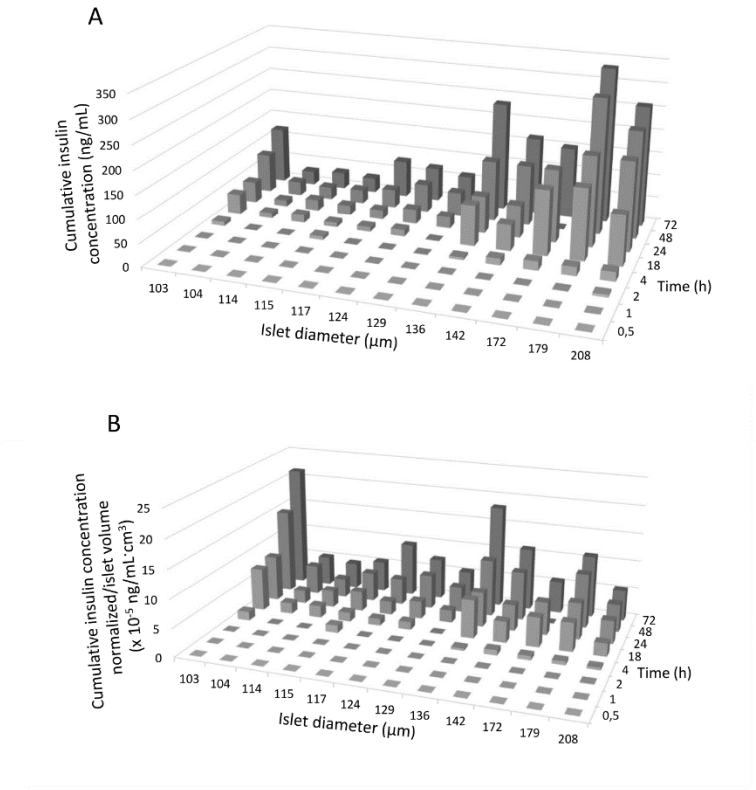

Figure 15. Histograms presenting a comparison of the measured cumulative insulin concentration over 72h for single islets maintained in 11.2mM glucose in function of time (A) and (B) normalized by islet volume. Three-dimensional histograms were made by combining data points, as those exemplified in Figure 11, from different single islets for a given glucose concentration.

5.3.4 Effect of glucose concentration on insulin secretion

Comparing averages of the cumulative insulin concentration at 72h presented in Figures 13 and 16 reveals that statistically (t-Test: Two-Sample Assuming Unequal Variances, $p < 0.05$), when the glucose concentrations are different, the average insulin secretion values are different; except between 5.6 and 11.2mM and between 11.2 and 20mM for single islets as well as between 11.2 and 20mM for groups of islets. Therefore, an augmentation in glucose concentration did not always correspond to an increase in the total insulin concentration at plateau.

From Supplemental Figures 18 and 19; Appendix A, there is no effect of glucose concentration on time constants. Time constants vary from a few hours up to nearly 100 hours. However, for all glucose concentrations tested, for a majority of single islets and groups of islets, time constants were below 30h. When visually inspecting Supplemental Figures 18 and 19; Appendix A, we can conclude that time constants for slow secretors, τ_1 and τ_2, are of similar timescale for most systems, indicating that two mechanisms of almost analogous dynamics are governing insulin secretion. When comparing time constants, τ_p, of fast secretors with those of slow secretors, they are also of similar timescale. Time constants and rates of insulin secretion give an indication on how fast a process is occurring. A time constant is the time for a system response to reach 63.2% of its final (asymptotic, at plateau) value. No effect of glucose concentration on the steady-state process gains could be observed (Supplemental Figs. 20 and 21; Appendix A). At high-glucose concentrations, insulin secretion from single islets is representative of islet populations, while under low-glucose conditions distinct behaviors were observed.

At 2.8mM glucose, for populations of 10 islets, although at low level, insulin secretion was detected in 8 of the 9 pools (Fig. 16A). At 5.6mM glucose for populations of 10 islets, fewer populations secreted insulin (Fig. 16B), and only two populations could be fitted for insulin secretion. At 5.6mM glucose, for pools of islets, curve fitting was often not possible due to the low level of insulin secretion. At 2.8 and 5.6mM, pooled islets did not behave in the same manner as single ones, but this was not the case at 11.2 and 20mM glucose.

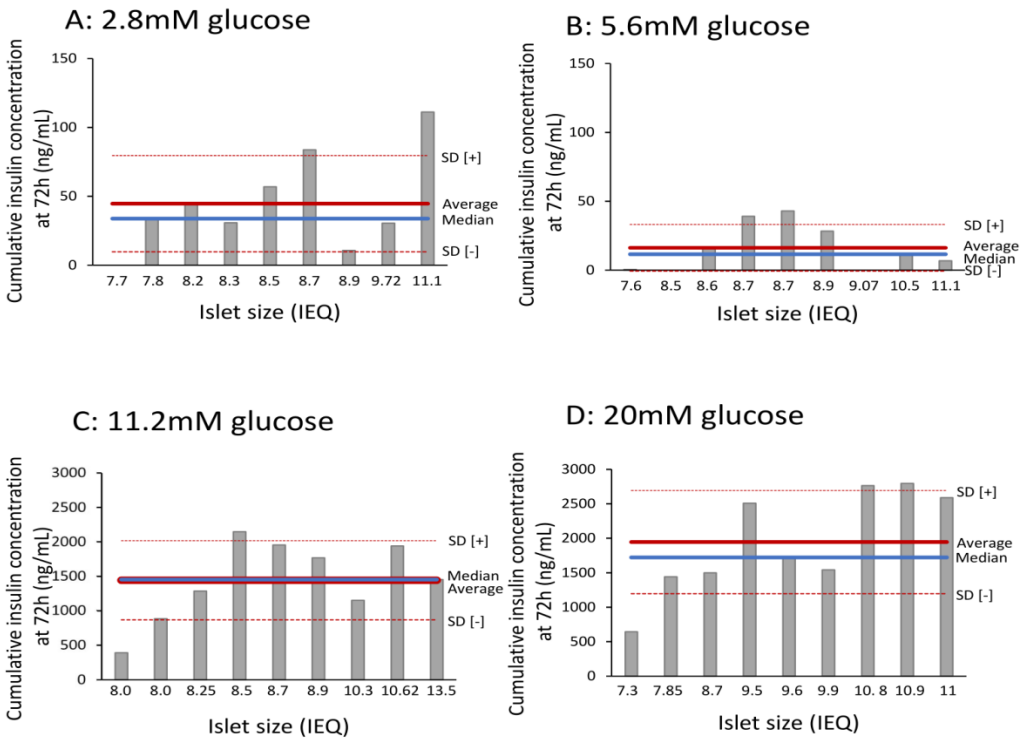

Figure 16. Measured cumulative insulin concentration over 72h from pools of 10 islets maintained in (A) 2.8mM glucose, (B) 5.6mM glucose, (C) 11.2mM glucose, and (D) 20mM glucose.

At 11.2mM glucose, the average value of insulin secretion was 132 ng mL^{-1} for single islets (Fig. 13C) and 1443 ng mL^{-1} for groups of 10 islets (Fig. 16C), which is approximately 10 fold higher. The same trend can be observed at 20mM i.e., the average value of insulin secretion was 175 ng mL^{-1} for single islets (Fig. 13D) and 1945 ng mL^{-1} for pools of 10 islets (Fig. 16D).

5.4 Discussion and Conclusion

An important finding in this study is that insulin secretion can be monitored and modeled over 72h from single pancreatic islets. Seventy-two (72) hours was chosen to avoid islet loss during the culture.[255] Also, we know that islets can be maintained in a healthy and functional state over 72h. The few studies reporting insulin release measurements from single islets were conducted

over short periods of time of up to 90 min, aiming to address a different hypothesis than ours.[256, 257] The microfluidic systems used previously to measure insulin secretion from single islets were early versions and would require further improvement in terms of reliability for future use.[258] Those microfluidic systems represent an interesting approach to further study insulin secretion in response to gradients of glucose concentration in perfused conditions. In static conditions, it is possible that insulin levels influence insulin secretion. Also, islets are usually cultured *in vitro* before being transplanted and can be exposed to high glucose concentrations over prolonged periods of time so, investigating the insulin secretion kinetics over time is therefore of importance.

Single islets and groups of islets secreted detectable insulin almost in all glucose concentrations, except for single islets at 2.8mM, and populations of islets at 5.6mM glucose. At 2.8mM glucose, for a majority of single islets, either no insulin was detected in the media or no significant detectable insulin was found i.e., the concentration of insulin was below the lower insulin concentration used to build the ELISA calibration curve. This was expected as the K_m for glucokinase, the rate-limiting step of glucose metabolism, is approximately 5mM.[259] For single islets at 5.6mM glucose, the percentage of islets secreting insulin was higher than that for pools of 10 islets. Paracrine, islet-islet and cell-cell mediated signals could influence groups of islets to secrete less insulin at 5.6mM glucose. In a previous study, human islets secreted low level of insulin when exposed to 5.6mM glucose, but when those islets were dissociated into single cells and further used to make small aggregates, they showed improved response.[260] Thus, paracrine-mediated signaling could be an explanation for the low level of insulin secretion observed at 5.6mM glucose for populations of islets. In another study, however, there was no insulin secretion when rat pancreata were perfused for 4h with solution of 1.3-2.5mM glucose.[261] In our study, insulin was detected only from the largest islets when exposed to 2.8mM glucose.

For 11.2mM and 20mM glucose, measuring insulin secretion from single islets is representative of populations of islets. At low-glucose concentrations i.e., 2.8 and 5.6mM glucose, working with single islets can allow identifying possible variation in islet response towards glucose. At glucose concentrations below 6mM, it is believed that several β-cells within an islet are non-responding, therefore, working with pools of islets at low glucose concentration could possibly mask this variation in insulin secretion.[262]

A majority of islets (ca. 50%) can be categorized as slow secretors for the four glucose concentrations. The functional connectivity of β-cells is high at high-glucose concentration, as

well as increasing glucose concentration results in an increasing number of responding β-cells to glucose within islets and therefore in an augmentation in insulin secretion with time.[262, 263] Hence, there is an initial slower response of the islets to recruit all β-cells to secrete insulin, and this would be explained by a slow, two-consecutive-step, model. In this study, at 20mM glucose, there was a partial decrease in the number of slow secretors with a corresponding increase in constant-rate secretors, and this was notable in pooled populations. This can be explained as, at 20mM glucose, >80% of β-cells are involved in insulin secretion when compared to other lower glucose concentrations.[264]

Studies presenting mathematical models revealed a pattern of increased insulin secretion with an augmentation in glucose concentration.[262, 264, 265] A study comparing *in vitro* and *in vivo* insulin release over 90 min in mice revealed that, both *in vitro* and *in vivo*, the second phase of insulin secretion showed an ascending pattern at 16.7mM.[247] Those findings correlate, in part, with our results showing that when glucose concentration increased, there was an augmentation in insulin secretion, but this was not always valid in our case. The lack of full correlation between glucose concentration and insulin secretion can be explained by two investigations. For instance, prolonged exposure (7 days) of human islets to 11mM and 28mM glucose revealed a decrease in insulin accumulation in the media when compared to 5.6mM.[266] Also, 72h exposure of murine islets to 15mM glucose resulted in impaired function of β-cells.[267]

Another possible mechanism that could potentially explain the observation of slow secretors is that caused by mass transport limitations. Mass transport of glucose into islets and of insulin that is released out of an islet is mainly caused by diffusion i.e., mass transport due to gradients of concentration. This would be represented by the slower secretion observed in slow secretors. In fast secretors, only one of the two mass transport steps would be in cause, explaining their faster dynamics. In constant-rate secretors, such diffusion barrier(s) would not be a step limiting insulin secretion. The different sub-populations of islets can perhaps be explained by the isolation procedures that can yield populations of islets with different physical states i.e., more or less damaged islets with different intercellular structures. Glucose-stimulated insulin secretion is expected to occur through a different mechanism *in vitro* compared to that *in vivo* where islets are vascularized. Such vasculature has been disrupted in isolated islets and passive diffusion become the main driving force for the glucose to reach the cells within the islets.

Nevertheless, our findings, extrapolated *in vivo*, would reveal that if the slow-secretors outnumber the fast-/constant-rate secretors, increased glucose levels *in vivo* would remain elevated for prolonged times, which we speculate may constitute a pre-diabetic condition.[268, 269]

When the islet size is converted to volume, the tendency is that smaller islets are more potent at higher glucose concentrations (11.2mM and 20mM). Smaller islets isolated from rat secreted more insulin per volume when compared to the larger ones incubated with 3 and 20mM glucose; small islets contain more cells per volume than big ones, possibly explaining why smaller islets would contain more insulin per volume or per surface area [270].

In summary, single islets show less variation in insulin release while working at high-glucose concentration and the values could be compared with pools of islets. For a majority of islets, the kinetics of insulin secretion can be modeled by a slow, two-consecutive-step, mechanism. Although no firm conclusion can be drawn about the effect of islet sizes, at 11.2 and 20mM glucose it can be seen that normalizing insulin secretion over their volumes reveals that smaller islets secrete similar level or more insulin than bigger ones. Our method and model also open the possibility to investigate effects of paracrine signaling action as well as islet sizes.

Results from traditional "static" GSIS assays do not reveal the full potential of insulin secretion from islets. Insulin secretion measurements done in a traditional GSIS represent the bottom of the cumulative insulin concentration *vs* time profile, well within the "slow release" period before insulin secretion increases in a large percentage of the islets. The same analysis prevails when interpreting the RRP mechanism of insulin secretion, at least with isolated islets. Is the RRP mechanism observed at short-term responsible for the behavior of the slow-secretors over longer periods of time (in our case 72h), remains a question to be investigated.

The method and model presented here could be a future prospect for drug discovery, as the use of single endocrine pancreatic islets opens the door for high-throughput pre-screening of drugs on primary tissue. This method could limit costs, save time, reduce the number of animals, and be adaptable to robotic pre-screening platforms for drug development, owing to the possibility to perform experiments on single islets. The assay is not without limitations. Handpicking islets is time consuming and there is a risk to lose islets during sampling, but those pitfalls could be addressed.

Funding and declaration of interest

This research project was supported by the Université de Sherbrooke and NSERC through a Discovery Grant awarded to Patrick Vermette (Grant # 250296-2012).

Rajesh Guruswamy Damodaran, Alexandre Poussard, Benoît Côté, Parker L. Andersen, and Patrick Vermette declare that they have no conflict of interest.

Acknowledgements

We thank Mr. Pavithran Iyer (Institut Quantique, Université de Sherbrooke) for writing and providing us the Python program. We thank Evan A. Dubiel, Jamie Sharp and Tim Spitters for their scientific insights.

Chapter 6

CONCLUSION

Conclusions – Français

Les travaux de cette thèse ont pour objectif la compréhension des mécanismes de survie et de fonctionnalité des îlots de Langerhans *in vitro*, pour améliorer les méthodes de transplantation d'îlots comme thérapie au diabète de type I. Cette thèse présente des données originales sur la cinétique de sécrétion de l'insuline et sur les effets de la matrice pancréatique dans la reconstruction de l'environnement natif des îlots.

Le premier travail expérimental, présenté dans le chapitre 3 « La matrice extracellulaire de pancréas décellularisé comme support natif aux îlots », propose une solution technique à la perte des greffons dans la transplantation d'ilots. Comme présenté précédemment, l'encapsulation des îlots les protège de la réponse immunitaire de l'hôte après transplantation. Les résultats de cette étude montrent que cette technique de décellularisation de pancréas de souris permet d'éliminer efficacement tous les composants cellulaires et de conserver la matrice extracellulaire (MEC) native du pancréas. L'injection des îlots par une seringue via le canal pancréatique pourrait être une nouvelle méthode d'implantation des îlots au sein de leur MEC native. L'utilisation d'une MEC native pour l'encapsulation des îlots pourrait être une avancée par rapport aux techniques actuelles qui utilisent l'alginate ou la fibrine, notamment pour éviter les effets néfastes sur la fonction des îlots de la poly-lysine utilisée pour stabiliser les gels d'alginate ou des grandes concentrations de fibrinogène et de thrombine utilisées pour former les gels de fibrine [8, 9]. Ainsi, la nécessité de disposer d'un matériau d'encapsulation adéquat, c'est-à-dire proche de l'environnement natif des îlots et faiblement immunogène, pourrait être réalisée par des supports faits à partir de pancréas décellularisés. Dans cette étude, nous avons observé que les îlots incubés dans des supports de MEC pancréatique décellularisée étaient viables et fonctionnels après 48h, et que ce support n'est pas cytotoxique après 120 jours de culture de cellules INS-1 exprimant la GFP. La littérature montre que plusieurs organes décellularisés ont été utilisés comme support natif de cellules, et une étude sur les supports pancréatiques a montré des résultats encourageants de recellularisation de pancréas décellularisé [9]. De plus, encapsuler des îlots dans des protéines de la MEC a montré une amélioration de la fonctionnalité des îlots [10]. Ainsi, nous pouvons conclure que les pancréas décellularisés peuvent être testés comme supports biocompatibles, non cytotoxiques et libres de tout contenu cellulaire, dans la transplantation d'îlots. Cependant, des expériences complémentaires doivent être réalisées pour valider ce support comme pancréas bio-

artificiel, notamment en faisant une évaluation *in vivo* de sa fonctionnalité, de la survie du greffon et de la réponse immunitaire liée à la greffe.

Le travail expérimental présenté au chapitre 4, « Solubilisation de pancréas décellularisé et immobilisation sur des surfaces anti-adhésives pour la culture d'îlots de Langerhans », a été fait pour éliminer les résultats faux positifs et faux négatifs quand les îlots sont dépourvus de leur MEC native, cet aspect n'étant pas considéré quand les îlots sont cultivés en 2D sur des surfaces de cultures en polystyrène (TCPS). Trois méthodes ont été utilisées pour extraire les protéines des pancréas décellularisés, et chacune des méthodes a été validée par la technique de Bradford. L'immobilisation des protéines de MEC sur les surfaces biomimétiques a été confirmée par spectrométrie photo-électronique par rayons X (XPS). Les îlots isolés cultivés pendant 5 jours sur ces surfaces se sont montrés viables et fonctionnels, avec une production d'insuline supérieure aux îlots cultivés sur des surfaces contrôles (carboxymethyl dextran) et sur TCPS. Une différence de morphologie des îlots a également été observée sur les surfaces biomimétiques comparées au TCPS. Ces travaux pourraient être poursuivis en identifiant les types cellulaires qui sont spécifiquement maintenus sur ces surfaces. Ces expérimentations ont été limitées par la faible quantité d'échantillons disponibles pour les réaliser.

Le dernier travail expérimental présenté dans ce manuscrit au chapitre 5, « La cinétique de sécrétion de l'insuline par des îlots individuels met en évidence différentes sous populations d'îlots », a eu pour but de déterminer les profils cinétiques de sécrétion de l'insuline suivant la concentration en glucose. Les profils cinétiques de sécrétion ont été évalués suivant le nombre d'îlots, seuls ou en groupe, et suivant leur taille. Un des résultats majeur de cette étude est d'avoir mesuré la quantité d'insuline secrétée *in vitro* par des îlots individuels à 8 points temporels différents sur une période de 72 heures. Nous avons observé trois profils cinétiques de sécrétion de l'insuline différents : sécrétion lente, sécrétion rapide, et sécrétion à taux constant. La majorité des îlots suivaient un profil de sécrétion lent (mécanisme à deux étapes consécutives). En normalisant la quantité d'insuline sécrétée à la taille des îlots, nous observons que les plus petits îlots secrètent plus d'insuline que les plus gros, même si nous ne pouvons proposer de modèle spécifique à cette observation. Cette étude montre également que le test traditionnel du « GSIS », qui est une méthode « statique », ne permet pas de mettre en évidence toute la dynamique de la sécrétion de l'insuline par les îlots. En effet, la méthode GSIS ne mesure qu'une portion cumulative

et terminale de la sécrétion d'insuline en fonction du temps, ce qui oblitère une partie du comportement sécrétoire des îlots. De ce fait, les indices de stimulation obtenus à partir de la méthode GSIS devront à l'avenir être considérés avec plus de prudence pour conclure sur les activités de sécrétion des îlots. La méthode de travail avec des îlots de Langerhans individuels pourrait ouvrir des perspectives pour du criblage à haut débit dans la pré-évaluation de médicaments, en particulier pour surmonter la rareté et le coût du tissu pancréatique. Cette méthode étant adaptable aux plateformes robotisées utilisées dans le développement de nouveaux candidats-médicaments, elle pourrait également diminuer le nombre d'animaux, les coûts et le temps nécessaires aux expérimentations, en offrant la possibilité de travailler avec des îlots individuels. Cependant, une des limites importante de cette méthode est l'isolement manuel des îlots qui peut être longue et délicate. De plus, des îlots peuvent être perdus pendant l'étape d'isolement ce qui diminue son rendement. Ces limitations pourront être étudiées par de futurs travaux.

En résumé, ce travail de thèse a mis en évidence l'intérêt de la MEC native du pancréas dans l'étude du comportement *in vitro* des îlots et son potentiel comme support de culture, et une description de la cinétique de sécrétion de l'insuline par les îlots. Ces résultats ouvrent des perspectives dans le développement d'un pancréas bio-artificiel transplantable.

Conclusions – English

All the experiments in this thesis are aimed at improving the understanding of islets survival and functionality *in vitro*, for transplantation as a therapy for type I diabetes mellitus, by knowing the kinetics of insulin release and by applying its own pancreatic environment to rebuild islets native niches.

The first experimental work described in chapter 3 titled "Decellularized pancreas as a native extracellular matrix scaffold for islets" attempted to address the issue of losing grafts after islet transplantation. As discussed earlier, islets encapsulation shields the tissue from the host immune system after transplantation. The results from this study convey that the techniques used for decellularization of the mouse pancreas could effectively remove the cellular components and retain the native ECM. Also, the infused mouse islets through the ductal port of a decellularized pancreas using a syringe would be a new way to embed islets within their native ECM. The use of native ECM for islets embedding would have an edge over the current techniques using alginate and fibrin gels for encapsulation and overcome the adverse effects on graft functions of using polylysine to stabilise alginate gels and using high concentrations of fibrinogen and thrombin causing negative impact on pancreatic islets [188, 189]. Therefore, the need of a suitable material for encapsulation, which is close to the native environment and has less host immune responses, could be met by using decellularized pancreatic scaffolds. In addition, in this study, it was observed that the infused islets in the decelluarized scaffolds are viable and functional after 48h *in vitro* and that the scaffold is free of cytotoxicity by culturing GFP-INS-1 cells for more than 120 days. Previously, it has been reported that scaffolds of many organs were successfully recellularized and a study on pancreatic scaffolds shows promising results in fabrication and recellularization of decellularized pancreas [189]. Further, encapsulating islets with ECM proteins has shown enhanced islets function [198]. Therefore, it can be concluded that decellularized pancreata can serve as biocompatible scaffolds with no cytotoxicity, and free of cellular components, to carry pancreatic islets for transplantation. However, it should be noted that further investigations must be made on this bio-artificial pancreas to study their responses following transplantation, including host immune rejections, functionality, and graft survival.

The experimental work of Chapter 4 titled, “Solubilisation of decellularized pancreata and immobilization on low-fouling surfaces for islet culture” was designed to eliminate any false positive or false negative results when the islets are devoid of their native ECM, typically not considered when islets are cultured on tissue culture polystyrene (TCPS) in 2D environment. Three methods were used to extract proteins from the decelluarized pancreata and all three methods extracted proteins, which was confirmed by a Bradford assay. The successful immobilization of proteins on the surfaces was confirmed by X-ray photoelectron spectroscopy (XPS) for the biomimetic surfaces. The isolated islets were cultured on these surfaces and found to be functional and viable at day 5 and the amount of insulin production was higher on all biomimetic surfaces when compared to TCPS and carboxymethyl-dextran (CMD) surfaces. In addition, the cell morphology was different on biomimetic surfaces compared to TCPS. It is suggested that future studies should involve identifying the different cell types supported by these immobilised biomimetics. It should also be noted that the main limitation in this experiment was dealing with a small sample size to perform certain studies in detail.

The final experimental work of this thesis described in Chapter 5 titled, " Insulin secretion kinetics from single islets reveals distinct sub-populations", aimed to address the kinetics of insulin release against different glucose concentrations. Differences between kinetics of insulin secretion from single islets and groups of islets as well as the effect of islet size towards insulin secretion were investigated. One of the major findings of this study is the detection of insulin secretion from single isolated islets at 8 different time points for 72h *in vitro*. It was found that the islets secrete insulin according to three different kinetic models: slow secretors, fast secretors and constant-rate secretors, out of which most of the islets were modeled by slow secretors (two-consecutive-step mechanism). Although no firm conclusions can be drawn on the effects of islet size towards insulin secretion, it was noted that, when the islet size was normalized to their volume, the small islets tend to secrete more insulin. The study also highlighted that the traditional “static” GSIS assay on isolated islets does not reveal the full potential of insulin secretion from islets. In fact, it represents only the bottom of the cumulative insulin secretion concentration *vs* time profile, revealing very less information on insulin released by the islets. Therefore, care should be taken in future studies when concluding stimulation indices from GSIS assays and determining the insulin release measurements on islets. The method of working with single endocrine pancreatic islets could open the door for high-throughput pre-screening of drugs, to overcome the usage and availability of

pancreatic tissues which involves high cost. This method could also limit the number of animals, cost and time, while be adaptable to robotic pre-screening platforms for drug development, owing to the possibility of performing experiments on single islets. However, some of the limitations associated with these techniques are islet handpicking which could be a time consuming and tedious process. Also, islets could be lost during sampling. These pitfalls need to be addressed in the future.

In summary, this thesis has verified that the use of native pancreatic ECM to study islet behaviour *in vitro* along with the insulin kinetics, in the hope of carrying islets in a natural bio-scaffold and implanting into a host, aims to offer a better solution in the field of tissue engineering and regenerative medicine towards the development of bio-artificial pancreas for transplantation treatments. Understanding and studying potential immune reactions and physiological changes in the host, post transplantation of these bio-scaffolds could provide a major insight in the development of these artificial organs. On the other hand, the emerging field of utilizing both decellularized scaffolds and stem cells to develop a bio-engineered organ would be a potential area to investigate the utility of these decellularized pancreas in the treatment of diabetes or pancreatitis conditions. Detailed characterization of the extracted ECM proteins and immobilization on the surfaces could be a natural source of *in vitro* test models for isolated islets to mimic the *in vivo* conditions and help in understanding islet biology and in developing drug discovery platforms for diabetes.

Bibliography

[1] Group, N.D.D. (1979). Classification and Diagnosis of Diabetes Mellitus and Other Categories of Glucose Intolerance. *Diabetes*, volume 28, p. 1039.

[2] Gepts, W. (1965). Pathologic anatomy of the pancreas in juvenile diabetes mellitus. *Diabetes*, volume 14, p. 619-633.

[3] van Belle, T.L., Coppieters, K.T. and von Herrath, M.G. (2011). Type 1 diabetes: etiology, immunology, and therapeutic strategies. *Physiological reviews*, volume 91, p. 79-118.

[4] Humar, A., Ramcharan, T., Kandaswamy, R., Gruessner, R.W., Gruessner, A.G. and Sutherland, D.E. (2004). The impact of donor obesity on outcomes after cadaver pancreas transplants. *American journal of transplantation : official journal of the American Society of Transplantation and the American Society of Transplant Surgeons*, volume 4, p. 605-610.

[5] Shapiro, A.M., Ricordi, C., Hering, B.J., Auchincloss, H., Lindblad, R., Robertson, R.P., Secchi, A., Brendel, M.D., Berney, T., Brennan, D.C., Cagliero, E., Alejandro, R., Ryan, E.A., DiMercurio, B., Morel, P., Polonsky, K.S., Reems, J.A., Bretzel, R.G., Bertuzzi, F., Froud, T., Kandaswamy, R., Sutherland, D.E., Eisenbarth, G., Segal, M., Preiksaitis, J., Korbutt, G.S., Barton, F.B., Viviano, L., Seyfert-Margolis, V., Bluestone, J. and Lakey, J.R. (2006). International trial of the Edmonton protocol for islet transplantation. *The New England journal of medicine*, volume 355, p. 1318-1330.

[6] Ryan, E.A., Paty, B.W., Senior, P.A., Bigam, D., Alfadhli, E., Kneteman, N.M., Lakey, J.R. and Shapiro, A.M. (2005). Five-year follow-up after clinical islet transplantation. *Diabetes*, volume 54, p. 2060-2069.

[7] Tatum, J.A., Meneveau, M.O. and Brayman, K.L. (2017). Single-donor islet transplantation in type 1 diabetes: patient selection and special considerations. *Diabetes, metabolic syndrome and obesity : targets and therapy*, volume 10, p. 73-78.

[8] Vorotnikova, E., McIntosh, D., Dewilde, A., Zhang, J., Reing, J.E., Zhang, L., Cordero, K., Bedelbaeva, K., Gourevitch, D., Heber-Katz, E., Badylak, S.F. and Braunhut, S.J. (2010). Extracellular matrix-derived products modulate endothelial and progenitor cell migration and proliferation in vitro and stimulate regenerative healing in vivo. *Matrix biology : journal of the International Society for Matrix Biology*, volume 29, p. 690-700.

[9] Cukierman, E., Pankov, R., Stevens, D.R. and Yamada, K.M. (2001). Taking cell-matrix adhesions to the third dimension. *Science*, volume 294, p. 1708-1712.

[10] Kimmel, H., Rahn, M. and Gilbert, T.W. (2010). The clinical effectiveness in wound healing with extracellular matrix derived from porcine urinary bladder matrix: a case series on severe chronic wounds. *The journal of the American College of Certified Wound Specialists*, volume 2, p. 55-59.

[11] Choi, J.S., Kim, J.D., Yoon, H.S. and Cho, Y.W. (2013). Full-thickness skin wound healing using human placenta-derived extracellular matrix containing bioactive molecules. *Tissue engineering. Part A*, volume 19, p. 329-339.

[12] Sandusky, G.E., Lantz, G.C. and Badylak, S.F. (1995). Healing comparison of small intestine submucosa and ePTFE grafts in the canine carotid artery. *The Journal of surgical research*, volume 58, p. 415-420.

[13] Brown, B., Lindberg, K., Reing, J., Stolz, D.B. and Badylak, S.F. (2006). The basement membrane component of biologic scaffolds derived from extracellular matrix. *Tissue engineering*, volume 12, p. 519-526.

[14] Ma, R., Li, M., Luo, J., Yu, H., Sun, Y., Cheng, S. and Cui, P. (2013). Structural integrity, ECM components and immunogenicity of decellularized laryngeal scaffold with preserved cartilage. *Biomaterials*, volume 34, p. 1790-1798.

[15] Lin, P., Chan, W.C., Badylak, S.F. and Bhatia, S.N. (2004). Assessing porcine liver-derived biomatrix for hepatic tissue engineering. *Tissue engineering*, volume 10, p. 1046-1053.

[16] Uygun, B.E., Soto-Gutierrez, A., Yagi, H., Izamis, M.L., Guzzardi, M.A., Shulman, C., Milwid, J., Kobayashi, N., Tilles, A., Berthiaume, F., Hertl, M., Nahmias, Y., Yarmush, M.L. and Uygun, K. (2010). Organ reengineering through development of a transplantable recellularized liver graft using decellularized liver matrix. *Nature medicine*, volume 16, p. 814-820.

[17] Sabetkish, S., Kajbafzadeh, A.M., Sabetkish, N., Khorramirouz, R., Akbarzadeh, A., Seyedian, S.L., Pasalar, P., Orangian, S., Beigi, R.S., Aryan, Z., Akbari, H. and Tavangar, S.M. (2015). Whole-organ tissue engineering: decellularization and recellularization of three-dimensional matrix liver scaffolds. *Journal of biomedical materials research. Part A*, volume 103, p. 1498-1508.

[18] Wu, Q., Bao, J., Zhou, Y.J., Wang, Y.J., Du, Z.G., Shi, Y.J., Li, L. and Bu, H. (2015). Optimizing perfusion-decellularization methods of porcine livers for clinical-scale whole-organ bioengineering. *BioMed research international*, volume 2015, p. 785474.

[19] Navarro-Tableros, V., Herrera Sanchez, M.B., Figliolini, F., Romagnoli, R., Tetta, C. and Camussi, G. (2015). Recellularization of rat liver scaffolds by human liver stem cells. *Tissue engineering. Part A*, volume 21, p. 1929-1939.

[20] Yagi, H., Fukumitsu, K., Fukuda, K., Kitago, M., Shinoda, M., Obara, H., Itano, O., Kawachi, S., Tanabe, M., Coudriet, G.M., Piganelli, J.D., Gilbert, T.W., Soto-Gutierrez, A. and Kitagawa, Y. (2013). Human-scale whole-organ bioengineering for liver transplantation: a regenerative medicine approach. *Cell transplantation*, volume 22, p. 231-242.

[21] Barakat, O., Abbasi, S., Rodriguez, G., Rios, J., Wood, R.P., Ozaki, C., Holley, L.S. and Gauthier, P.K. (2012). Use of decellularized porcine liver for engineering humanized liver organ. *The Journal of surgical research*, volume 173, p. e11-25.

[22] Kasimir, M.T., Rieder, E., Seebacher, G., Silberhumer, G., Wolner, E., Weigel, G. and Simon, P. (2003). Comparison of different decellularization procedures of porcine heart valves. *The International journal of artificial organs*, volume 26, p. 421-427.

[23] Rieder, E., Kasimir, M.T., Silberhumer, G., Seebacher, G., Wolner, E., Simon, P. and Weigel, G. (2004). Decellularization protocols of porcine heart valves differ importantly in efficiency of cell removal and susceptibility of the matrix to recellularization with human vascular cells. *The Journal of thoracic and cardiovascular surgery*, volume 127, p. 399-405.

[24] Kasimir, M.T., Weigel, G., Sharma, J., Rieder, E., Seebacher, G., Wolner, E. and Simon, P. (2005). The decellularized porcine heart valve matrix in tissue engineering: platelet adhesion and activation. *Thrombosis and haemostasis*, volume 94, p. 562-567.

[25] Ott, H.C., Matthiesen, T.S., Goh, S.K., Black, L.D., Kren, S.M., Netoff, T.I. and Taylor, D.A. (2008). Perfusion-decellularized matrix: using nature's platform to engineer a bioartificial heart. *Nature medicine*, volume 14, p. 213-221.

[26] Ng, S.L., Narayanan, K., Gao, S. and Wan, A.C. (2011). Lineage restricted progenitors for the repopulation of decellularized heart. *Biomaterials*, volume 32, p. 7571-7580.

[27] Akhyari, P., Aubin, H., Gwanmesia, P., Barth, M., Hoffmann, S., Huelsmann, J., Preuss, K. and Lichtenberg, A. (2011). The quest for an optimized protocol for whole-heart

decellularization: a comparison of three popular and a novel decellularization technique and their diverse effects on crucial extracellular matrix qualities. *Tissue engineering. Part C, Methods*, volume 17, p. 915-926.

[28] Remlinger, N.T., Wearden, P.D. and Gilbert, T.W. (2012). Procedure for decellularization of porcine heart by retrograde coronary perfusion. *Journal of visualized experiments : JoVE*, p. e50059.

[29] Wainwright, J.M., Czajka, C.A., Patel, U.B., Freytes, D.O., Tobita, K., Gilbert, T.W. and Badylak, S.F. (2010). Preparation of cardiac extracellular matrix from an intact porcine heart. *Tissue engineering. Part C, Methods*, volume 16, p. 525-532.

[30] Park, K.M. and Woo, H.M. (2012). Porcine bioengineered scaffolds as new frontiers in regenerative medicine. *Transplantation proceedings*, volume 44, p. 1146-1150.

[31] Kitahara, H., Yagi, H., Tajima, K., Okamoto, K., Yoshitake, A., Aeba, R., Kudo, M., Kashima, I., Kawaguchi, S., Hirano, A., Kasai, M., Akamatsu, Y., Oka, H., Kitagawa, Y. and Shimizu, H. (2016). Heterotopic transplantation of a decellularized and recellularized whole porcine heart. *Interactive cardiovascular and thoracic surgery*, volume 22, p. 571-579.

[32] Guyette, J.P., Charest, J.M., Mills, R.W., Jank, B.J., Moser, P.T., Gilpin, S.E., Gershlak, J.R., Okamoto, T., Gonzalez, G., Milan, D.J., Gaudette, G.R. and Ott, H.C. (2016). Bioengineering Human Myocardium on Native Extracellular Matrix. *Circulation Research*, volume 118, p. 56-72.

[33] Ott, H.C., Clippinger, B., Conrad, C., Schuetz, C., Pomerantseva, I., Ikonomou, L., Kotton, D. and Vacanti, J.P. (2010). Regeneration and orthotopic transplantation of a bioartificial lung. *Nature medicine*, volume 16, p. 927-933.

[34] Tsuchiya, T., Mendez, J., Calle, E.A., Hatachi, G., Doi, R., Zhao, L., Suematsu, T., Nagayasu, T. and Niklason, L.E. (2016). Ventilation-Based Decellularization System of the Lung. *BioResearch open access*, volume 5, p. 118-126.

[35] Cortiella, J., Niles, J., Cantu, A., Brettler, A., Pham, A., Vargas, G., Winston, S., Wang, J., Walls, S. and Nichols, J.E. (2010). Influence of acellular natural lung matrix on murine embryonic stem cell differentiation and tissue formation. *Tissue engineering. Part A*, volume 16, p. 2565-2580.

[36] Wagner, D.E., Bonenfant, N.R., Parsons, C.S., Sokocevic, D., Brooks, E.M., Borg, Z.D., Lathrop, M.J., Wallis, J.D., Daly, A.B., Lam, Y.W., Deng, B., DeSarno, M.J., Ashikaga, T., Loi, R. and Weiss, D.J. (2014). Comparative decellularization and recellularization of normal versus emphysematous human lungs. *Biomaterials*, volume 35, p. 3281-3297.

[37] O'Neill, J.D., Anfang, R., Anandappa, A., Costa, J., Javidfar, J., Wobma, H.M., Singh, G., Freytes, D.O., Bacchetta, M.D., Sonett, J.R. and Vunjak-Novakovic, G. (2013). Decellularization of human and porcine lung tissues for pulmonary tissue engineering. *The Annals of thoracic surgery*, volume 96, p. 1046-1055; discussion 1055-1046.

[38] Doi, R., Tsuchiya, T., Mitsutake, N., Nishimura, S., Matsuu-Matsuyama, M., Nakazawa, Y., Ogi, T., Akita, S., Yukawa, H., Baba, Y., Yamasaki, N., Matsumoto, K., Miyazaki, T., Kamohara, R., Hatachi, G., Sengyoku, H., Watanabe, H., Obata, T., Niklason, L.E. and Nagayasu, T. (2017). Transplantation of bioengineered rat lungs recellularized with endothelial and adipose-derived stromal cells. *Scientific reports*, volume 7, p. 8447.

[39] Crabbe, A., Liu, Y., Sarker, S.F., Bonenfant, N.R., Barrila, J., Borg, Z.D., Lee, J.J., Weiss, D.J. and Nickerson, C.A. (2015). Recellularization of decellularized lung scaffolds is enhanced by dynamic suspension culture. *PloS one*, volume 10, p. e0126846.

[40] Gilpin, S.E., Ren, X., Okamoto, T., Guyette, J.P., Mou, H., Rajagopal, J., Mathisen, D.J., Vacanti, J.P. and Ott, H.C. (2014). Enhanced Lung Epithelial Specification of Human iPSCs on Decellularized Lung Matrix. *The Annals of thoracic surgery*, volume 98, p. 1721-1729.

[41] Baptista, P.M., Orlando, G., Mirmalek-Sani, S.H., Siddiqui, M., Atala, A. and Soker, S. (2009). Whole organ decellularization - a tool for bioscaffold fabrication and organ bioengineering. *Conference proceedings : ... Annual International Conference of the IEEE Engineering in Medicine and Biology Society. IEEE Engineering in Medicine and Biology Society. Annual Conference*, volume 2009, p. 6526-6529.

[42] Goh, S.K., Bertera, S., Olsen, P., Candiello, J.E., Halfter, W., Uechi, G., Balasubramani, M., Johnson, S.A., Sicari, B.M., Kollar, E., Badylak, S.F. and Banerjee, I. (2013). Perfusion-decellularized pancreas as a natural 3D scaffold for pancreatic tissue and whole organ engineering. *Biomaterials*, volume 34, p. 6760-6772.

[43] Mirmalek-Sani, S.H., Orlando, G., McQuilling, J.P., Pareta, R., Mack, D.L., Salvatori, M., Farney, A.C., Stratta, R.J., Atala, A., Opara, E.C. and Soker, S. (2013). Porcine pancreas

extracellular matrix as a platform for endocrine pancreas bioengineering. *Biomaterials*, volume 34, p. 5488-5495.

[44] Wu, D., Wan, J., Huang, Y., Guo, Y., Xu, T., Zhu, M., Fan, X., Zhu, S., Ling, C., Li, X., Lu, J., Zhu, H., Zhou, P., Lu, Y. and Wang, Z. (2015). 3D Culture of MIN-6 Cells on Decellularized Pancreatic Scaffold: In Vitro and In Vivo Study. *BioMed research international*, volume 2015, p. 432645.

[45] Napierala, H., Hillebrandt, K.H., Haep, N., Tang, P., Tintemann, M., Gassner, J., Noesser, M., Everwien, H., Seiffert, N., Kluge, M., Teegen, E., Polenz, D., Lippert, S., Geisel, D., Reutzel Selke, A., Raschzok, N., Andreou, A., Pratschke, J., Sauer, I.M. and Struecker, B. (2017). Engineering an endocrine Neo-Pancreas by repopulation of a decellularized rat pancreas with islets of Langerhans. *Scientific reports*, volume 7, p. 41777.

[46] Rajesh, G.D. and Patrick, V. (2018). Decellularized pancreas as a native extracellular matrix scaffold for pancreatic islet seeding and culture. *Journal of tissue engineering and regenerative medicine*, volume 12, p. 1230-1237.

[47] Badylak, S.F., Lantz, G.C., Coffey, A. and Geddes, L.A. (1989). Small intestinal submucosa as a large diameter vascular graft in the dog. *The Journal of surgical research*, volume 47, p. 74-80.

[48] Fiala, R., Vidlar, A., Vrtal, R., Belej, K. and Student, V. (2007). Porcine small intestinal submucosa graft for repair of anterior urethral strictures. *European urology*, volume 51, p. 1702-1708; discussion 1708.

[49] Oliveira, A.C., Garzon, I., Ionescu, A.M., Carriel, V., Cardona Jde, L., Gonzalez-Andrades, M., Perez Mdel, M., Alaminos, M. and Campos, A. (2013). Evaluation of small intestine grafts decellularization methods for corneal tissue engineering. *PloS one*, volume 8, p. e66538.

[50] Syed, O., Walters, N.J., Day, R.M., Kim, H.W. and Knowles, J.C. (2014). Evaluation of decellularization protocols for production of tubular small intestine submucosa scaffolds for use in oesophageal tissue engineering. *Acta biomaterialia*, volume 10, p. 5043-5054.

[51] Crapo, P.M. and Wang, Y. (2010). Small intestinal submucosa gel as a potential scaffolding material for cardiac tissue engineering. *Acta biomaterialia*, volume 6, p. 2091-2096.

[52] Zhang, L., Du, A., Li, J., Pan, M., Han, W. and Xiao, Y. (2016). Development of a cell-seeded modified small intestinal submucosa for urethroplasty. *Heliyon*, volume 2, p. e00087.

[53] Goulle, F. (2012). Use of porcine small intestinal submucosa for corneal reconstruction in dogs and cats: 106 cases. *Journal of Small Animal Practice*, volume 53, p. 34-43.

[54] Wei, R.Q., Tan, B., Tan, M.Y., Luo, J.C., Deng, L., Chen, X.H., Li, X.Q., Zuo, X., Zhi, W., Yang, P., Xie, H.Q. and Yang, Z.M. (2009). Grafts of porcine small intestinal submucosa with cultured autologous oral mucosal epithelial cells for esophageal repair in a canine model. *Experimental biology and medicine*, volume 234, p. 453-461.

[55] Chang, C.W., Petrie, T., Clark, A., Lin, X., Sondergaard, C.S. and Griffiths, L.G. (2016). Mesenchymal Stem Cell Seeding of Porcine Small Intestinal Submucosal Extracellular Matrix for Cardiovascular Applications. *PloS one*, volume 11, p. e0153412.

[56] Lanteri Parcells, A., Abernathie, B. and Datiashvili, R. (2014). The use of urinary bladder matrix in the treatment of complicated open wounds. *Wounds : a compendium of clinical research and practice*, volume 26, p. 189-196.

[57] Tukmachev, D., Forostyak, S., Koci, Z., Zaviskova, K., Vackova, I., Vyborny, K., Sandvig, I., Sandvig, A., Medberry, C.J., Badylak, S.F., Sykova, E. and Kubinova, S. (2016). Injectable Extracellular Matrix Hydrogels as Scaffolds for Spinal Cord Injury Repair. *Tissue engineering. Part A*, volume 22, p. 306-317.

[58] Faust, A., Kandakatla, A., van der Merwe, Y., Ren, T., Huleihel, L., Hussey, G., Naranjo, J.D., Johnson, S., Badylak, S. and Steketee, M. (2017). Urinary bladder extracellular matrix hydrogels and matrix-bound vesicles differentially regulate central nervous system neuron viability and axon growth and branching. *Journal of biomaterials applications*, volume 31, p. 1277-1295.

[59] Li, J., Wang, W., An, H., Wang, F., Rexiati, M. and Wang, Y. (2016). In vitro culture of rat hair follicle stem cells on rabbit bladder acellular matrix. *SpringerPlus*, volume 5, p. 1461.

[60] Remlinger, N.T., Gilbert, T.W., Yoshida, M., Guest, B.N., Hashizume, R., Weaver, M.L., Wagner, W.R., Brown, B.N., Tobita, K. and Wearden, P.D. (2013). Urinary bladder matrix promotes site appropriate tissue formation following right ventricle outflow tract repair. *Organogenesis*, volume 9, p. 149-160.

[61] Merguerian, P.A., Reddy, P.P., Barrieras, D.J., Wilson, G.J., Woodhouse, K., Bagli, D.J., McLorie, G.A. and Khoury, A.E. (2000). Acellular bladder matrix allografts in the regeneration of functional bladders: evaluation of large-segment (> 24 cm2) substitution in a porcine model. *BJU International*, volume 85, p. 894-898.

[62] Ross, E.A., Williams, M.J., Hamazaki, T., Terada, N., Clapp, W.L., Adin, C., Ellison, G.W., Jorgensen, M. and Batich, C.D. (2009). Embryonic stem cells proliferate and differentiate when seeded into kidney scaffolds. *Journal of the American Society of Nephrology : JASN*, volume 20, p. 2338-2347.

[63] Song, J.J., Guyette, J.P., Gilpin, S.E., Gonzalez, G., Vacanti, J.P. and Ott, H.C. (2013). Regeneration and experimental orthotopic transplantation of a bioengineered kidney. *Nature medicine*, volume 19, p. 646-651.

[64] Du, C., Narayanan, K., Leong, M.F., Ibrahim, M.S., Chua, Y.P., Khoo, V.M. and Wan, A.C. (2016). Functional Kidney Bioengineering with Pluripotent Stem-Cell-Derived Renal Progenitor Cells and Decellularized Kidney Scaffolds. *Advanced healthcare materials*, volume 5, p. 2080-2091.

[65] Kheir, E., Stapleton, T., Shaw, D., Jin, Z., Fisher, J. and Ingham, E. (2011). Development and characterization of an acellular porcine cartilage bone matrix for use in tissue engineering. *Journal of Biomedical Materials Research Part A*, volume 99A, p. 283-294.

[66] Kang, H., Peng, J., Lu, S., Liu, S., Zhang, L., Huang, J., Sui, X., Zhao, B., Wang, A., Xu, W., Luo, Z. and Guo, Q. (2014). In vivo cartilage repair using adipose-derived stem cell-loaded decellularized cartilage ECM scaffolds. *Journal of tissue engineering and regenerative medicine*, volume 8, p. 442-453.

[67] Gawlitta, D., Benders, K.E., Visser, J., van der Sar, A.S., Kempen, D.H., Theyse, L.F., Malda, J. and Dhert, W.J. (2015). Decellularized cartilage-derived matrix as substrate for endochondral bone regeneration. *Tissue engineering. Part A*, volume 21, p. 694-703.

[68] Gershlak, J.R., Hernandez, S., Fontana, G., Perreault, L.R., Hansen, K.J., Larson, S.A., Binder, B.Y., Dolivo, D.M., Yang, T., Dominko, T., Rolle, M.W., Weathers, P.J., Medina-Bolivar, F., Cramer, C.L., Murphy, W.L. and Gaudette, G.R. (2017). Crossing kingdoms: Using decellularized plants as perfusable tissue engineering scaffolds. *Biomaterials*, volume 125, p. 13-22.

[69] Chang, T.T., Zhou, V.X. and Rubinsky, B. (2017). Using non-thermal irreversible electroporation to create an in vivo niche for exogenous cell engraftment. *BioTechniques*, volume 62, p. 229-231.

[70] Shupe, T., Williams, M., Brown, A., Willenberg, B. and Petersen, B.E. (2010). Method for the decellularization of intact rat liver. *Organogenesis*, volume 6, p. 134-136.

[71] Struecker, B., Butter, A., Hillebrandt, K., Polenz, D., Reutzel-Selke, A., Tang, P., Lippert, S., Leder, A., Rohn, S., Geisel, D., Denecke, T., Aliyev, K., Johrens, K., Raschzok, N., Neuhaus, P., Pratschke, J. and Sauer, I.M. (2017). Improved rat liver decellularization by arterial perfusion under oscillating pressure conditions. *Journal of tissue engineering and regenerative medicine*, volume 11, p. 531-541.

[72] Orlando, G., Farney, A.C., Iskandar, S.S., Mirmalek-Sani, S.H., Sullivan, D.C., Moran, E., AbouShwareb, T., De Coppi, P., Wood, K.J., Stratta, R.J., Atala, A., Yoo, J.J. and Soker, S. (2012). Production and implantation of renal extracellular matrix scaffolds from porcine kidneys as a platform for renal bioengineering investigations. *Annals of surgery*, volume 256, p. 363-370.

[73] Guyette, J.P., Gilpin, S.E., Charest, J.M., Tapias, L.F., Ren, X. and Ott, H.C. (2014). Perfusion decellularization of whole organs. *Nature protocols*, volume 9, p. 1451-1468.

[74] Chen, W.C., Wang, Z., Missinato, M.A., Park, D.W., Long, D.W., Liu, H.J., Zeng, X., Yates, N.A., Kim, K. and Wang, Y. (2016). Decellularized zebrafish cardiac extracellular matrix induces mammalian heart regeneration. *Science advances*, volume 2, p. e1600844.

[75] Roosens, A., Somers, P., De Somer, F., Carriel, V., Van Nooten, G. and Cornelissen, R. (2016). Impact of Detergent-Based Decellularization Methods on Porcine Tissues for Heart Valve Engineering. *Annals of biomedical engineering*, volume 44, p. 2827-2839.

[76] Ye, X., Wang, H., Gong, W., Li, S., Li, H., Wang, Z. and Zhao, Q. (2016). Impact of decellularization on porcine myocardium as scaffold for tissue engineered heart tissue. *Journal of materials science. Materials in medicine*, volume 27, p. 70.

[77] de Sousa Iwamoto, L.A., Duailibi, M.T., Iwamoto, G.Y., Juliano, Y., Duailibi, M.S., Ossamu Tanaka, F.A. and Duailibi, S.E. (2016). Tooth tissue engineering: tooth decellularization for natural scaffold. *Future science OA*, volume 2, p. FSO121.

[78] Lee, D.J., Diachina, S., Lee, Y.T., Zhao, L., Zou, R., Tang, N., Han, H., Chen, X. and Ko, C.C. (2016). Decellularized bone matrix grafts for calvaria regeneration. *Journal of tissue engineering*, volume 7, p. 2041731416680306.

[79] Gao, S., Yuan, Z., Xi, T., Wei, X. and Guo, Q. (2016). Characterization of decellularized scaffold derived from porcine meniscus for tissue engineering applications. *Frontiers of Materials Science*, volume 10, p. 101-112.

[80] Erten, E., Sezgin Arslan, T., Derkus, B. and Arslan, Y.E. (2016). Detergent-free decellularization of bovine costal cartilage for chondrogenic differentiation of human adipose mesenchymal stem cells in vitro. *RSC Advances*, volume 6, p. 94236-94246.

[81] Fu, Y., Fan, X., Tian, C., Luo, J., Zhang, Y., Deng, L., Qin, T. and Lv, Q. (2016). Decellularization of porcine skeletal muscle extracellular matrix for the formulation of a matrix hydrogel: a preliminary study. *Journal of cellular and molecular medicine*, volume 20, p. 740-749.

[82] Vasudevan, S., Huang, J., Botterman, B., Matloub, H.S., Keefer, E. and Cheng, J. (2014). Detergent-free Decellularized Nerve Grafts for Long-gap Peripheral Nerve Reconstruction. *Plastic and Reconstructive Surgery Global Open*, volume 2, p. e201.

[83] Farrokhi, A., Pakyari, M., Nabai, L., Pourghadiri, A., Hartwell, R., Jalili, R. and Ghahary, A. (2018) *Evaluation of detergent-free and detergent-based methods for decellularization of murine skin*, p.

[84] Hung, S.H., Su, C.H., Lin, S.E. and Tseng, H. (2016). Preliminary experiences in trachea scaffold tissue engineering with segmental organ decellularization. *The Laryngoscope*, volume 126, p. 2520-2527.

[85] Xiang, J., Zheng, X., Liu, P., Yang, L., Dong, D., Wu, W., Liu, X., Li, J. and Lv, Y. (2016). Decellularized spleen matrix for reengineering functional hepatic-like tissue based on bone marrow mesenchymal stem cells. *Organogenesis*, volume 12, p. 128-142.

[86] Gao, R., Wu, W., Xiang, J., Lv, Y., Zheng, X., Chen, Q., Wang, H., Wang, B., Liu, Z. and Ma, F. (2015). Hepatocyte culture in autologous decellularized spleen matrix. *Organogenesis*, volume 11, p. 16-29.

[87] Hasan, A. (2017) *Tissue Engineering for Artificial Organs: Regenerative Medicine, Smart Diagnostics and Personalized Medicine*, Wiley, Doha, p.

[88] Gilpin, A. and Yang, Y. (2017). Decellularization Strategies for Regenerative Medicine: From Processing Techniques to Applications. *BioMed research international*, volume 2017, p. 9831534.

[89] Koley, D. and Bard, A.J. (2010). Triton X-100 concentration effects on membrane permeability of a single HeLa cell by scanning electrochemical microscopy (SECM). *Proceedings of the National Academy of Sciences of the United States of America*, volume 107, p. 16783-16787.

[90] Kalipatnapu, S. and Chattopadhyay, A. (2005). Membrane protein solubilization: recent advances and challenges in solubilization of serotonin1A receptors. *IUBMB life*, volume 57, p. 505-512.

[91] Jamur, M.C. and Oliver, C. (2010). Permeabilization of cell membranes. *Methods in molecular biology*, volume 588, p. 63-66.

[92] Ji, H. (2010). Lysis of cultured cells for immunoprecipitation. *Cold Spring Harbor protocols*, volume 2010, p. pdb prot5466.

[93] Vavken, P., Joshi, S. and Murray, M.M. (2009). TRITON-X Is Most Effective among Three Decellularization Agents for ACL Tissue Engineering. *Journal of orthopaedic research : official publication of the Orthopaedic Research Society*, volume 27, p. 1612-1618.

[94] Xu, H., Xu, B., Yang, Q., Li, X., Ma, X., Xia, Q., Zhang, Y., Zhang, C., Wu, Y. and Zhang, Y. (2014). Comparison of decellularization protocols for preparing a decellularized porcine annulus fibrosus scaffold. *PloS one*, volume 9, p. e86723.

[95] Meyer, S.R., Chiu, B., Churchill, T.A., Zhu, L., Lakey, J.R. and Ross, D.B. (2006). Comparison of aortic valve allograft decellularization techniques in the rat. *Journal of biomedical materials research. Part A*, volume 79, p. 254-262.

[96] Ren, H., Shi, X., Tao, L., Xiao, J., Han, B., Zhang, Y., Yuan, X. and Ding, Y. (2013). Evaluation of two decellularization methods in the development of a whole-organ decellularized rat liver scaffold. *Liver international : official journal of the International Association for the Study of the Liver*, volume 33, p. 448-458.

[97] Bertanha, M., Moroz, A., Jaldin, R.G., Silva, R.A.M., Rinaldi, J.C., Golim, M.A., Felisbino, S.L., Domingues, M.A.C., Sobreira, M.L., Reis, P.P. and Deffune, E. (2014). Morphofunctional characterization of decellularized vena cava as tissue engineering scaffolds. *Experimental cell research*, volume 326, p. 103-111.

[98] González-Andrades, M., Carriel, V., Rivera-Izquierdo, M., Garzón, I., González-Andrades, E., Medialdea, S., Alaminos, M. and Campos, A. (2015). Effects of Detergent-Based Protocols on Decellularization of Corneas With Sclerocorneal Limbus. Evaluation of Regional Differences. *Translational Vision Science & Technology*, volume 4, p. 13.

[99] Simoes, I.N., Vale, P., Soker, S., Atala, A., Keller, D., Noiva, R., Carvalho, S., Peleteiro, C., Cabral, J.M., Eberli, D., da Silva, C.L. and Baptista, P.M. (2017). Acellular Urethra Bioscaffold: Decellularization of Whole Urethras for Tissue Engineering Applications. *Scientific reports*, volume 7, p. 41934.

[100] Nakayama, K.H., Batchelder, C.A., Lee, C.I. and Tarantal, A.F. (2010). Decellularized rhesus monkey kidney as a three-dimensional scaffold for renal tissue engineering. *Tissue engineering. Part A*, volume 16, p. 2207-2216.

[101] Bhuyan, A.K. (2010). On the mechanism of SDS-induced protein denaturation. *Biopolymers*, volume 93, p. 186-199.

[102] Lichtenberg, D., Ahyayauch, H. and Goni, F.M. (2013). The mechanism of detergent solubilization of lipid bilayers. *Biophysical journal*, volume 105, p. 289-299.

[103] Helder, M.R.K., Stoyles, N.J., Tefft, B.J., Hennessy, R.S., Hennessy, R.R.C., Dyer, R., Witt, T., Simari, R.D. and Lerman, A. (2017). Xenoantigenicity of porcine decellularized valves. *Journal of cardiothoracic surgery*, volume 12, p. 56.

[104] Xu, K., Kuntz, L.A., Foehr, P., Kuempel, K., Wagner, A., Tuebel, J., Deimling, C.V. and Burgkart, R.H. (2017). Efficient decellularization for tissue engineering of the tendon-bone interface with preservation of biomechanics. *PloS one*, volume 12, p. e0171577.

[105] Caralt, M., Uzarski, J.S., Iacob, S., Obergfell, K.P., Berg, N., Bijonowski, B.M., Kiefer, K.M., Ward, H.H., Wandinger-Ness, A., Miller, W.M., Zhang, Z.J., Abecassis, M.M. and Wertheim, J.A. (2015). Optimization and critical evaluation of decellularization strategies to develop renal extracellular matrix scaffolds as biological templates for organ engineering and transplantation. *American journal of transplantation : official journal of the American Society of Transplantation and the American Society of Transplant Surgeons*, volume 15, p. 64-75.

[106] Iglic, A. (2011) *Advances in Planar Lipd Bilayers and Liposomes*, Academic Press, Oxford, p.

[107] Hellstrom, M., El-Akouri, R.R., Sihlbom, C., Olsson, B.M., Lengqvist, J., Backdahl, H., Johansson, B.R., Olausson, M., Sumitran-Holgersson, S. and Brannstrom, M. (2014). Towards the development of a bioengineered uterus: comparison of different protocols for rat uterus decellularization. *Acta biomaterialia*, volume 10, p. 5034-5042.

[108] Rodi, P.M., Bocco Gianello, M.D., Corregido, M.C. and Gennaro, A.M. (2014). Comparative study of the interaction of CHAPS and Triton X-100 with the erythrocyte membrane. *Biochimica et biophysica acta*, volume 1838, p. 859-866.

[109] Petersen, T.H., Calle, E.A., Colehour, M.B. and Niklason, L.E. (2012). Matrix composition and mechanics of decellularized lung scaffolds. *Cells, tissues, organs*, volume 195, p. 222-231.

[110] Crapo, P.M., Gilbert, T.W. and Badylak, S.F. (2011). An overview of tissue and whole organ decellularization processes. *Biomaterials*, volume 32, p. 3233-3243.

[111] Dong, X., Wei, X., Yi, W., Gu, C., Kang, X., Liu, Y., Li, Q. and Yi, D. (2009). RGD-modified acellular bovine pericardium as a bioprosthetic scaffold for tissue engineering. *Journal of Materials Science: Materials in Medicine*, volume 20, p. 2327.

[112] Wang, Y., Bao, J., Wu, Q., Zhou, Y., Li, Y., Wu, X., Shi, Y., Li, L. and Bu, H. (2015). Method for perfusion decellularization of porcine whole liver and kidney for use as a scaffold for clinical-scale bioengineering engrafts. *Xenotransplantation*, volume 22, p. 48-61.

[113] Lu, W.D., Zhang, L., Wu, C.L., Liu, Z.G., Lei, G.Y., Liu, J., Gao, W. and Hu, Y.R. (2014). Development of an acellular tumor extracellular matrix as a three-dimensional scaffold for tumor engineering. *PloS one*, volume 9, p. e103672.

[114] Morris, A.H., Chang, J. and Kyriakides, T.R. (2016). Inadequate Processing of Decellularized Dermal Matrix Reduces Cell Viability In Vitro and Increases Apoptosis and Acute Inflammation In Vivo. *BioResearch open access*, volume 5, p. 177-187.

[115] Albanna, M.Z. and Holmes, J.H. (2016) *Skin Tissue Engineering and Regenerative Medicine*, Academic Press, p.

[116] Lumpkins, S.B., Pierre, N. and McFetridge, P.S. (2008). A mechanical evaluation of three decellularization methods in the design of a xenogeneic scaffold for tissue engineering the temporomandibular joint disc. *Acta biomaterialia*, volume 4, p. 808-816.

[117] Sayk, F., Bos, I., Schubert, U., Wedel, T. and Sievers, H.H. (2005). Histopathologic findings in a novel decellularized pulmonary homograft: an autopsy study. *The Annals of thoracic surgery*, volume 79, p. 1755-1758.

[118] Dubiel, E.A., Martin, Y. and Vermette, P. (2011). Bridging the gap between physicochemistry and interpretation prevalent in cell-surface interactions. *Chemical reviews*, volume 111, p. 2900-2936.

[119] Bonnans, C., Chou, J. and Werb, Z. (2014). Remodelling the extracellular matrix in development and disease. *Nature reviews. Molecular cell biology*, volume 15, p. 786-801.

[120] Yao, L., Phan, F. and Li, Y. (2013). Collagen microsphere serving as a cell carrier supports oligodendrocyte progenitor cell growth and differentiation for neurite myelination in vitro. *Stem Cell Research & Therapy*, volume 4, p. 109-109.

[121] Leszczak, V., Baskett, D.A. and Popat, K.C. (2015). Endothelial Cell Growth and Differentiation on Collagen-Immobilized Polycaprolactone Nanowire Surfaces. *Journal of biomedical nanotechnology*, volume 11, p. 1080-1092.

[122] Tate, C.C., Shear, D.A., Tate, M.C., Archer, D.R., Stein, D.G. and LaPlaca, M.C. (2009). Laminin and fibronectin scaffolds enhance neural stem cell transplantation into the injured brain. *Journal of tissue engineering and regenerative medicine*, volume 3, p. 208-217.

[123] Weber, L.M., Hayda, K.N. and Anseth, K.S. (2008). Cell–Matrix Interactions Improve β-Cell Survival and Insulin Secretion in Three-Dimensional Culture. *Tissue engineering. Part A*, volume 14, p. 1959-1968.

[124] Bramfeldt, H. and Vermette, P. (2009). Enhanced smooth muscle cell adhesion and proliferation on protein-modified polycaprolactone-based copolymers. *Journal of biomedical materials research. Part A*, volume 88, p. 520-530.

[125] Dubiel, E.A., Lakey, J.R., T, Lamb, M.W. and Vermette, P. (2014). Culturing Free-Floating and Fibrin-Embedded Islets with Endothelial Cells: Effects on Insulin Secretion and Apoptosis. *Cel. Mol. Bioeng*, volume 7, p. 243.

[126] Kuehn, C., Lakey, J.R.T., Lamb, M.W. and Vermette, P. (2013). Young porcine endocrine pancreatic islets cultured in fibrin show improved resistance toward hydrogen peroxide. *Islets*, volume 5, p. 207-215.

[127] Kuehn, C., Dubiel, E.A., Sabra, G. and Vermette, P. (2012). Culturing INS-1 cells on CDPGYIGSR-, RGD- and fibronectin surfaces improves insulin secretion and cell proliferation. *Acta biomaterialia*, volume 8, p. 619-626.

[128] Dubiel, E.A., Kuehn, C., Wang, R. and Vermette, P. (2012). In vitro morphogenesis of PANC-1 cells into islet-like aggregates using RGD-covered dextran derivative surfaces. *Colloids and surfaces. B, Biointerfaces*, volume 89, p. 117-125.

[129] Andersen, P.L. and Vermette, P. (2017). Biomimetic Surfaces Supporting Dissociated Pancreatic Islet Cultures. *Colloids and Surfaces B: Biointerfaces*, volume 159, p. 166-173.

[130] Monchaux, E. and Vermette, P. (2007). Bioactive microarrays immobilized on low-fouling surfaces to study specific endothelial cell adhesion. *Biomacromolecules*, volume 8, p. 3668-3673.

[131] Cooke, M.J., Phillips, S.R., Shah, D.S., Athey, D., Lakey, J.H. and Przyborski, S.A. (2008). Enhanced cell attachment using a novel cell culture surface presenting functional domains from extracellular matrix proteins. *Cytotechnology*, volume 56, p. 71-79.

[132] Nguyen, H., Qian, J.J., Bhatnagar, R.S. and Li, S. (2003). Enhanced cell attachment and osteoblastic activity by P-15 peptide-coated matrix in hydrogels. *Biochemical and biophysical research communications*, volume 311, p. 179-186.

[133] Antonova, L.V., Seifalian, A.M., Kutikhin, A.G., Sevostyanova, V.V., Matveeva, V.G., Velikanova, E.A., Mironov, A.V., Shabaev, A.R., Glushkova, T.V., Senokosova, E.A., Vasyukov, G.Y., Krivkina, E.O., Burago, A.Y., Kudryavtseva, Y.A., Barbarash, O.L. and Barbarash, L.S. (2016). Conjugation with RGD Peptides and Incorporation of Vascular Endothelial Growth Factor Are Equally Efficient for Biofunctionalization of Tissue-Engineered Vascular Grafts. *International journal of molecular sciences*, volume 17, p.

[134] Dumbleton, J., Agarwal, P., Huang, H., Hogrebe, N., Han, R., Gooch, K.J. and He, X. (2016). The effect of RGD peptide on 2D and miniaturized 3D culture of HEPM cells, MSCs, and ADSCs with alginate hydrogel. *Cell Mol Bioeng*, volume 9, p. 277-288.

[135] Hunt, N.C., Hallam, D., Karimi, A., Mellough, C.B., Chen, J., Steel, D.H. and Lako, M. (2017). 3D culture of human pluripotent stem cells in RGD-alginate hydrogel improves retinal tissue development. *Acta biomaterialia*, volume 49, p. 329-343.

[136] Park, S.H., Zheng, J.H., Nguyen, V.H., Jiang, S.N., Kim, D.Y., Szardenings, M., Min, J.H., Hong, Y., Choy, H.E. and Min, J.J. (2016). RGD Peptide Cell-Surface Display Enhances

the Targeting and Therapeutic Efficacy of Attenuated Salmonella-mediated Cancer Therapy. *Theranostics*, volume 6, p. 1672-1682.

[137] Sobers, C.J., Wood, S.E. and Mrksich, M. (2015). A gene expression-based comparison of cell adhesion to extracellular matrix and RGD-terminated monolayers. *Biomaterials*, volume 52, p. 385-394.

[138] Gerecht, S., Burdick, J.A., Ferreira, L.S., Townsend, S.A., Langer, R. and Vunjak-Novakovic, G. (2007). Hyaluronic acid hydrogel for controlled self-renewal and differentiation of human embryonic stem cells. *Proceedings of the National Academy of Sciences of the United States of America*, volume 104, p. 11298-11303.

[139] Schizas, N., Rojas, R., Kootala, S., Andersson, B., Pettersson, J., Hilborn, J. and Hailer, N.P. (2014). Hyaluronic acid-based hydrogel enhances neuronal survival in spinal cord slice cultures from postnatal mice. *Journal of biomaterials applications*, volume 28, p. 825-836.

[140] Wight, T.N., Kinsella, M.G. and Qwarnstrom, E.E. (1992). The role of proteoglycans in cell adhesion, migration and proliferation. *Current opinion in cell biology*, volume 4, p. 793-801.

[141] von der Mark, K., Park, J., Bauer, S. and Schmuki, P. (2010). Nanoscale engineering of biomimetic surfaces: cues from the extracellular matrix. *Cell and tissue research*, volume 339, p. 131-153.

[142] Higuchi, A., Ling, Q.D., Hsu, S.T. and Umezawa, A. (2012). Biomimetic cell culture proteins as extracellular matrices for stem cell differentiation. *Chemical reviews*, volume 112, p. 4507-4540.

[143] Gilbert, T.W., Stewart-Akers, A.M., Simmons-Byrd, A. and Badylak, S.F. (2007). Degradation and remodeling of small intestinal submucosa in canine Achilles tendon repair. *The Journal of bone and joint surgery. American volume*, volume 89, p. 621-630.

[144] Beattie, A.J., Gilbert, T.W., Guyot, J.P., Yates, A.J. and Badylak, S.F. (2009). Chemoattraction of progenitor cells by remodeling extracellular matrix scaffolds. *Tissue engineering. Part A*, volume 15, p. 1119-1125.

[145] Brennan, E.P., Tang, X.H., Stewart-Akers, A.M., Gudas, L.J. and Badylak, S.F. (2008). Chemoattractant activity of degradation products of fetal and adult skin extracellular matrix

for keratinocyte progenitor cells. *Journal of tissue engineering and regenerative medicine*, volume 2, p. 491-498.

[146] Reing, J.E., Zhang, L., Myers-Irvin, J., Cordero, K.E., Freytes, D.O., Heber-Katz, E., Bedelbaeva, K., McIntosh, D., Dewilde, A., Braunhut, S.J. and Badylak, S.F. (2009). Degradation products of extracellular matrix affect cell migration and proliferation. *Tissue engineering. Part A*, volume 15, p. 605-614.

[147] Tran, K.T., Lamb, P. and Deng, J.S. (2005). Matrikines and matricryptins: Implications for cutaneous cancers and skin repair. *Journal of dermatological science*, volume 40, p. 11-20.

[148] Mahfouz, W., Elsalmy, S., Corcos, J. and Fayed, A.S. (2013). Fundamentals of bladder tissue engineering. *African Journal of Urology*, volume 19, p. 51-57.

[149] Wong, M.L. and Griffiths, L.G. (2014). Immunogenicity in xenogeneic scaffold generation: Antigen removal versus decellularization. *Acta biomaterialia*, volume 10, p. 1806-1816.

[150] Vadori, M. and Cozzi, E. (2015). The immunological barriers to xenotransplantation. *Tissue antigens*, volume 86, p. 239-253.

[151] Chen, G., Qian, H., Starzl, T., Sun, H., Garcia, B., Wang, X., Wise, Y., Liu, Y., Xiang, Y., Copeman, L., Liu, W., Jevnikar, A., Wall, W., Cooper, D.K., Murase, N., Dai, Y., Wang, W., Xiong, Y., White, D.J. and Zhong, R. (2005). Acute rejection is associated with antibodies to non-Gal antigens in baboons using Gal-knockout pig kidneys. *Nature medicine*, volume 11, p. 1295-1298.

[152] Campbell, P.M., Salam, A., Ryan, E.A., Senior, P., Paty, B.W., Bigam, D., McCready, T., Halpin, A., Imes, S., Al Saif, F., Lakey, J.R. and Shapiro, A.M. (2007). Pretransplant HLA antibodies are associated with reduced graft survival after clinical islet transplantation. *American journal of transplantation : official journal of the American Society of Transplantation and the American Society of Transplant Surgeons*, volume 7, p. 1242-1248.

[153] Zheng, M.H., Chen, J., Kirilak, Y., Willers, C., Xu, J. and Wood, D. (2005). Porcine small intestine submucosa (SIS) is not an acellular collagenous matrix and contains porcine DNA: possible implications in human implantation. *Journal of biomedical materials research. Part B, Applied biomaterials*, volume 73, p. 61-67.

[154] Shim, G., Kim, M.G., Park, J.Y. and Oh, Y.K., (2013). 11 - Small interfering RNAs (siRNAs) as cancer therapeutics. In: *Biomaterials for Cancer Therapeutics*, Woodhead Publishing, p. 237-269.

[155] Valentin, J.E., Badylak, J.S., McCabe, G.P. and Badylak, S.F. (2006). Extracellular matrix bioscaffolds for orthopaedic applications. A comparative histologic study. *The Journal of bone and joint surgery. American volume*, volume 88, p. 2673-2686.

[156] Hawkins, J.A., Hillman, N.D., Lambert, L.M., Jones, J., Di Russo, G.B., Profaizer, T., Fuller, T.C., Minich, L.L., Williams, R.V. and Shaddy, R.E. (2003). Immunogenicity of decellularized cryopreserved allografts in pediatric cardiac surgery: comparison with standard cryopreserved allografts. *The Journal of thoracic and cardiovascular surgery*, volume 126, p. 247-252; discussion 252-243.

[157] Konstantinovic, M.L., Lagae, P., Zheng, F., Verbeken, E.K., De Ridder, D. and Deprest, J.A. (2005). Comparison of host response to polypropylene and non-cross-linked porcine small intestine serosal-derived collagen implants in a rat model. *BJOG : an international journal of obstetrics and gynaecology*, volume 112, p. 1554-1560.

[158] Prevel, C.D., Eppley, B.L., Summerlin, D.J., Jackson, J.R., McCarty, M. and Badylak, S.F. (1995). Small intestinal submucosa: utilization for repair of rodent abdominal wall defects. *Annals of plastic surgery*, volume 35, p. 374-380.

[159] Wang, D., Ding, X., Xue, W., Zheng, J., Tian, X., Li, Y., Wang, X., Song, H., Liu, H. and Luo, X. (2017). A new scaffold containing small intestinal submucosa and mesenchymal stem cells improves pancreatic islet function and survival in vitro and in vivo. *International Journal of Molecular Medicine*, volume 39, p. 167-173.

[160] Keane, T.J. and Badylak, S.F. (2015). The host response to allogeneic and xenogeneic biological scaffold materials. *Journal of tissue engineering and regenerative medicine*, volume 9, p. 504-511.

[161] Aamodt, J.M. and Grainger, D.W. (2016). Extracellular Matrix-based Biomaterial Scaffolds and the Host Response. *Biomaterials*, volume 86, p. 68-82.

[162] Sandrin, M.S. and McKenzie, I.F. (1994). Gal alpha (1,3)Gal, the major xenoantigen(s) recognised in pigs by human natural antibodies. *Immunological reviews*, volume 141, p. 169-190.

[163] Lu, T.Y., Lin, B., Kim, J., Sullivan, M., Tobita, K., Salama, G. and Yang, L. (2013). Repopulation of decellularized mouse heart with human induced pluripotent stem cell-derived cardiovascular progenitor cells. *Nature communications*, volume 4, p. 2307.

[164] Stabler, C.T., Caires, L.C., Mondrinos, M.J., Marcinkiewicz, C., Lazarovici, P., Wolfson, M.R. and Lelkes, P.I. (2016). Enhanced Re-Endothelialization of Decellularized Rat Lungs. *Tissue engineering. Part C, Methods*, volume 22, p. 439-450.

[165] Lichtenberg, A., Tudorache, I., Cebotari, S., Ringes-Lichtenberg, S., Sturz, G., Hoeffler, K., Hurscheler, C., Brandes, G., Hilfiker, A. and Haverich, A. (2006). In vitro re-endothelialization of detergent decellularized heart valves under simulated physiological dynamic conditions. *Biomaterials*, volume 27, p. 4221-4229.

[166] Badylak, S.F. (2004). Xenogeneic extracellular matrix as a scaffold for tissue reconstruction. *Transplant Immunology*, volume 12, p. 367-377.

[167] Dickinson, L.E. and Gerecht, S. (2016). Engineered Biopolymeric Scaffolds for Chronic Wound Healing. *Frontiers in Physiology*, volume 7, p.

[168] Ren-Ke Li, R.D.W. (2014) *Cardiac Regeneration and Repair: Biomaterials and Tissue Engineering*, Woodhead Publishing Limited, Cambridge, p.

[169] U.S. Food and Drug Administration, (2017). 510(k) Clearances.https://www.fda.gov/MedicalDevices/ProductsandMedicalProcedures/DeviceApprovalsandClearances/510kClearances/default.htm, in.

[170] U.S. Food and Drug Administration, (2017). Classification of 510 (k) medical devices. https://www.fda.gov/MedicalDevices/DeviceRegulationandGuidance/Overview/ClassifyYourDevice. , in.

[171] U.S. Food and Drug Administration, (2017). FDA Regulation of Human Cells, Tissues, and Cellular and Tissue-Based Products (HCT/P's) Product List 2017. https://www.fda.gov/biologicsbloodvaccines/tissuetissueproducts/regulationoftissues/ucm150485.htm. p.

[172] U.S.Food and Drug Administration, (2017). Evaluating Substantial Equivalence in Premarket Notifications [510(k)] https://www.fda.gov/downloads/MedicalDevices/.../UCM284443.pdf., in.

[173] Snyder, D.L., Sullivan, N. and Schoelles, K.M., (2012). In: *Skin Substitutes for Treating Chronic Wounds*, Rockville (MD).

[174] Mitchell, R.I., Rappaport, A.M. and Davidson, J.K. (1966). Autotransplantation of the pancreas. *Canadian journal of surgery. Journal canadien de chirurgie*, volume 9, p. 192-198.

[175] Shapiro, A.M., Pokrywczynska, M. and Ricordi, C. (2017). Clinical pancreatic islet transplantation. *Nature reviews. Endocrinology*, volume 13, p. 268-277.

[176] Correa-Giannella, M.L. and Raposo do Amaral, A.S. (2009). Pancreatic islet transplantation. *Diabetology & metabolic syndrome*, volume 1, p. 9.

[177] Ichii, H. and Ricordi, C. (2009). Current status of islet cell transplantation. *Journal of hepato-biliary-pancreatic surgery*, volume 16, p. 101-112.

[178] Ryan, E.A., Lakey, J.R., Paty, B.W., Imes, S., Korbutt, G.S., Kneteman, N.M., Bigam, D., Rajotte, R.V. and Shapiro, A.M. (2002). Successful islet transplantation: continued insulin reserve provides long-term glycemic control. *Diabetes*, volume 51, p. 2148-2157.

[179] Bennet, W., Sundberg, B., Groth, C.G., Brendel, M.D., Brandhorst, D., Brandhorst, H., Bretzel, R.G., Elgue, G., Larsson, R., Nilsson, B. and Korsgren, O. (1999). Incompatibility between human blood and isolated islets of Langerhans: a finding with implications for clinical intraportal islet transplantation? *Diabetes*, volume 48, p. 1907-1914.

[180] Moberg, L., Johansson, H., Lukinius, A., Berne, C., Foss, A., Kallen, R., Ostraat, O., Salmela, K., Tibell, A., Tufveson, G., Elgue, G., Nilsson Ekdahl, K., Korsgren, O. and Nilsson, B. (2002). Production of tissue factor by pancreatic islet cells as a trigger of detrimental thrombotic reactions in clinical islet transplantation. *Lancet*, volume 360, p. 2039-2045.

[181] Bottino, R., Fernandez, L.A., Ricordi, C., Lehmann, R., Tsan, M.F., Oliver, R. and Inverardi, L. (1998). Transplantation of allogeneic islets of Langerhans in the rat liver: effects of macrophage depletion on graft survival and microenvironment activation. *Diabetes*, volume 47, p. 316-323.

[182] Barshes, N.R., Wyllie, S. and Goss, J.A. (2005). Inflammation-mediated dysfunction and apoptosis in pancreatic islet transplantation: implications for intrahepatic grafts. *Journal of leukocyte biology*, volume 77, p. 587-597.

[183] Thomas, F.T., Contreras, J.L., Bilbao, G., Ricordi, C., Curiel, D. and Thomas, J.M. (1999). Anoikis, extracellular matrix, and apoptosis factors in isolated cell transplantation. *Surgery*, volume 126, p. 299-304.

[184] de Groot, M., Schuurs, T.A. and van Schilfgaarde, R. (2004). Causes of limited survival of microencapsulated pancreatic islet grafts. *The Journal of surgical research*, volume 121, p. 141-150.

[185] Lim, F. and Sun, A.M. (1980). Microencapsulated islets as bioartificial endocrine pancreas. *Science*, volume 210, p. 908-910.

[186] Jacobs-Tulleneers-Thevissen, D., Chintinne, M., Ling, Z., Gillard, P., Schoonjans, L., Delvaux, G., Strand, B.L., Gorus, F., Keymeulen, B., Pipeleers, D. and Beta Cell Therapy Consortium, E.-F. (2013). Sustained function of alginate-encapsulated human islet cell implants in the peritoneal cavity of mice leading to a pilot study in a type 1 diabetic patient. *Diabetologia*, volume 56, p. 1605-1614.

[187] Kuehn, C., Lakey, J.R., Lamb, M.W. and Vermette, P. (2013). Young porcine endocrine pancreatic islets cultured in fibrin show improved resistance toward hydrogen peroxide. *Islets*, volume 5, p. 207-215.

[188] Safley, S.A., Cui, H., Cauffiel, S., Tucker-Burden, C. and Weber, C.J. (2008). Biocompatibility and immune acceptance of adult porcine islets transplanted intraperitoneally in diabetic NOD mice in calcium alginate poly-L-lysine microcapsules versus barium alginate microcapsules without poly-L-lysine. *Journal of diabetes science and technology*, volume 2, p. 760-767.

[189] Andrades, P., Asiedu, C., Rodriguez, C., Goodwin, J., Deckard, L.A., Jargal, U., Balgansuren, G. and Thomas, J.M. (2007). Insulin secretion from pancreatic islets in fibrin glue clots at different fibrinogen and thrombin concentrations. *Transplantation proceedings*, volume 39, p. 1607-1608.

[190] Weber, L.M., Hayda, K.N. and Anseth, K.S. (2008). Cell-matrix interactions improve beta-cell survival and insulin secretion in three-dimensional culture. *Tissue engineering. Part A*, volume 14, p. 1959-1968.

[191] Hynes, R.O. (2009). The extracellular matrix: not just pretty fibrils. *Science*, volume 326, p. 1216-1219.

[192] Kaido, T., Perez, B., Yebra, M., Hill, J., Cirulli, V., Hayek, A. and Montgomery, A.M. (2004). Alphav-integrin utilization in human beta-cell adhesion, spreading, and motility. *The Journal of biological chemistry*, volume 279, p. 17731-17737.

[193] Daoud, J., Petropavlovskaia, M., Rosenberg, L. and Tabrizian, M. (2010). The effect of extracellular matrix components on the preservation of human islet function in vitro. *Biomaterials*, volume 31, p. 1676-1682.

[194] Wang, R.N. and Rosenberg, L. (1999). Maintenance of beta-cell function and survival following islet isolation requires re-establishment of the islet-matrix relationship. *The Journal of endocrinology*, volume 163, p. 181-190.

[195] Mazza, G., Rombouts, K., Rennie Hall, A., Urbani, L., Vinh Luong, T., Al-Akkad, W., Longato, L., Brown, D., Maghsoudlou, P., Dhillon, A.P., Fuller, B., Davidson, B., Moore, K., Dhar, D., De Coppi, P., Malago, M. and Pinzani, M. (2015). Decellularized human liver as a natural 3D-scaffold for liver bioengineering and transplantation. *Scientific reports*, volume 5, p. 13079.

[196] Rosario, D.J., Reilly, G.C., Ali Salah, E., Glover, M., Bullock, A.J. and Macneil, S. (2008). Decellularization and sterilization of porcine urinary bladder matrix for tissue engineering in the lower urinary tract. *Regenerative medicine*, volume 3, p. 145-156.

[197] Oberwallner, B., Brodarac, A., Choi, Y.H., Saric, T., Anic, P., Morawietz, L. and Stamm, C. (2014). Preparation of cardiac extracellular matrix scaffolds by decellularization of human myocardium. *Journal of biomedical materials research. Part A*, volume 102, p. 3263-3272.

[198] Davis, N.E., Beenken-Rothkopf, L.N., Mirsoian, A., Kojic, N., Kaplan, D.L., Barron, A.E. and Fontaine, M.J. (2012). Enhanced function of pancreatic islets co-encapsulated with ECM proteins and mesenchymal stromal cells in a silk hydrogel. *Biomaterials*, volume 33, p. 6691-6697.

[199] Andersen, P.L. and Vermette, P. (2016). Intracellular insulin quantification by cell-ELISA. *Experimental cell research*, volume 347, p. 14-23.

[200] Gilbert, T.W., Sellaro, T.L. and Badylak, S.F. (2006). Decellularization of tissues and organs. *Biomaterials*, volume 27, p. 3675-3683.

[201] Gilbert, T.W. (2012). Strategies for tissue and organ decellularization. *Journal of cellular biochemistry*, volume 113, p. 2217-2222.

[202] Schaner, P.J., Martin, N.D., Tulenko, T.N., Shapiro, I.M., Tarola, N.A., Leichter, R.F., Carabasi, R.A. and Dimuzio, P.J. (2004). Decellularized vein as a potential scaffold for vascular tissue engineering. *J Vasc Surg*, volume 40, p. 146-153.

[203] Phillips, G.O., DM, S., R, v.V. and A, N. (1998) *Advances in Tissue Banking*, World Scientific Publishing Company, Singapore, p.

[204] Liao, Q., Chiu, N.H., Shen, C., Chen, Y. and Vouros, P. (2007). Investigation of enzymatic behavior of benzonase/alkaline phosphatase in the digestion of oligonucleotides and DNA by ESI-LC/MS. *Analytical chemistry*, volume 79, p. 1907-1917.

[205] Sun H, Z.Y., Herzog EL, (2016). Experimental Approaches for the Investigation of Innate Immunity. In, World Scientific Publishing Co. Pte. Ltd., USA, p. 55-65.

[206] Ucuzian, A.A., Gassman, A.A., East, A.T. and Greisler, H.P. (2010). Molecular mediators of angiogenesis. *J Burn Care Res*, volume 31, p. 158-175.

[207] Lodish H, B.A., Zipursky SL, et al (2000) *Molecular Cell Biology*, 4th, W. H. Freeman, New York, p.

[208] Bouwens, L. (2004). Islet morphogenesis and stem cell markers. *Cell biochemistry and biophysics*, volume 40, p. 81-88.

[209] Bosco, D., Meda, P., Halban, P.A. and Rouiller, D.G. (2000). Importance of cell-matrix interactions in rat islet beta-cell secretion in vitro: role of alpha6beta1 integrin. *Diabetes*, volume 49, p. 233-243.

[210] Bertelli E, R.M., Orazioli D, Bendayan M. (2001). Association between islets of Langerhans and pancreatic ductal system in adult rat. Where endocrine and exocrine meet together? *Diabetologia*, volume 44, p. 575-584.

[211] Evan A.Dubiel, J.R.T.L., Morgan W.Lamb, and Patrick Vermette (2014). Culturing Free-Floating and Fibrin-Embedded Islets with Endothelial Cells: Effects on Insulin Secretion and Apoptosis. *Cellular and Molecular Bioengineering*, volume 7, p. 243–253.

[212] Riopel, M., Stuart, W. and Wang, R. (2013). Fibrin improves beta (INS-1) cell function, proliferation and survival through integrin alphavbeta3. *Acta biomaterialia*, volume 9, p. 8140-8148.

[213] Yap, W.T., Salvay, D.M., Silliman, M.A., Zhang, X., Bannon, Z.G., Kaufman, D.B., Lowe, W.L., Jr. and Shea, L.D. (2013). Collagen IV-modified scaffolds improve islet survival and function and reduce time to euglycemia. *Tissue engineering. Part A*, volume 19, p. 2361-2372.

[214] Nagata, N., Gu, Y., Hori, H., Balamurugan, A.N., Touma, M., Kawakami, Y., Wang, W., Baba, T.T., Satake, A., Nozawa, M., Tabata, Y. and Inoue, K. (2001). Evaluation of insulin

secretion of isolated rat islets cultured in extracellular matrix. *Cell transplantation*, volume 10, p. 447-451.

[215] Hammar, E.B., Irminger, J.C., Rickenbach, K., Parnaud, G., Ribaux, P., Bosco, D., Rouiller, D.G. and Halban, P.A. (2005). Activation of NF-kappaB by extracellular matrix is involved in spreading and glucose-stimulated insulin secretion of pancreatic beta cells. *The Journal of biological chemistry*, volume 280, p. 30630-30637.

[216] Bendayan, M., Duhr, M.A. and Gingras, D. (1986). Studies on pancreatic acinar cells in tissue culture: basal lamina (basement membrane matrix promotes three-dimensional reorganization. *European journal of cell biology*, volume 42, p. 60-67.

[217] Hulinsky, I., Cooney, S., Harrington, J. and Silink, M. (1995). In vitro growth of neonatal rat islet cells is stimulated by adhesion to matrix. *Hormone and metabolic research = Hormon- und Stoffwechselforschung = Hormones et metabolisme*, volume 27, p. 209-215.

[218] Zhang, Z., Vuori, K., Reed, J.C. and Ruoslahti, E. (1995). The alpha 5 beta 1 integrin supports survival of cells on fibronectin and up-regulates Bcl-2 expression. *Proceedings of the National Academy of Sciences of the United States of America*, volume 92, p. 6161-6165.

[219] Daoud, J., Petropavlovskaia, M., Rosenberg, L. and Tabrizian, M. (2010). The effect of extracellular matrix components on the preservation of human islet function in vitro. *Biomaterials*, volume 31, p. 1676-1682.

[220] Beattie, G.M., Montgomery, A.M., Lopez, A.D., Hao, E., Perez, B., Just, M.L., Lakey, J.R., Hart, M.E. and Hayek, A. (2002). A novel approach to increase human islet cell mass while preserving beta-cell function. *Diabetes*, volume 51, p. 3435-3439.

[221] Chaimov, D., Baruch, L., Krishtul, S., Meivar-levy, I., Ferber, S. and Machluf, M. (2017). Innovative encapsulation platform based on pancreatic extracellular matrix achieve substantial insulin delivery. *Journal of Controlled Release*, volume 257, p. 91-101.

[222] Naba, A., Clauser, K.R., Mani, D.R., Carr, S.A. and Hynes, R.O. (2017). Quantitative proteomic profiling of the extracellular matrix of pancreatic islets during the angiogenic switch and insulinoma progression. *Scientific reports*, volume 7, p. 40495.

[223] Damodaran, R.G. and Vermette, P. (2017). Decellularized pancreas as a native extracellular matrix scaffold for islets. submitted for publication. p.

[224] Cassel, J.M. and Kanagy, J.R. (1949). Studies on the Purification of Collagen. *Journal of research of the National Bureau of Standards* volume 42, p. 557-565.

[225] Bradford, M.M. (1976). A rapid and sensitive method for the quantitation of microgram quantities of protein utilizing the principle of protein-dye binding. *Analytical biochemistry*, volume 72, p. 248-254.

[226] Vigier, S., Gagnon, H., Bourgade, K., Klarskov, K., Fülöp, T. and Vermette, P. (2017). Composition and organization of the pancreatic extracellular matrix by combined methods of immunohistochemistry, proteomics and scanning electron microscopy. *Current Research in Translational Medicine*, volume 65, p. 31-39.

[227] Hill, R.C., Calle, E.A., Dzieciatkowska, M., Niklason, L.E. and Hansen, K.C. (2015). Quantification of Extracellular Matrix Proteins from a Rat Lung Scaffold to Provide a Molecular Readout for Tissue Engineering. *Molecular & Cellular Proteomics : MCP*, volume 14, p. 961-973.

[228] Martin, Y., Boutin, D. and Vermette, P. (2007). Study of the effect of process parameters for n-heptylamine plasma polymerization on final layer properties. *Thin Solid Films*, volume 515, p. 6844-6852.

[229] Dubiel, E.A. and Vermette, P. (2012). Solution composition impacts fibronectin immobilization on carboxymethyl-dextran surfaces and INS-1 insulin secretion. *Colloids and Surfaces B: Biointerfaces*, volume 95, p. 266-273.

[230] Morini, S., Braun, M., Onori, P., Cicalese, L., Elias, G., Gaudio, E. and Rastellini, C. (2006). Morphological changes of isolated rat pancreatic islets: a structural, ultrastructural and morphometric study. *Journal of Anatomy*, volume 209, p. 381-392.

[231] Carter, J.D., Dula, S.B., Corbin, K.L., Wu, R. and Nunemaker, C.S. (2009). A Practical Guide to Rodent Islet Isolation and Assessment. *Biological Procedures Online*, volume 11, p. 3-31.

[232] Rajesh, G.D., Alexandre, P., Benoît, C., L., A.P. and Patrick, V. Insulin secretion kinetics from single islets reveals distinct subpopulations. *Biotechnology Progress*, volume 0, p.

[233] Hopcroft, D.W., Mason, D.R. and Scott, R.S. (1985). Standardization of insulin secretion from pancreatic islets: validation of a DNA assay. *Hormone and metabolic research = Hormon- und Stoffwechselforschung = Hormones et metabolisme*, volume 17, p. 559-561.

[234] Reaven, E.P., Gold, G., Walker, W. and Reaven, G.M. (1981). Effect of variations in islet size and shape on glucose-stimulated insulin secretion. *Hormone and metabolic research = Hormon- und Stoffwechselforschung = Hormones et metabolisme*, volume 13, p. 673-674.

[235] Lehmann, R., Zuellig, R.A., Kugelmeier, P., Baenninger, P.B., Moritz, W., Perren, A., Clavien, P.A., Weber, M. and Spinas, G.A. (2007). Superiority of small islets in human islet transplantation. *Diabetes*, volume 56, p. 594-603.

[236] Farhat, B., Almelkar, A., Ramachandran, K., Williams, S.J., Huang, H.H., Zamierowksi, D., Novikova, L. and Stehno-Bittel, L. (2013). Small human islets comprised of more beta-cells with higher insulin content than large islets. *Islets*, volume 5, p. 87-94.

[237] MacGregor, R.R., Williams, S.J., Tong, P.Y., Kover, K., Moore, W.V. and Stehno-Bittel, L. (2006). Small rat islets are superior to large islets in in vitro function and in transplantation outcomes. *American journal of physiology. Endocrinology and metabolism*, volume 290, p. E771-779.

[238] Curry, D.L., Bennett, L.L. and Grodsky, G.M. (1968). Dynamics of insulin secretion by the perfused rat pancreas. *Endocrinology*, volume 83, p. 572-584.

[239] Barg, S., Eliasson, L., Renstrom, E. and Rorsman, P. (2002). A subset of 50 secretory granules in close contact with L-type Ca2+ channels accounts for first-phase insulin secretion in mouse beta-cells. *Diabetes*, volume 51 Suppl 1, p. S74-82.

[240] Gerich, J.E. (2002). Is reduced first-phase insulin release the earliest detectable abnormality in individuals destined to develop type 2 diabetes? *Diabetes*, volume 51 Suppl 1, p. S117-121.

[241] Grodsky, G.M. (1972). A threshold distribution hypothesis for packet storage of insulin and its mathematical modeling. *The Journal of clinical investigation*, volume 51, p. 2047-2059.

[242] Rorsman, P. and Renstrom, E. (2003). Insulin granule dynamics in pancreatic beta cells. *Diabetologia*, volume 46, p. 1029-1045.

[243] Gerich, J.E. (1993). Control of glycaemia. *Bailliere's clinical endocrinology and metabolism*, volume 7, p. 551-586.

[244] Kahn, S.E. (2001). Clinical review 135: The importance of beta-cell failure in the development and progression of type 2 diabetes. *The Journal of clinical endocrinology and metabolism*, volume 86, p. 4047-4058.

[245] Duckworth, W.C., Bennett, R.G. and Hamel, F.G. (1998). Insulin degradation: progress and potential. *Endocrine reviews*, volume 19, p. 608-624.

[246] Chen, J., Nittala, A., Gao, S., Ghosh, S., Wang, X. and Patel, S. (2010). Kinetics of insulin secretion to acute, repetitive stimulation of islets in vivo in Sprague Dawley rats. *Islets*, volume 2, p. 10-17.

[247] Henquin, J.C., Nenquin, M., Stiernet, P. and Ahren, B. (2006). In vivo and in vitro glucose-induced biphasic insulin secretion in the mouse: pattern and role of cytoplasmic Ca2+ and amplification signals in beta-cells. *Diabetes*, volume 55, p. 441-451.

[248] Zhu, S., Larkin, D., Lu, S., Inouye, C., Haataja, L., Anjum, A., Kennedy, R., Castle, D. and Arvan, P. (2016). Monitoring C-Peptide Storage and Secretion in Islet beta-Cells In Vitro and In Vivo. *Diabetes*, volume 65, p. 699-709.

[249] de Haan, B.J., Faas, M.M., Spijker, H., van Willigen, J.W., de Haan, A. and de Vos, P. (2004). Factors influencing isolation of functional pancreatic rat islets. *Pancreas*, volume 29, p. e15-22.

[250] Lacy, P.E. and Kostianovsky, M. (1967). Method for the isolation of intact islets of Langerhans from the rat pancreas. *Diabetes*, volume 16, p. 35-39.

[251] Kin, T., Zhai, X., Murdoch, T.B., Salam, A., Shapiro, A.M. and Lakey, J.R. (2007). Enhancing the success of human islet isolation through optimization and characterization of pancreas dissociation enzyme. *American journal of transplantation : official journal of the American Society of Transplantation and the American Society of Transplant Surgeons*, volume 7, p. 1233-1241.

[252] Dyrskog, S.E., Erlandsen, M., Chen, J., Hong, J., Abudula, R. and Hermansen, K. (2007). Comparison of insulin responses in experiments using pooled mice islets versus islets from individual animals in the study of diabetes. *Metabolism: clinical and experimental*, volume 56, p. 304-307.

[253] Ulloa-Aguirre, A. and Conn, P.M. (2014) *Cellular Endocrinology in Health and Disease*, 1st, Academic press, Elsevier., London,UK., p.

[254] Ricordi, C. (1991). Quantitative and qualitative standards for islet isolation assessment in humans and large mammals. *Pancreas*, volume 6, p. 242-244.

[255] Kin, T., Senior, P., O'Gorman, D., Richer, B., Salam, A. and Shapiro, A.M. (2008). Risk factors for islet loss during culture prior to transplantation. *Transplant international :*

official journal of the European Society for Organ Transplantation, volume 21, p. 1029-1035.

[256] Dishinger, J.F., Reid, K.R. and Kennedy, R.T. (2009). Quantitative monitoring of insulin secretion from single islets of Langerhans in parallel on a microfluidic chip. *Analytical chemistry*, volume 81, p. 3119-3127.

[257] Song, S.H., Kjems, L., Ritzel, R., McIntyre, S.M., Johnson, M.L., Veldhuis, J.D. and Butler, P.C. (2002). Pulsatile insulin secretion by human pancreatic islets. *The Journal of clinical endocrinology and metabolism*, volume 87, p. 213-221.

[258] Barbulovic-Nad and Wheeler, A.R. (2008) *Encyclopedia of Micro- and Nanofluidics*, Springer, Heidelberg p.

[259] Storer, A.C. and Cornish-Bowden, A. (1976). Kinetics of rat liver glucokinase. Co-operative interactions with glucose at physiologically significant concentrations. *The Biochemical journal*, volume 159, p. 7-14.

[260] Ramachandran, K., Peng, X., Bokvist, K. and Stehno-Bittel, L. (2014). Assessment of re-aggregated human pancreatic islets for secondary drug screening. *British journal of pharmacology*, volume 171, p. 3010-3022.

[261] Grodsky, G.M., Batts, A.A., Bennett, L.L., Vcella, C., McWilliams, N.B. and Smith, D.F. (1963). Effects of Carbohydrates on Secretion of Insulin from Isolated Rat Pancreas. *The American journal of physiology*, volume 205, p. 638-644.

[262] Low, J.T., Mitchell, J.M., Do, O.H., Bax, J., Rawlings, A., Zavortink, M., Morgan, G., Parton, R.G., Gaisano, H.Y. and Thorn, P. (2013). Glucose principally regulates insulin secretion in mouse islets by controlling the numbers of granule fusion events per cell. *Diabetologia*, volume 56, p. 2629-2637.

[263] Markovic, R., Stozer, A., Gosak, M., Dolensek, J., Marhl, M. and Rupnik, M.S. (2015). Progressive glucose stimulation of islet beta cells reveals a transition from segregated to integrated modular functional connectivity patterns. *Scientific reports*, volume 5, p. 7845.

[264] Schuit, F.C., In't Veld, P.A. and Pipeleers, D.G. (1988). Glucose stimulates proinsulin biosynthesis by a dose-dependent recruitment of pancreatic beta cells. *Proceedings of the National Academy of Sciences of the United States of America*, volume 85, p. 3865-3869.

[265] Buchwald, P. (2011). A local glucose-and oxygen concentration-based insulin secretion model for pancreatic islets. *Theoretical biology & medical modelling*, volume 8, p. 20.

[266] Eizirik, D.L., Korbutt, G.S. and Hellerstrom, C. (1992). Prolonged exposure of human pancreatic islets to high glucose concentrations in vitro impairs the beta-cell function. *The Journal of clinical investigation*, volume 90, p. 1263-1268.

[267] Olofsson, C.S., Collins, S., Bengtsson, M., Eliasson, L., Salehi, A., Shimomura, K., Tarasov, A., Holm, C., Ashcroft, F. and Rorsman, P. (2007). Long-term exposure to glucose and lipids inhibits glucose-induced insulin secretion downstream of granule fusion with plasma membrane. *Diabetes*, volume 56, p. 1888-1897.

[268] Campos, C. (2012). Chronic Hyperglycemia and Glucose Toxicity: Pathology and Clinical Sequelae. *Postgraduate Medicine*, volume 124, p. 90-97.

[269] Alqahtani, N., Khan, W.A.G., Alhumaidi, M.H. and Ahmed, Y.A.A.R. (2013). Use of Glycated Hemoglobin in the Diagnosis of Diabetes Mellitus and Pre-diabetes and Role of Fasting Plasma Glucose, Oral Glucose Tolerance Test. *International Journal of Preventive Medicine*, volume 4, p. 1025-1029.

[270] Huang, H.H., Novikova, L., Williams, S.J., Smirnova, I.V. and Stehno-Bittel, L. (2011). Low insulin content of large islet population is present in situ and in isolated islets. *Islets*, volume 3, p. 6-13.

Appendix A

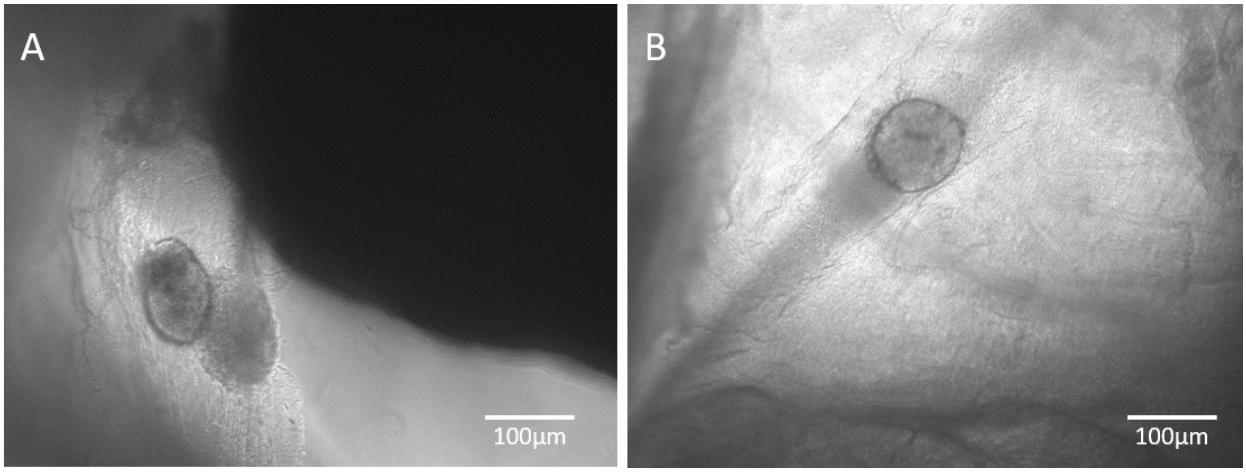

Supplemental Figure 1. Optical microscope images of infused islets inside a decellularized pancreas.

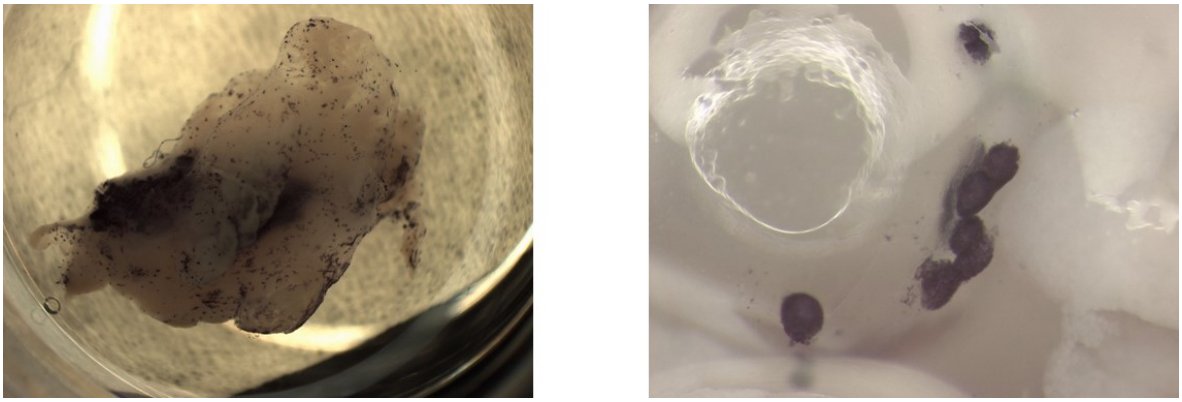

Supplemental Figure 2. Metabolic activity by 3-(4,5-dimethylthiazol-2-Yl)-2,5-diphenyltetrazolium bromide (MTT) staining of (A) INS-1 cells following 6 days of culture in decellularized pancreas and (B) islets following 48 hours of culture in decellularized pancreas.

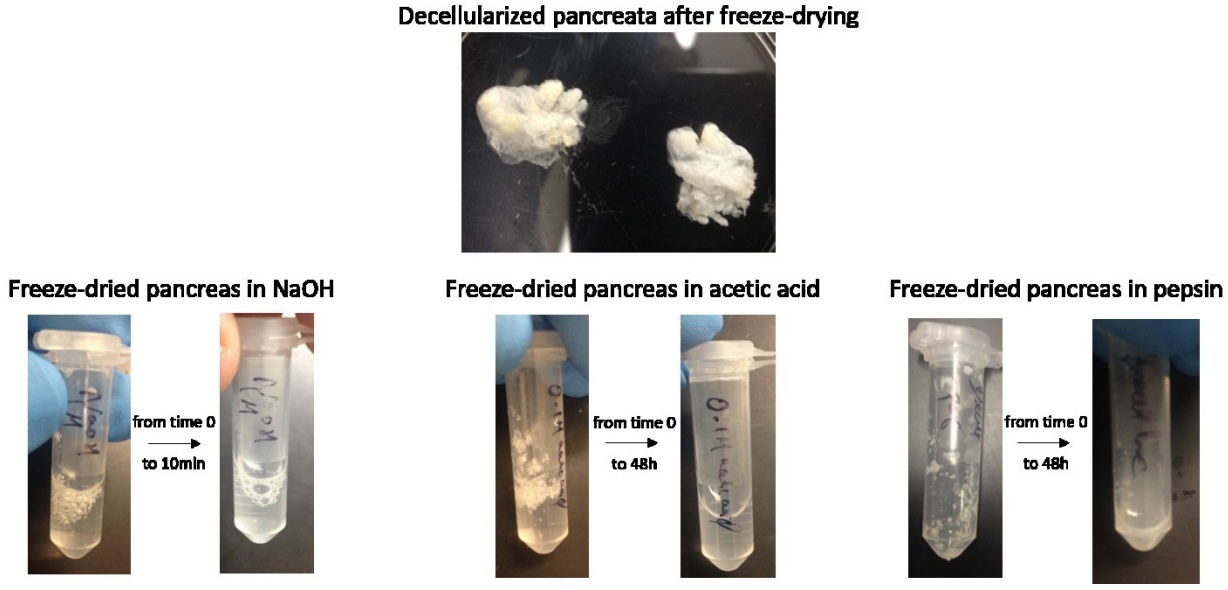

Supplemental Figure 3. Decellularized pancreata before and after solubilisation using the three methods.

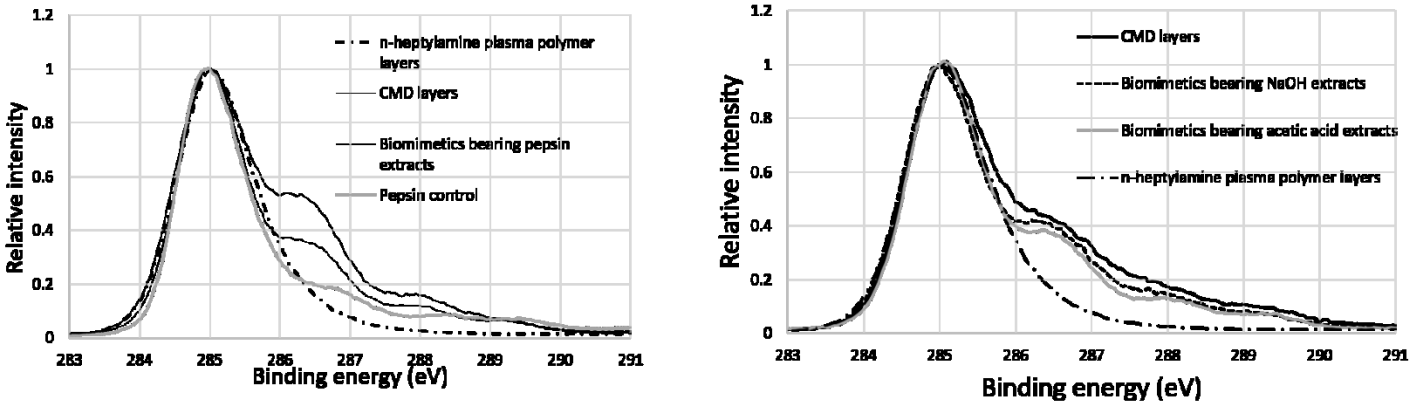

Supplemental Figure 4. High-resolution X-ray photoelectron spectroscopy (XPS) C 1s spectra of the different surfaces. Pepsin control refers to activated CMD surfaces incubated in a solution with only pepsin without decellularized pancreata.

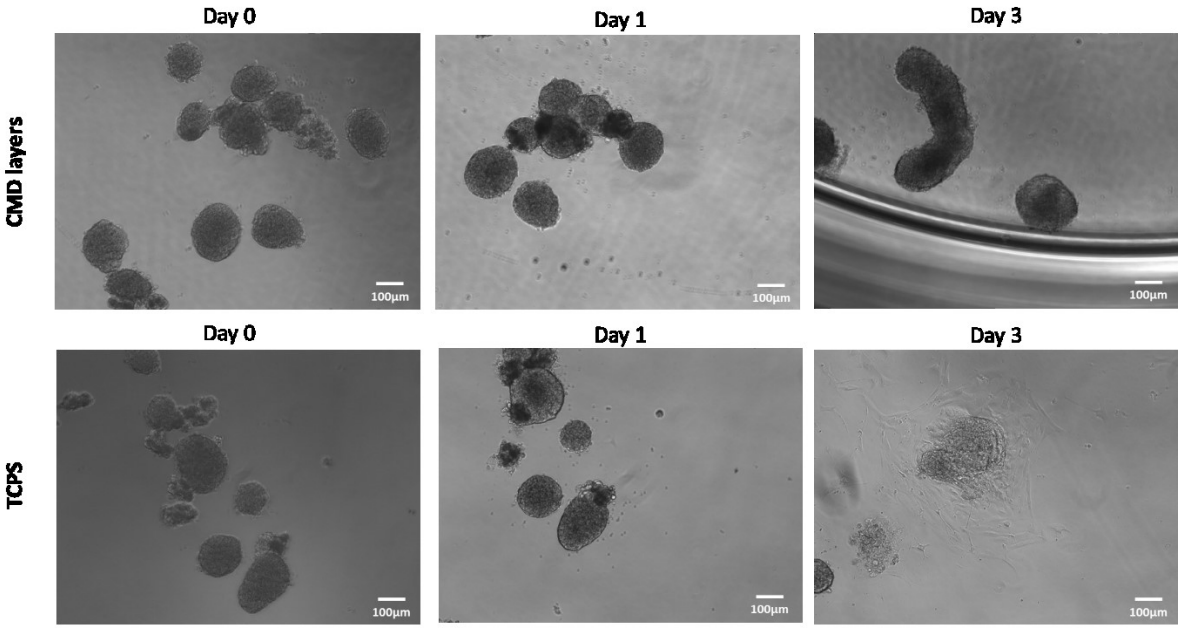

Supplemental Figure 5. Islet morphology from Day 0 to Day 3 for islets cultured on CMD layers and tissue culture polystyrene (TCPS).

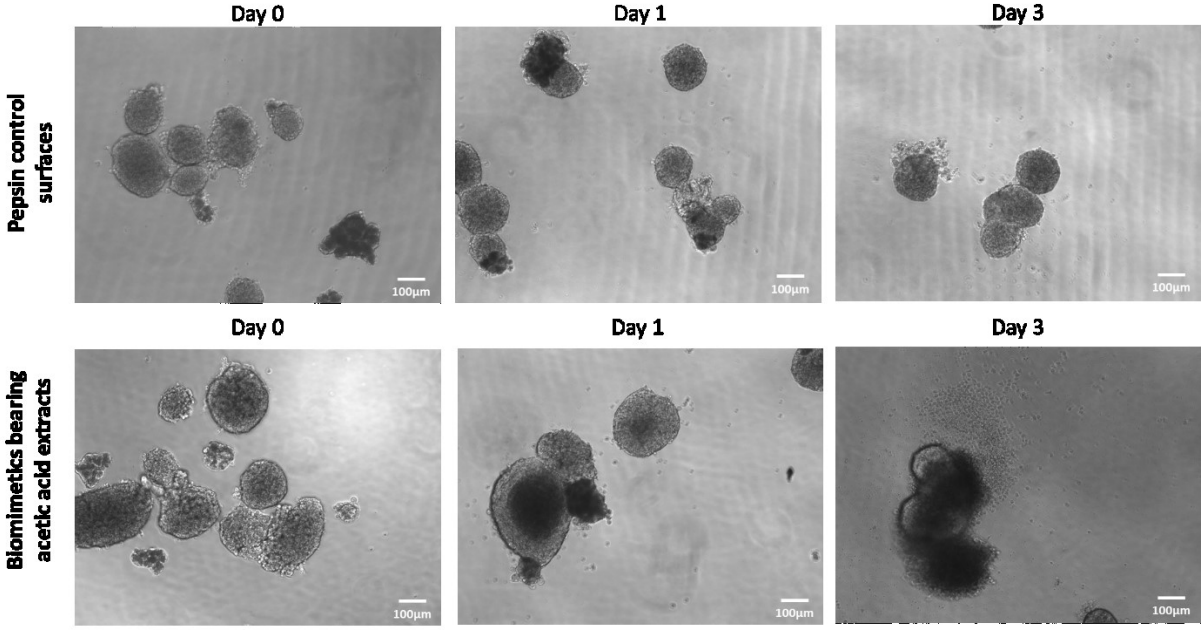

Supplemental Figure 6. Islet morphology from Day 0 to Day 3 for islets cultured on pepsin control surfaces and biomimetics bearing acetic acid extracts.

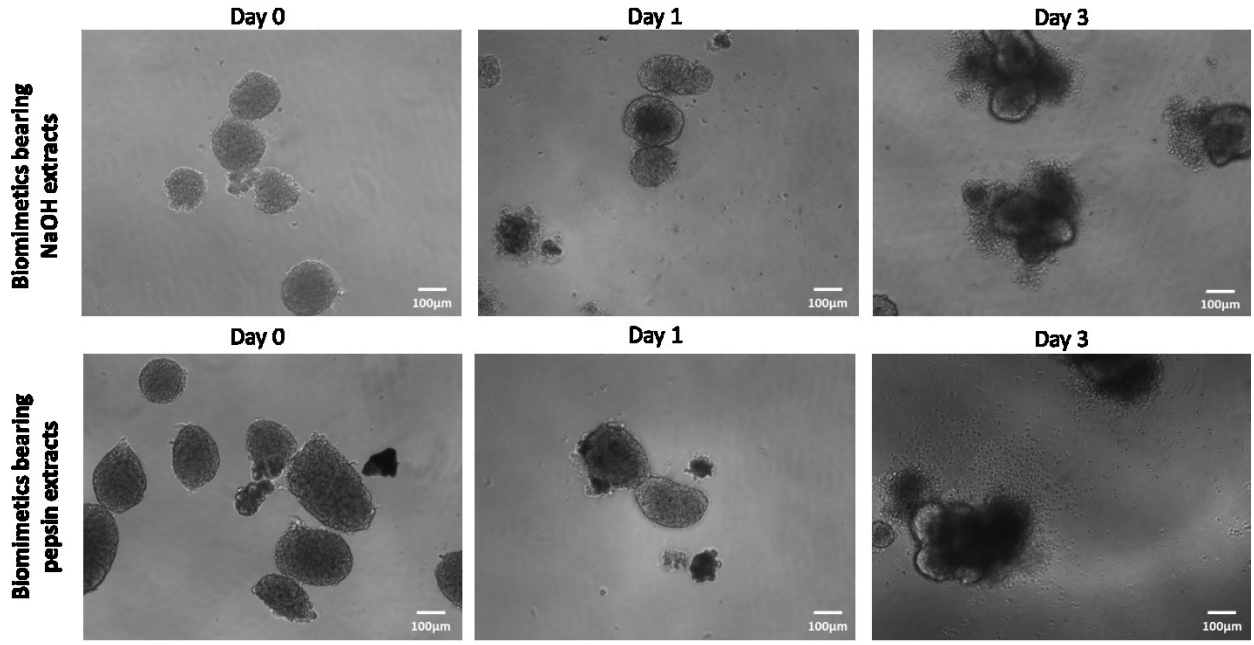

Supplemental Figure 7. Islet morphology from Day 0 to Day 3 for islets cultured on biomimetics bearing NaOH and pepsin extracts.

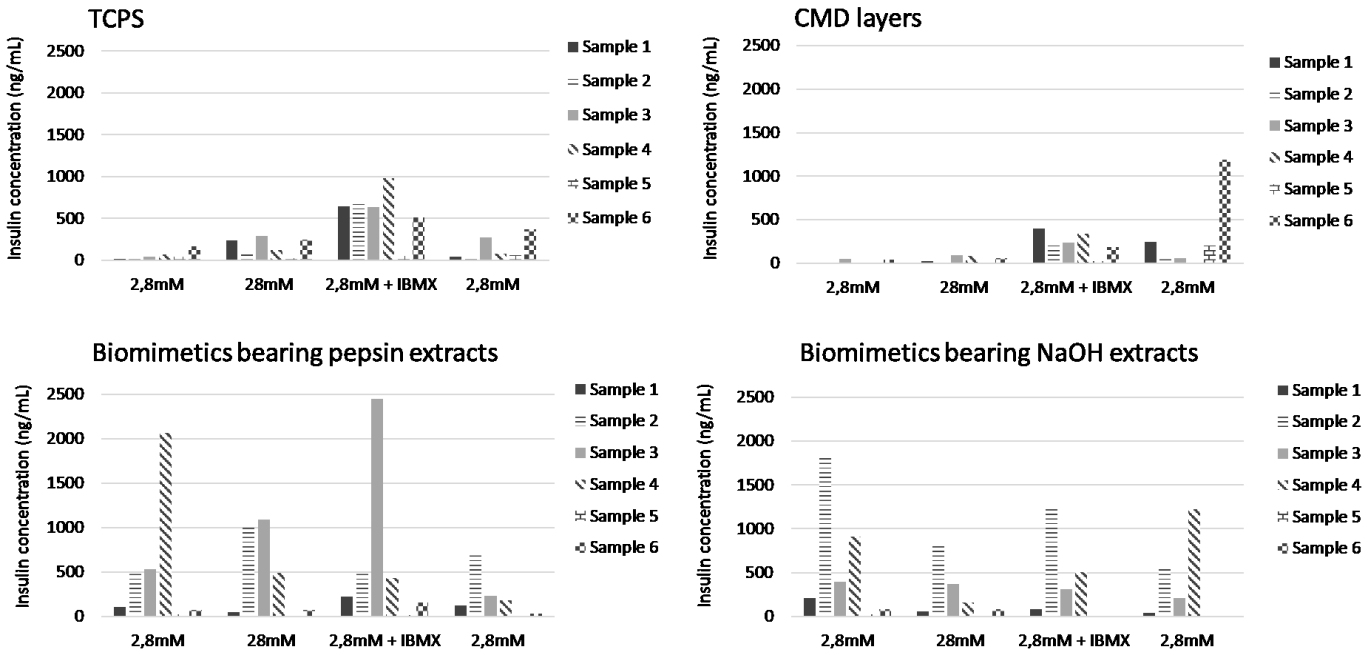

Supplemental Figure 8. Glucose-stimulated insulin secretion (GSIS) of islets cultured 5 days on TCPS, CMD layers, biomimetics bearing pepsin extracts and biomimetics bearing NaOH extracts.

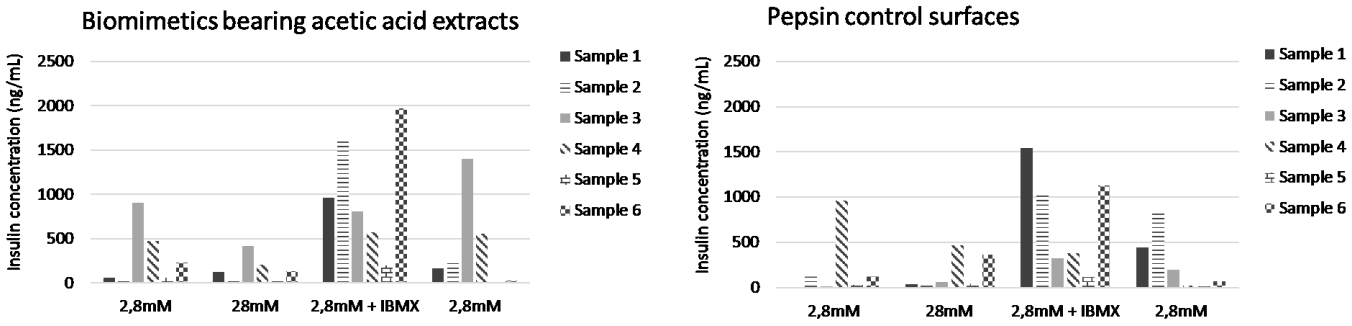

Supplemental Figure 9. Glucose-stimulated insulin secretion (GSIS) of islets cultured 5 days on biomimetics bearing acetic acid extracts and pepsin control surfaces.

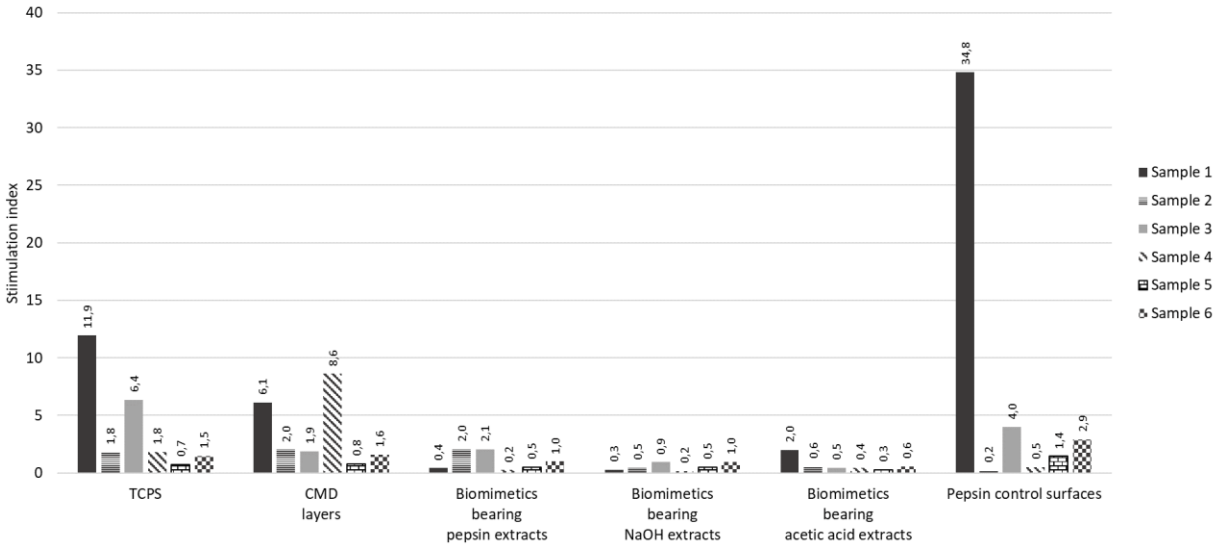

Supplemental Figure 10. Stimulation indices calculated from the glucose-stimulated insulin secretion (GSIS) assay of islets cultured 5 days on the different surfaces.
These stimulation indices are calculated by taking ratios of insulin concentration at high glucose to that at the first low glucose.

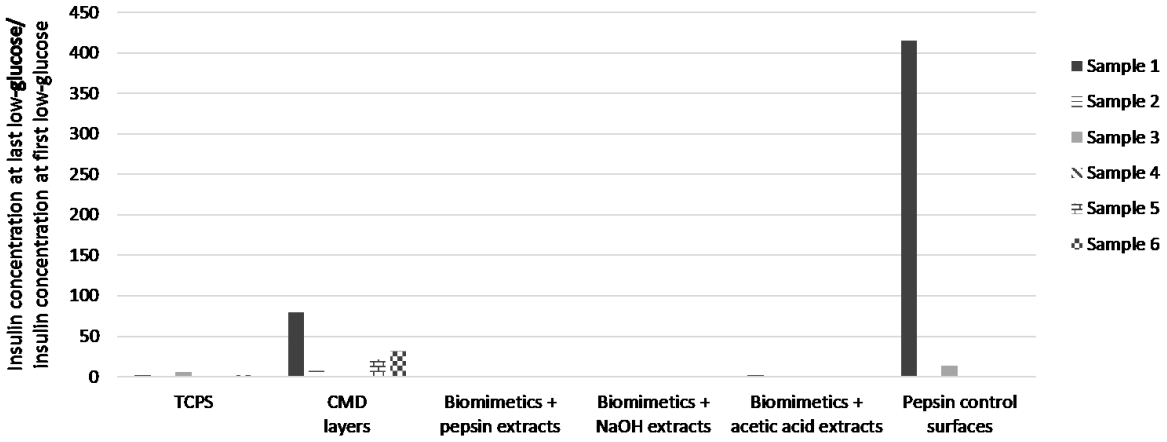

Supporting Figure 11. Ratios of insulin concentration measured at last low glucose to that at first low glucose from glucose-stimulated insulin secretion (GSIS) assays of islets cultured 5 days on the different surfaces.

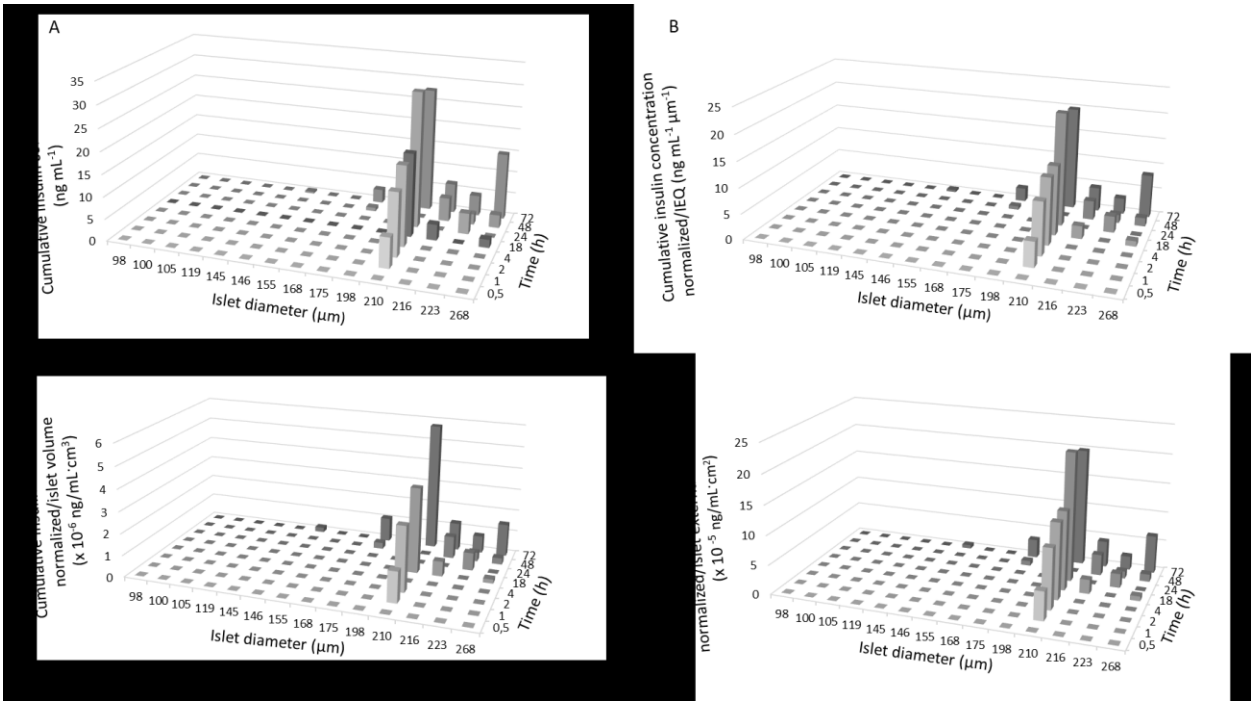

Supplemental Figure 12. (A) Measured cumulative insulin concentration, (B) normalized per IEQ, (C) normalized per islet volume, and (D) normalized per islet external surface area from single islets exposed to 2.8mM glucose for 72h.

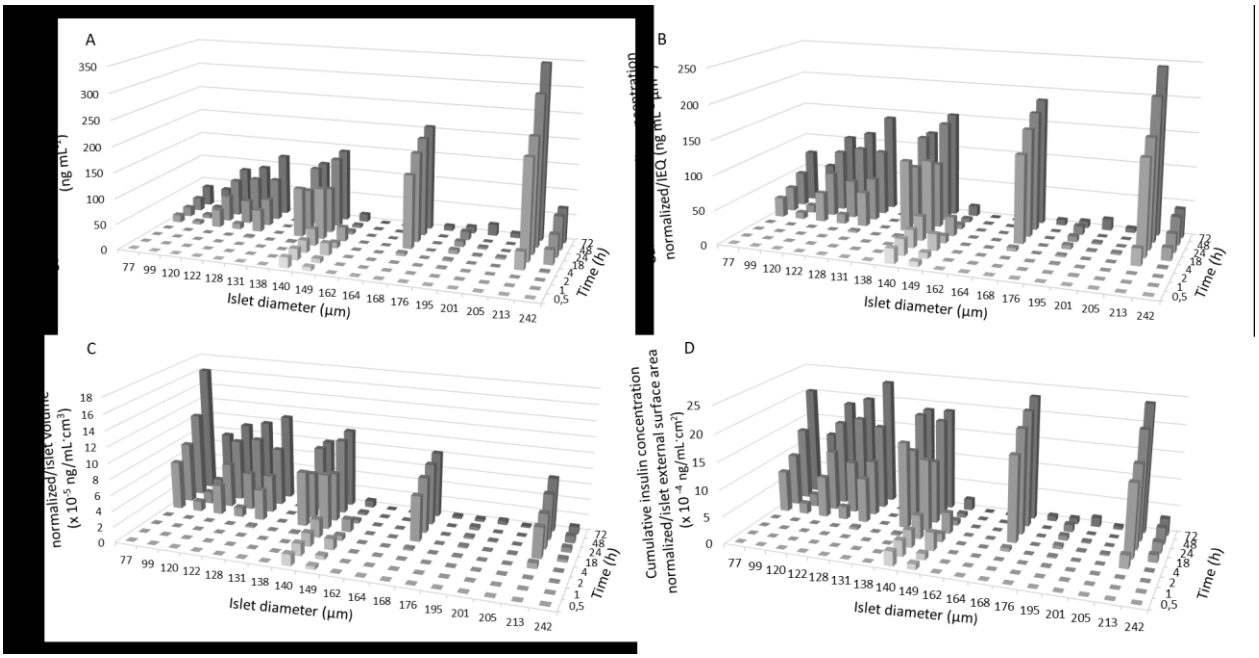

Supplemental Figure 13. (A) Measured cumulative insulin concentration, (B) normalized per IEQ, (C) normalized per islet volume, and (D) normalized per islet external surface area from single islets exposed to 5.6mM glucose for 72h.

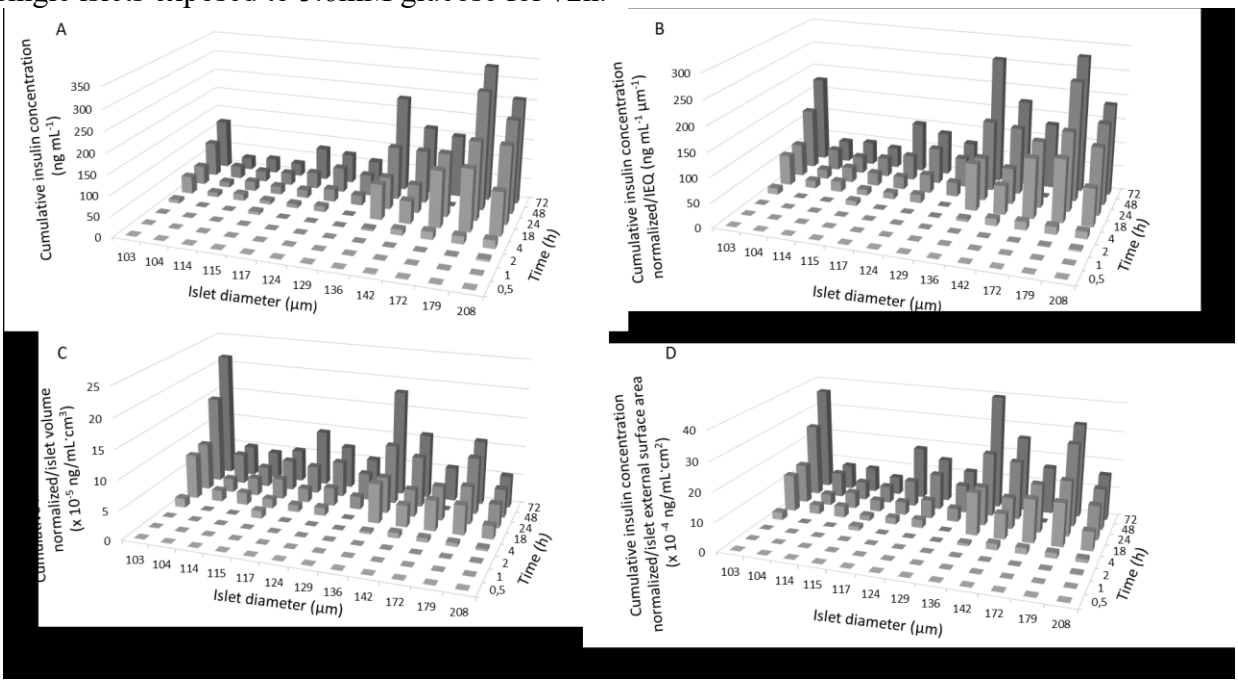

Supplemental Figure 14. (A) Measured cumulative insulin concentration, (B) normalized per IEQ, (C) normalized per islet volume, and (D) normalized per islet external surface area from single islets exposed to 11.2mM glucose for 72h.

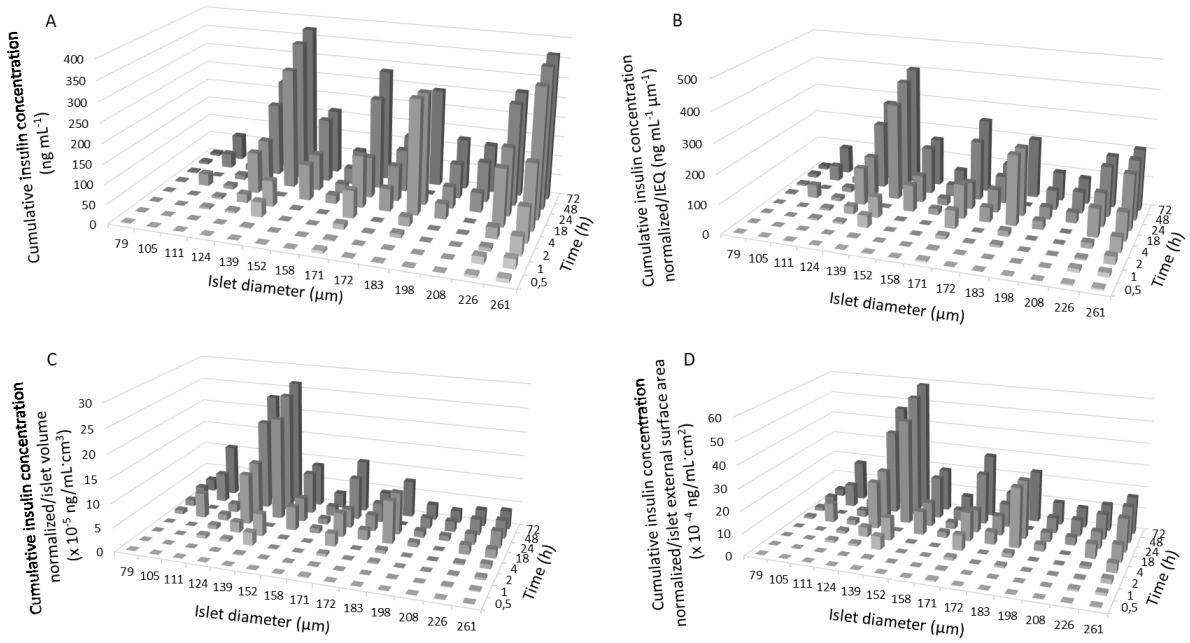

Supplemental Figure 15. (A) Measured cumulative insulin concentration, (B) normalized per IEQ, (C) normalized per islet volume, and (D) normalized per islet external surface area from single islets exposed to 20mM glucose for 72h.

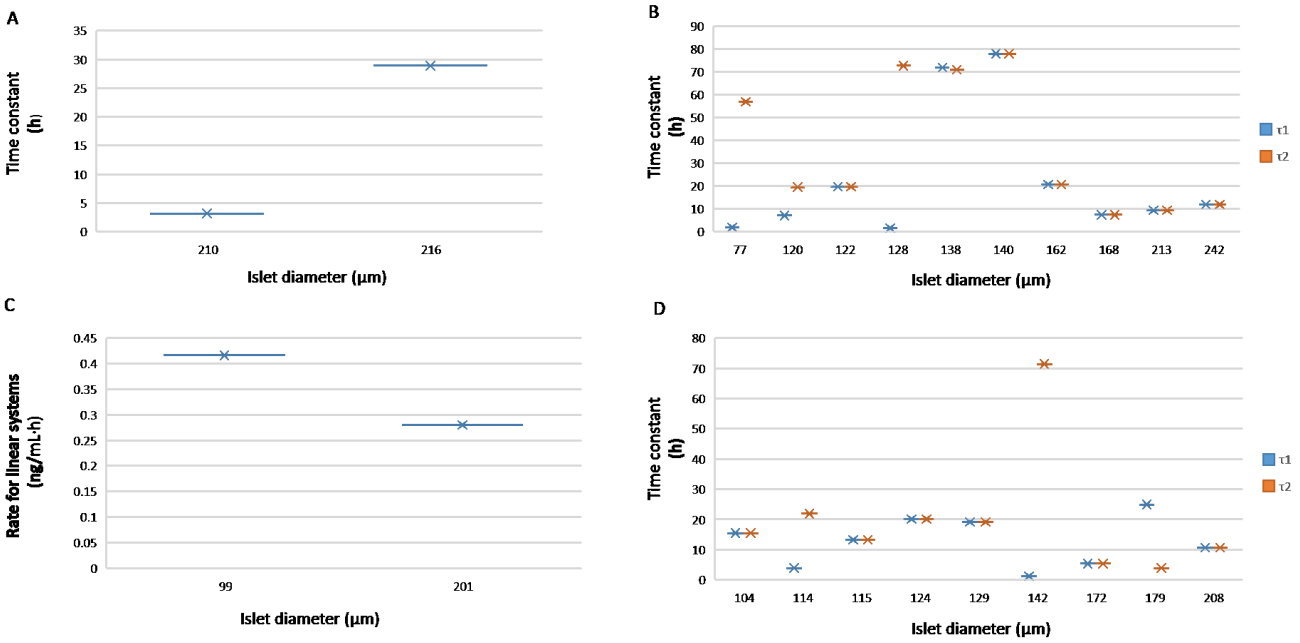

Supplemental Figure 16. Time constants for single islets modeled from (A) fast secretors in 2.8mM glucose and (B) slow secretors in 5.6mM glucose. (C) Rates of insulin secretion for constant-rate secretors (single islets) in 5.6mM glucose. (D) Time constants of insulin secretion for single islets modeled from slow secretors in 11.2mM glucose.

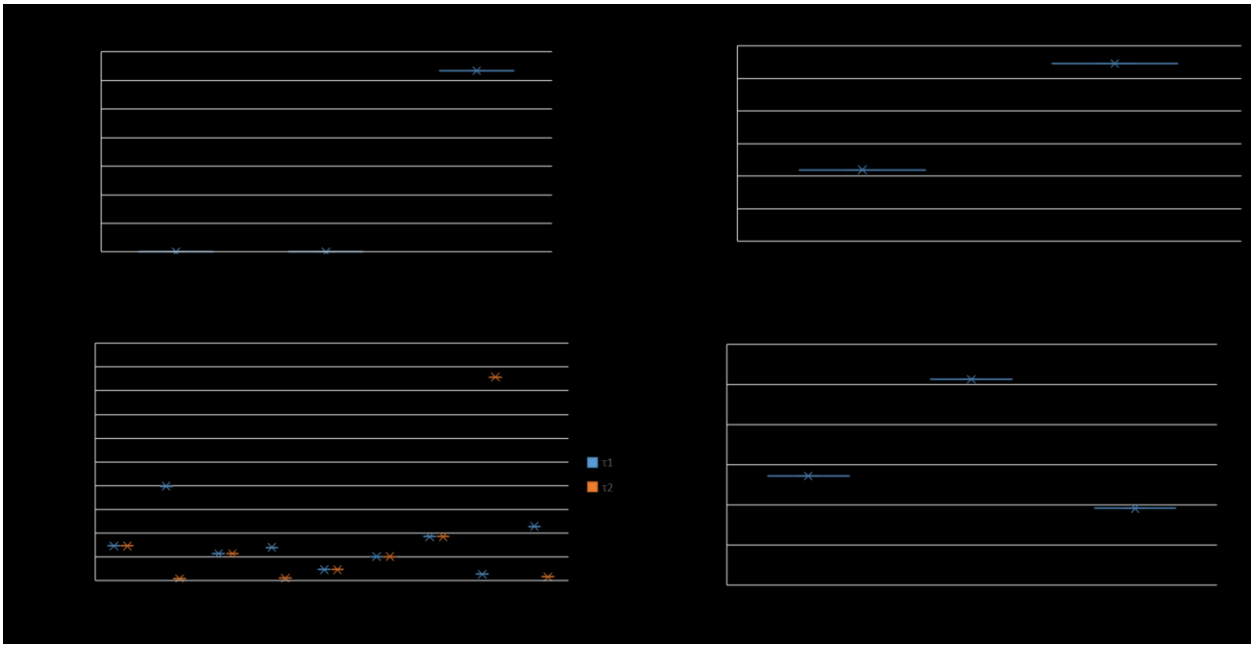

Supplemental Figure 17. Rates of insulin secretion for single islets modeled from constant-rate secretors in (A) 11.2mM glucose and (B) 20mM glucose. Time constants for single islets modeled from (C) slow secretors and (D) fast secretors in 20mM glucose.

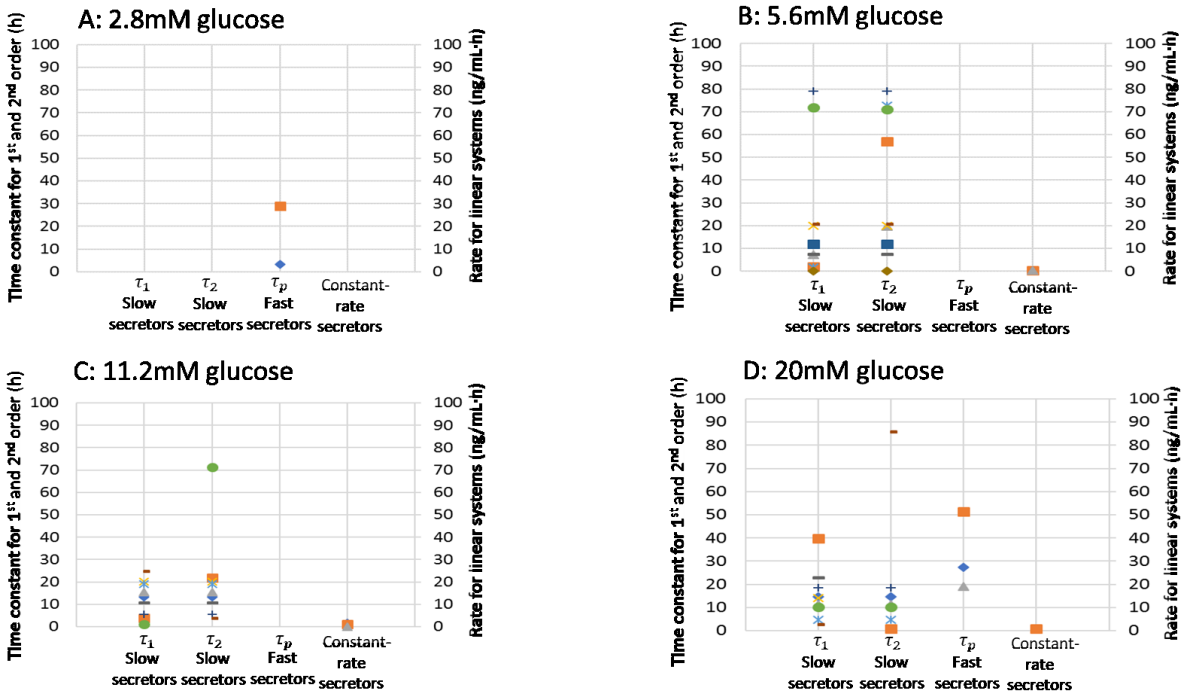

Supplemental Figure 18. From single islet experiments, time constants of fast and slow secretors or rates of insulin secretion of constant-rate secretors (i.e., linear systems) maintained 72h in (A) 2.8mM glucose, (B) 5.6mM glucose, (C) 11.2mM glucose and (D) 20mM glucose.

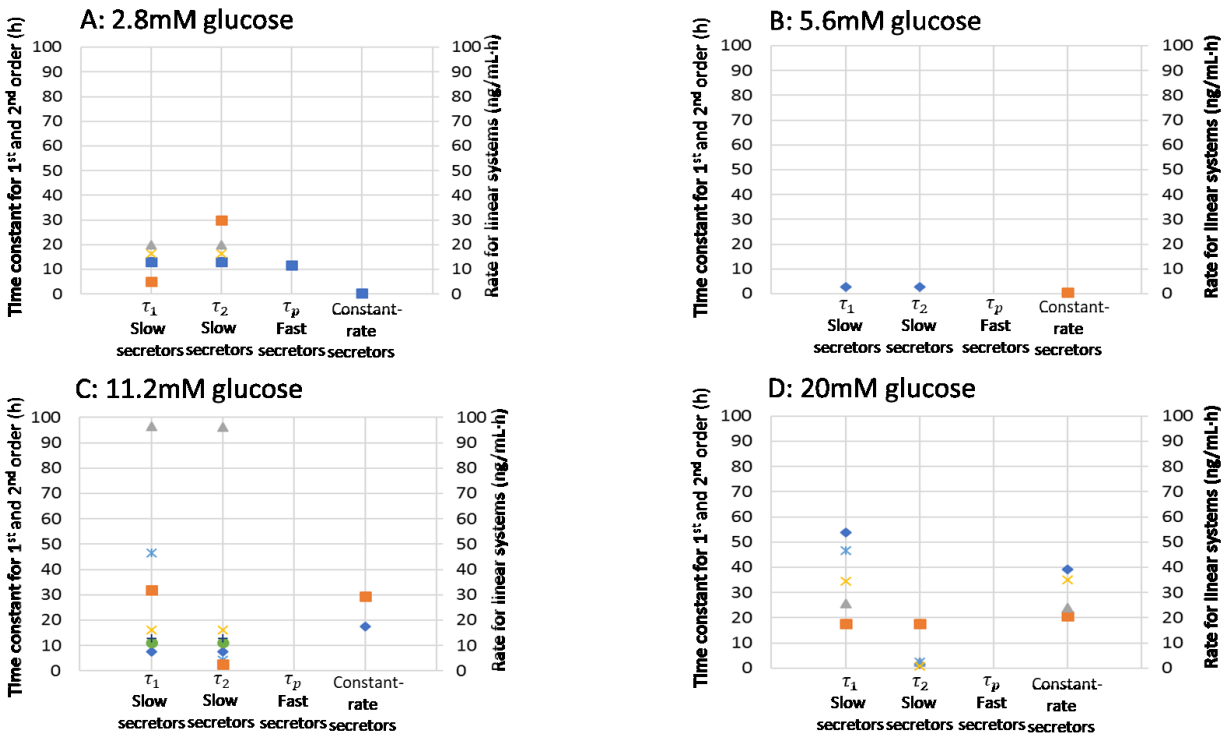

Supplemental Figure 19. From pools of 10-islet experiments, time constants of fast and slow secretors or rates of insulin secretion of constant-rate secretors (i.e., linear systems) maintained 72h in (A) 2.8mM glucose, (B) 5.6mM glucose, (C) 11.2mM glucose and (D) 20mM glucose.

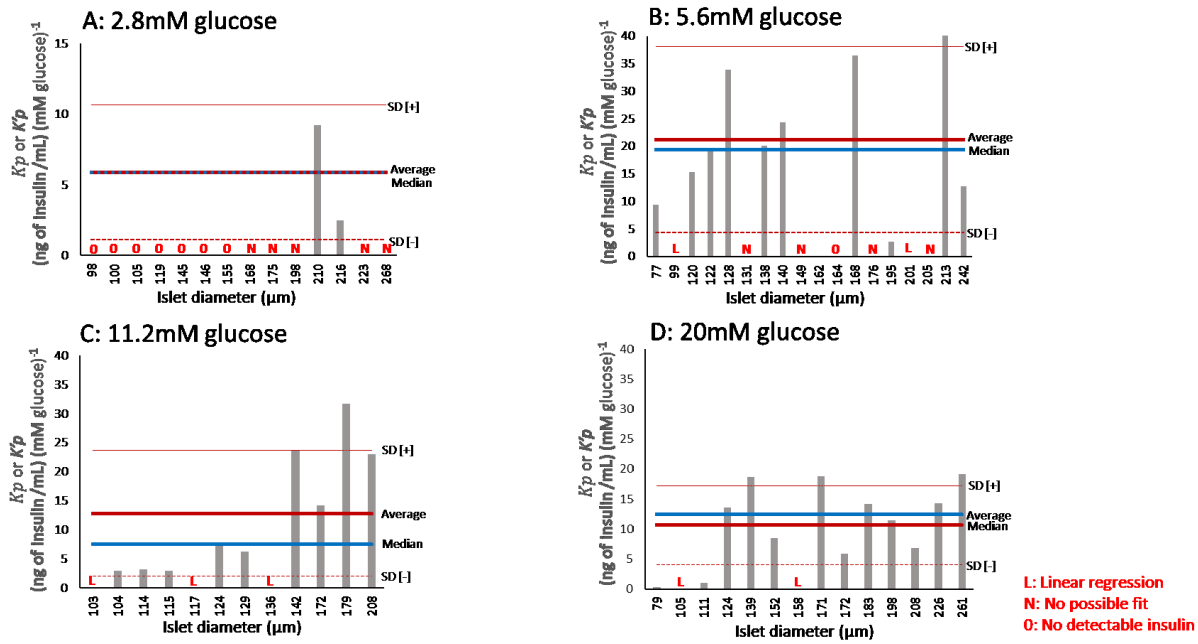

Supplemental Figure 20. From single islet experiments, the steady-state process gains, K_p and $〚K'〛\_p$, of fast and slow secretors maintained 72h in (A) 2.8mM glucose, (B) 5.6mM glucose, (C) 11.2mM glucose and (D) 20mM glucose. K_p and $〚K'〛\_p$ can be interpreted as the ratios of the predicted (modeled) cumulative insulin concentration at plateau to the glucose concentration used to incubate the islets.

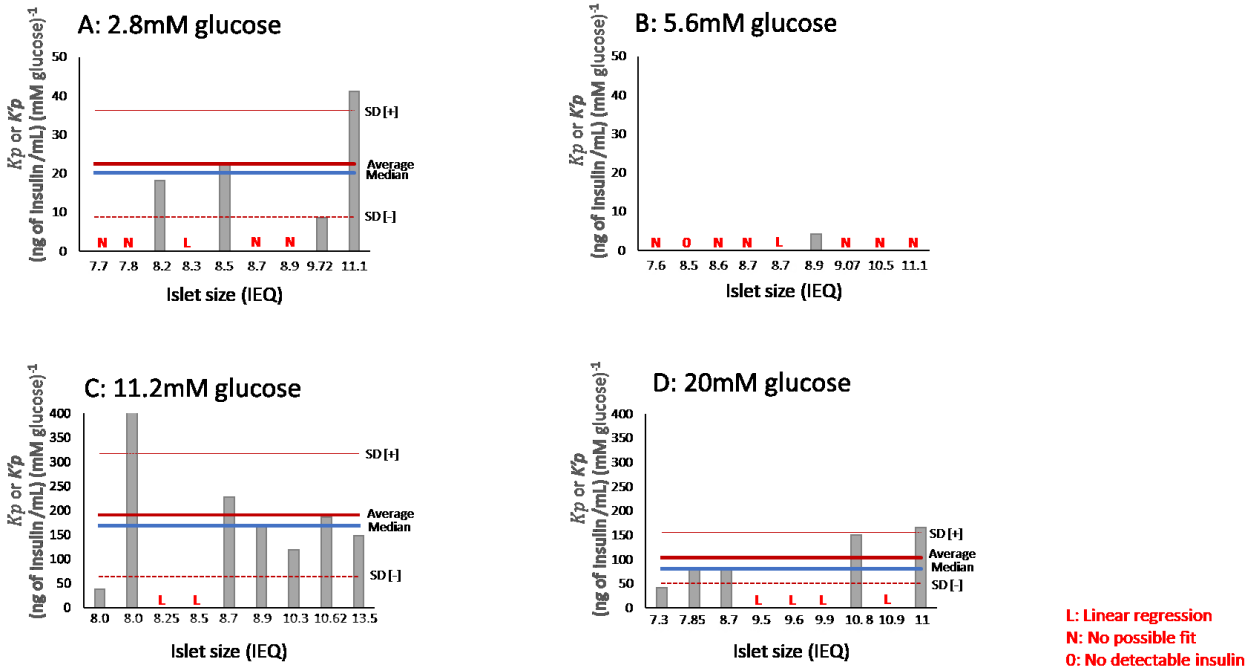

Supplemental Figure 21. From pools of 10-islet experiments, the steady-state process gains, K_p and $〚K'〛\_p$, of fast and slow secretors maintained 72h in (A) 2.8mM glucose, (B) 5.6mM glucose, (C) 11.2mM glucose and (D) 20mM glucose. K_p and $〚K'〛\_p$ can be interpreted as the ratios of the predicted (modeled) cumulative insulin concentration at plateau to the glucose concentration used to incubate the islets.

Appendix B

Development of first-order function

In this study, fast-secretor islets appear to follow the dynamics of a first-order system. A first-order system is represented by the equation:

$$\tau_p \frac{dy}{dt} + y = K_p f(t) \quad \text{(E1)}$$

y is the response of the system (output) submitted to a forcing function *f* (input). τ_p is the time constant indicative of the response speed. Smaller value τ_p will produce faster response. K_p is the static gain representing the ultimate variation of the output (*y*) to a variation of the input (*f*).

For a step change of amplitude *A* in the input i.e., *f(t) = A*, equation (E1) becomes:

$$\tau_p \frac{dy}{dt} + y = K_p A \quad \text{(E2)}$$

Solution of this equation gives:

$$y = K_p A \left(1 - e^{-t/\tau_p}\right) \quad \text{(E3)}$$

In this study, A represents different concentrations of glucose at *t=0* and *y*, the resulting measured concentration of insulin. Parameters τ_p and K_p can be determined by fitting experimental data.

To explain the significance of parameters τ_p and K_p, an analogy could be represented by the following irreversible reaction where component A is transformed into component B:

$$A \rightarrow B \quad \text{(E4)}$$

In a batch reactor, since there is no flowrate in or out of the reactor, the material balance on component *j* is:

Rate of accumulation of component j = Rate of creation of component j by reaction (E5)

Thus:

$$\frac{d}{dt}\int C_j\, dV = \int r_j\, dV \tag{E6}$$

C_j and r_j are, respectively, the concentration and reaction rate for component *j*, and *V* is the reactor volume. For a well-stirred reactor and assuming constant volume:

$$\int C_j\, dV = C_j \mathrm{V} \quad \text{and} \quad \int r_j\, dV = r_j V \tag{E7}$$

For a first-order rate reaction, the reaction rate is:

$$r = kC_A \tag{E8}$$

k is the specific reaction rate in (time unit)$^{-1}$ and C_A is the concentration of component A. Since B will be produced at the same rate as A is consumed, we can then write:

$$r_B = -r_A = kC_A \tag{E9}$$

The negative sign indicates that A is disappearing. Inserting equations (E7) and (E8) in (E6), leads to, for component A:

$$\frac{dC_A}{dt} = -kC_A \tag{E10}$$

Considering an initial concentration C_{A0} at $t=0$, solving the equation gives:

$$C_A = C_{A0}e^{-kt} \tag{E11}$$

For component B:

$$\frac{dC_B}{dt} = r_B = kC_A = kC_{A0}e^{-kt} \tag{E12}$$

Solving:

$$C_B = C_{B0} + C_{A0}(1 - e^{-kt}) \tag{E13}$$

Hence, for this system with $C_{B0} = 0$, a step change C_{A0} at $t=0$ gives:

$$\tau_p = \frac{1}{k} \tag{E14}$$

$$K_p = \frac{C_{B\infty}}{C_{A0}} \tag{E15}$$

Where $C_{B\infty}$ is the concentration on component B when $t \rightarrow \infty$. If the reaction is complete i.e., all reactive are consumed, $C_{B\infty} = C_{A0}$ and $K_p = 1$. An example of first-order response for both species is presented in Figure S1 for $C_{A0} = 1$ and $k = 1$.

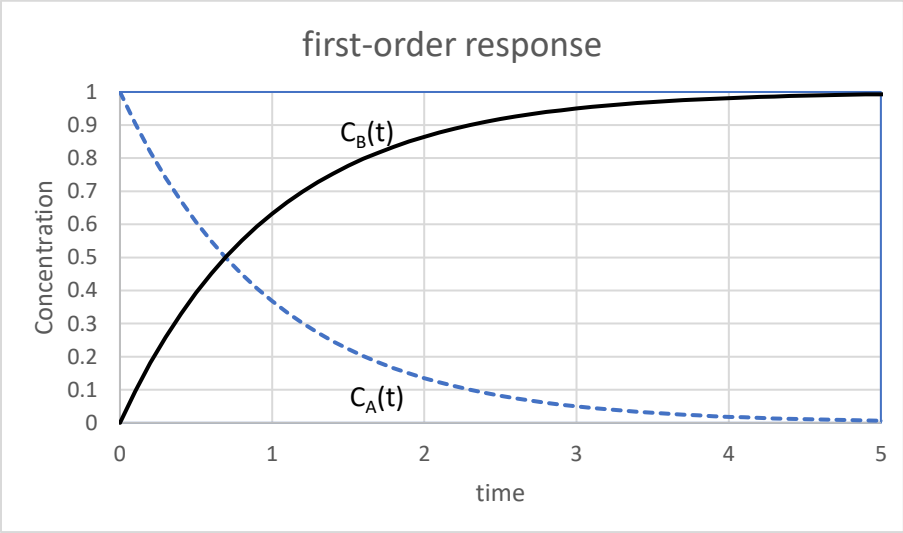

Figure S1

Development of second-order function

Contrary to fast secretors which start to produce insulin rapidly at the beginning of a kinetic experiment, slow-secretor islets initial response is sluggish. The sigmoidal response obtained are typical of a second-order system. This type of response can be the results of two different processes that operate in series. For example, a component which requires a significant time to diffuse through a porous solid phase before a reaction can occur could display a second-order response. As an analogy, we can demonstrate the dynamic of two irreversible reactions in series. In the first reaction, component A decomposes to form the intermediate B. In the second reaction, B forms the final product C:

$$A \rightarrow B \rightarrow C \tag{E16}$$

If for both reactions, the reaction rates are of first-order:

$$r_1 = k_1 C_A \quad , \quad r_2 = k_2 C_B \tag{E17}$$

The material balances on the components give:

$$\frac{dC_A}{dt} = -r_1 = -k_1 C_A \tag{E18}$$

$$\frac{dC_B}{dt} = r_1 - r_2 = k_1 C_A - k_2 C_B \tag{E19}$$

$$\frac{dC_C}{dt} = r_2 = k_2 C_B \tag{E20}$$

For component A, the material balance can be solved like before:

$$C_A = C_{A0} e^{-k_1 t} \tag{E21}$$

For component B, inserting (E21) in (E19):

$$\frac{dC_B}{dt} + k_2 C_B = k_1 C_{A0} e^{-k_1 t} \tag{E22}$$

The solution of this equation is:

$$C_B = C_{B0}\, e^{-k_2 t} + C_{A0} \frac{k_1}{k_1 - k_2} \left(e^{-k_1 t} - e^{-k_2 t}\right) \tag{E23}$$

If $C_{B0} = 0$, (E23) is reduced to:

$$C_B = C_{A0} \frac{k_1}{k_1 - k_2} \left(e^{-k_1 t} - e^{-k_2 t}\right) \tag{E24}$$

For component C, inserting (E24) in (E20):

$$\frac{dC_C}{dt} = C_{A0} \frac{k_1 k_2}{k_1 - k_2} \left(e^{-k_1 t} - e^{-k_2 t}\right) \tag{E25}$$

Assuming $C_{C0} = 0$, the solution of (E25) is:

$$C_C = C_{A0}\left[1 - \frac{1}{k_2 - k_1}\left(k_2 e^{-k_1 t} - k_1 e^{-k_2 t}\right)\right] \quad \text{(E26)}$$

Since $\tau_{p1} = 1/k_1$ and $\tau_{p2} = 1/k_2$, equation (E26) is equivalent to equation 2.

Figure S2 presents the second-order response of two reactions in series with conditions $C_{A0} = 1$, $k_1 = 1$ and $k_2 = 3$.

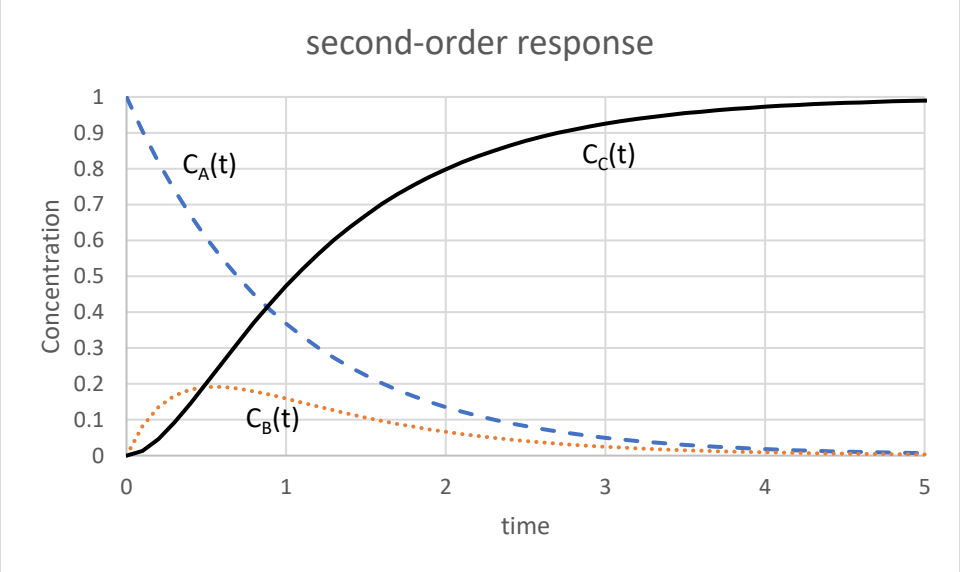

Figure S2

Appendix C

Python program used to determine percentage of live and dead cells

```
import os
from PIL import Image
import matplotlib as mpl
mpl.use("Agg")
import matplotlib.pyplot as plt
class image():
	def __init__(self):
		# image name
		self.name = "NAN"
		# image file name
		self.file = "NAN"
		# image dimensions: height and width
		self.size = []
		# file type of the image
		self.type = "NAN"
		# number of pixels of with colors R, G and B
		self.RGB = {'R':-1, 'G':-1, 'B':-1}
		# image histogram data -- Tonal variations in R, G and B
		self.HData = {'R':[], 'G':[], 'B':[]}
##############################################################################
#######
def Load(imageFName):
	# Load an image by filename
	if os.path.isfile(imageFName):
		img = Image.open(imageFName)
```

```
            # Create an image object and set its name
            imageObject = image()
            imageObject.file = imageFName
            imageObject.name = imageFName[imageFName.index("."):]
            imageObject.type = imageObject.name = imageFName[:imageFName.index(".")]
            imageObject.size = img.size
            return imageObject
        else:
            print("\033[91m File %s does not exist \033[0m" % imageFName)
################################################################################
#######
def IsImageFile(name):
        # determine if a file/folder is an image file
        if os.path.exists(name):
            return 0
        else:
            imageExtensions = [".pdf", ".png", ".jpg", ".jpeg", ".tiff"]
            for extn in imageExtensions:
                if extn in name[-len(extn):]:
                    return 1;
            return 0;
################################################################################
#######
def LoadDir(dirName):
```